AR-009-944

DSTO-TR-0454

DSTO

Elastic/Plastic Finite Element Analysis of the F-111 Fuel Flow Vent Hole Number 13

J. Paul, P. Chapman and A. Searl

DEPARTMENT OF DEFENCE
DEFENCE SCIENCE AND TECHNOLOGY ORGANISATION

Mar-04

DISCLAIMER NOTICE

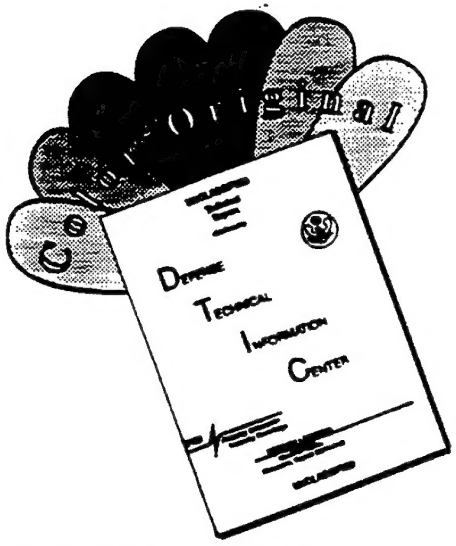

THIS DOCUMENT IS BEST QUALITY AVAILABLE. THE COPY FURNISHED TO DTIC CONTAINED A SIGNIFICANT NUMBER OF COLOR PAGES WHICH DO NOT REPRODUCE LEGIBLY ON BLACK AND WHITE MICROFICHE.

Elastic/Plastic Finite Element Analysis of the F-111 Fuel Flow Vent Hole Number 13

J. Paul, P. Chapman and A. Searl

Airframes and Engines Division
Aeronautical and Maritime Research Laboratory

DSTO-TR-0454

ABSTRACT

A detailed plasticity finite element stress analysis is presented for a fatigue critical location, at Fuel Flow Vent Hole #13 (FFVH#13) in the Wing Pivot Fitting of the Royal Australian Air Force's F-111 aircraft. The D6ac material behaviour was represented by a unified constitutive model which is considered to be particularly accurate for modelling plastic deformation through several cycles of non-symmetric loading. The aim of the present work is to generate the residual stress distributions following one (or more) applications of Cold Proof Load Test, as an input to the Durability And Damage Tolerance Analyses (DADTA) for FFVH#13. The mesh refinements and the selection of boundary conditions for a substructure model representing the immediate vicinity of FFVH#13 are discussed in detail. The results from the numerical analysis were correlated with full-scale wing test strain data and showed good agreement. The residual stress distributions obtained here are considered to be significantly more accurate than what has previously been used for the DADTA of FFVH#13.

RELEASE LIMITATION

Approved for public release

DEPARTMENT OF DEFENCE

DEFENCE SCIENCE AND TECHNOLOGY ORGANISATION

Published by

DSTO Aeronautical and Maritime Research Laboratory
PO Box 4331
Melbourne Victoria 3001

Telephone: (03) 9626 8111
Fax: (03) 9626 8999

AR-009-944
November 1996

APPROVED FOR PUBLIC RELEASE

Elastic/Plastic Finite Element Analysis of the F-111 Fuel Flow Vent Hole Number 13

Executive Summary

The conditions under which the RAAF operate the F-111 aircraft have been shown to be conducive to cracking in the structurally critical wing pivot fitting. Lockheed Martin Tactical Aircraft Systems (LMTAS) are contracted by the RAAF to perform Durability And Damage Tolerance Analyses in order to determine safe inspection intervals for the F-111 aircraft. Two control points of current concern are the upper outboard and the lower inboard corners of the Fuel Flow Vent Hole Number 13 (FFVH#13), in the wing pivot fitting. There have been numerous incidences of fatigue cracks detected at the lower inboard corner of FFVH#13 in the RAAF F-111 fleet. A significant factor is the residual stress caused by local yielding in the cold proof load test (CPLT). In order to calculate inspection intervals, a detailed knowledge of the elastic and residual stress fields is required for these locations.

The RAAF manages the cracking at FFVH#13 by re-working the hole to a larger shape to remove a crack when one is detected. AMRL has conducted extensive full-scale strain surveys of the F-111 wing pivot fitting with various FFVH#13 geometries, in order to provide detailed experimental strain data for the correlation of finite element analysis models. In the present work, a detailed plasticity finite element analysis was performed on FFVH#13 on three geometries which are representative of the variation within the RAAF fleet.

The D6ac material behaviour was represented by a unified constitutive model which is considered to be particularly accurate for modelling plastic deformation through several cycles of non-symmetric loading. The results from the numerical analysis correlated well with the full-scale wing test strain data, and the residual stress fields in the critical region were produced for each geometry.

The elastic and residual stress fields developed in this report will be used by LMTAS as an important ingredient for the determination of the inspection interval for this critical location in the F-111.

Authors

J. Paul
Airframes and Engines Division

Mr Paul has a degree in Aeronautical Engineering and a Masters in Mechanical Engineering in the repair of thick composite structures. He has worked in the finite element field for 13 years providing AMRL with a high level of expertise in the area of computational analysis which has been utilised to solve a variety of RAAF related stress/strain problems seen on the F-111 and F/A-18 aircraft. He is currently the Functional Head of the Computational Stress Analysis Facilities within AED and leads the team working on the F-111 Structural Integrity Task, which provides the residual stress input required for the calculation of the inspection interval for the Fuel Flow Vent Hole #13 location in the F-111 Wing Pivot Fitting.

P. Chapman
Airframes and Engines Division

Mr Chapman graduated with an Aerospace Engineering degree from RMIT in 1994 with first class honours. He has been working at AMRL since 1995, where he has been involved with the finite element modelling and analysis of the Fuel Flow Vent Hole #13 location in the F-111 Wing Pivot Fitting, and the research of bonded composite reinforcements of cracked aluminium panelling. His current work involves a review of the life assessment of the F/A-18.

A. Searl
Airframes and Engines Division

Mr Searl has a degree in Aerospace Engineering having graduated from RMIT in 1994 with first class honours, and is currently studying for a doctor of philosophy in Aerospace Engineering at RMIT as a Cadet Research Scientist. Since commencing work with AMRL in 1995, he has been involved with the finite element modelling and analysis of the Fuel Flow Vent Hole #13 location in the F-111 Wing Pivot Fitting, and the investigation of composite bonded reinforcements for the F/A-18 fuselage bulkhead re-entrant corner. His current research involves investigation into the structural optimisation of complex composite structures for the CRC-AS and AMRL.

Contents

LIST OF TABLES

LIST OF FIGURES

1. INTRODUCTION

1.1 BACKGROUND

The Royal Australian Airforce (RAAF) currently has in service a fleet of F-111 aircraft. The conditions under which the RAAF operates this aircraft have shown to be conducive to cracking in the structurally critical Wing Pivot Fitting (WPF). Fuel Flow Vent Hole number 13 (FFVH#13), shown in Figure 1, is the most critical of many such holes in the WPF upper and lower plate Stiffeners. In early fatigue testing by the F-111 Original Equipment Manufacturer (OEM[1]) [1] cracking was detected at FFVH#13, and there have been numerous incidences of fatigue cracks detected at its lower inboard corner in the RAAF fleet.

Initially any cracks found in FFVH#13 were locally blended out and the RAAF, who were concerned about this technique, tasked AMRL to determine optimum rework shapes [2]. That work developed a family of rework geometries, (see Figure 2) based upon an idealised elastic finite element analysis (FEA) of the rework shape in a plate. Since AMRL's recommendation, any rework by the RAAF of FFVH#13 to remove cracks is performed strictly to the rework shape configurations. This has resulted in a wide variation in size of FFVH#13's within the RAAF fleet, in which a few wings have even been reworked out to size F in Figure 2. AMRL has worked over the past few years to standardise and improve the techniques used by the RAAF to rework FFVH#13 geometries [3].

The RAAF contracts Lockheed Martin Tactical Aircraft Systems to perform Durability And Damage Tolerance Analyses (DADTAs) on its F-111 aircraft. These fatigue analyses determine the inspection intervals for locations on the aircraft which are designated as critical or have been known to give problems. Two such control points of significant concern are the upper outboard and lower inboard corners of FFVH#13, in the WPF. To perform an accurate DADTA, the OEM requires a detailed knowledge of the flight spectrum, material crack growth data and the cyclic and residual stress fields at the location of concern. Whilst the FFVH#13 control points have been analysed in previous DADTAs, the RAAF considered that those analyses did not include an accurate account of residual stresses, and therefore, may have been unconservative. Accordingly, the RAAF tasked AMRL to accurately determine both the cyclic and residual stress fields around FFVH#13, for the range of sizes and shapes in the RAAF fleet, as inputs to a special DADTA of these control points. This work has been performed using detailed Finite Element (FE) modeling of the local FFVH#13 WPF region.

---

[1] The Original Equipment Manufacturer changed name from General Dynamics (GD) to Lockheed Fort Worh Corporation and is now known as Lockheed Martin Tactical Aircraft Systems (LMTAS).

1.2 COLD PROOF LOAD TESTING

CPLT involves the application of approximate limit loads to the aircraft at -40 deg C. At this temperature the WPF material, D6ac steel, is considered to be fracture critical. If the aircraft survives this severe structural test then an additional period of safe operation, nominally 2,000 flight hours or about 7 years life, is accredited to the airframe.

However, the application of the CPLT causes localised yielding and leaves certain regions of the aircraft with large plastic residual stresses that otherwise, under normal flight conditions, would not be present. The residual stresses occur at stress concentrations such as holes. In some areas, such as the lower WPF plate, the residual stresses are compressive and beneficial, but in the upper plate, particularly at FFVH#13, they are tensile and detrimental.

The CPLT cycle is defined by the particular phase of the Structural Inspection Program (SIP), currently phase III is active for the RAAF fleet. SIP III requires a -2.4g, +7.33g load cycle at 56° wing sweep and a -3.0g, +7.33g load cycle at 26° wing sweep to be applied to the aircraft.

1.3 AMRL FE MODELING

The gross plastic yielding which occurs in FFVH#13 when the wing is subjected to the CPLT loading makes analysing the residual stress fields very difficult. Classical techniques of modeling the plastic behaviour of materials have difficulties in representing high inelastic strain behaviour under cyclic loading. Consequently, AMRL developed and utilised a set of unified constitutive equations to represent the non-linear material behaviour of D6ac steel [4]. These equations have been implemented into the PAFEC Finite Element Analysis Package [5], and all plastic analyses in this report utilised this material model.

Previously, AMRL received an F-111 Stub Wing FE model from the OEM, which contained a simple representation of the WPF coupled to a reduced section of the outer wing. Early work at AMRL [6] converted the supplied NASTRAN Data Deck of that model into a PAFEC FE model. From this, a local detailed substructure model of the upper wing pivot fitting plate and FFVH#13 was developed. The region extended between Stiffeners #2 and #4 in the chordwise direction and from the center hub to the stiffener run out regions in the spanwise direction, see Figure 3.

The approach undertaken by AMRL was to use the substructure FE model to perform the detailed FE analysis of the FFVH#13 region. A number of variants of this model were created for different FFVH#13 sizes and shapes. In order to obtain the best possible boundary conditions, as input to these models, the original OEM Stub Wing model was enhanced to improve a number of deficient aspects. This enhancement also included the insertion of the AMRL substructure FE model for each rework geometry

analysed, and then the displacement boundary conditions were extracted for use on the separate substructure FE models.

The FE models were correlated against strain data from full-scale wing tests performed at AMRL [7, 8 and 9]. Three FFVH#13 shapes were tested: Baseline, Intermediate and Large; and corresponding FE models were developed for correlation. Then, for the analyses to create the DADTA input, models of virtually the same three shapes were used. The DADTA reworked shapes were classified as Blueprint, Intermediate and Large, and corresponded to the original profile and shapes C and F respectively in Figure 2. The only difference from the correlation shapes was that the Blueprint geometry was representative of the true drawing geometry, whereas the Baseline geometry was that of the actual AMRL wing. The Intermediate and Large geometries were the same for both the correlation and DADTA analyses. The three DADTA rework shapes adequately cover the full range of shapes in the RAAF fleet.

2. FINITE ELEMENT MODELS

2.1 MODIFIED OEM WING STUB FE MODEL

The initial course meshed FE model used for the F-111 FFVH#13 Finite Element DADTA work was originally obtained from a General Dynamics F-111 Stub Wing FE model used to analyse the upper wing skin of the WPF in the F-111 fatigue test. This FE model was created for the NASTRAN FE analysis system and was converted to the PAFEC package using a PAFEC product called NAPEC [6]. The converted model has provided the basis for all previous F-111 WPF FE analysis work performed by AMRL, and was therefore employed for this work as the initial model to be correlated against the most recent set of full-scale wing tests.

2.1.1 Model description

Structurally the Stub Wing model consisted of the WPF with underlying detail, the wing sweep actuator attachment structure, the wing pivot hub and approximately 2.3m (90 inches) of the outboard wing assembly. This model was constructed of one, two and three dimensional elements, which are listed in Table 1 along with their number of occurrences throughout the model.

The Stub Wing FE model had the upper wing skin of the WPF and central hub region represented by three-dimensional (3D) brick elements. All other skin surfaces were represented by two-dimensional (2D) shell elements. The underlying Stiffeners,

including the Titanium shear web[2] were all of 2D shell element representation, with additional beams used to enhance the stiffness representation. See Figure 4 for a view of the complete FE model.

One major inconsistency between the Stub Wing model and the RAAF and AMRL wings is that the model had no lower plate boron doubler representation. The effect of this deficiency would be to change the lower plate strains and to a lesser extent the upper plate strains and the overall deflection of the model. This is not compensated for in AMRL's analyses and is discussed in detail in Section 6.

Close examination of the Stub Wing FE model showed deficiencies in representing the RAAF F-111s and the AMRL test wing. A number of modifications and refinements were made to create an improved representation. Details of the modifications made to this model can be found in Appendix 1.1.

2.1.2 Loading

The original OEM Stub Wing FE model incorporated applied loads and restraints to the structure. These loads were located around the outer boundaries of the stub wing. Concentrated loads and restraints were applied to the hub region to react the main loads. Figure 5 and Figure 6 show the complex sets of loads applied to this model for the -2.4g and +7.33g load cases respectively.

2.2 COMBINED OEM/AMRL FE MODEL

2.2.1 Introduction

In order to accurately model the complex geometry and stiffness of the WPF area of interest, a substructure model of the local region around FFVH#13 was previously constructed [2, 6]. This substructure FE model utilised the loading distribution from the OEM Wing Stub FE model for the analysis of stresses around FFVH#13. The coarseness of the meshing in the original OEM Wing Stub FE model limited the accuracy of the extracted boundary conditions around the critical region. For the current work reported here, the AMRL substructure FE model was inserted into the OEM Stub Wing FE model. The combined OEM/AMRL FE models were used to improve the representation of the boundary conditions, particularly in the region of the Stiffener #3/Titanium web interface.

The representation of the FFVH#13 region in the OEM Wing Stub FE model was not detailed enough to adequately represent the local stiffness changes in the region. In

[2] The Titanium shear web is oriented vertically and approximately spanwise. It is a main shear carrying element of the wing pivot fitting and is attached at the top to the upper plate stiffener number 3, which contains FFVH#13 (see Figure 17).

addition, the bolt loads being provided by the connection of Stiffener #3 to the Titanium web were inadequate and even numerically singular. A single element had been used to depict the load transfer through each individual bolt. Inserting the detailed AMRL substructure model accounted for some of the deficiencies associated with the OEM Wing Stub FE model. This extra detail provided a more accurate structural and stiffness representation of the region, including an improved load transfer representation between the Titanium web and Stiffener #3.

The three wing test reworked geometries were inserted into three different combined OEM/AMRL FE models. This was necessitated by differences seen in the displacement fields around the substructure boundary when analysing the substructure models in isolation. The main differences occurred in the region where Stiffener #3 was attached via bolts to the Titanium web. As the FFVH#13 hole size is increased, the local compliance of the Stiffener is changed, thereby changing the load transferred through the bolts. Each set of reworked geometry boundary conditions derived from elastic analyses of the combined OEM/AMRL FE models was then used in the corresponding AMRL substructure model described in Section 2.3.

2.2.2 Model description

The OEM/AMRL combined FE models consist of a combination of beam, 2D shell and 3D isoparametric elements. Table 2 shows the number of nodes, elements and degrees of freedom for each reworked model (defined as Baseline, Intermediate and Large in Section 4.5). In addition, the inserted AMRL substructure region contains higher order elements with mid-side nodes, and the upper wing skin region of the model was modified to be represented by two elements through the thickness. The effect of incorporating the AMRL detailed FFVH#13 substructure model into the OEM Stub Wing FE model resulted in a more accurate representation of the local region's stiffness. This one enhancement contributed significantly to the improved correlation of strain gauges for the Stiffener #3 region. It should be noted that this combined model was too large for the current AMRL computer system to perform the required detailed plasticity analysis. This necessitated the use of the smaller more detailed AMRL substructure model to perform this section of the analysis.

2.2.3 Model modifications

The modifications made to these series of models mainly concentrated on maintaining mesh compatibility between the OEM Wing Stub FE model and the inserted substructure model. The model enhancements described in Section 2.1.1 were included in these models. A description of the modifications performed is provided in Appendix 1.2.

2.3 AMRL SUBSTRUCTURE MODEL

2.3.1 Introduction

Substructure FE models of sections of the F-111 WPF have been used extensively by AMRL over the years as the basis of previous analyses work on FFVH#13, Stiffener Runout Number 2 [10] and the effect of AMRL applied boron doubler to the F-111 wing [2, 6]. In each case a substructure model was generated either in 2D for the Stiffener Runout Number 2 analyses or combined 2D/3D for the FFVH#13 analyses. This section describes the enhancements made to a substructure FE model of FFVH#13 inherited from previous AMRL work [2].

2.3.2 Model description

The current development of the AMRL substructure FE model of FFVH#13 actually consists of three models depicting each of the three FFVH#13 reworked shape geometries described in detail in Section 4.5. Table 3 shows the number of nodes, elements and degrees of freedom for each reworked model. The region extracted from the original OEM Wing Stub model consists of Stiffener #3 and the section of the upper wing skin between Stiffeners #2 and #4. The Titanium web was not included in the substructure because it has a complex 3D shape, yet its influence is readily and effectively conveyed through the connecting bolt loads applied to the model via their displacement fields. Specific details of the enhancements and modifications for the current development of the AMRL substructure FFVH#13 model can be found in Appendix 1.3. The overall substructure mesh can be seen in Figure 7 with the specific meshes for the three reworked geometries seen in Figure 8 to Figure 10.

2.3.3 Loading

Unlike the original OEM Stub Wing FE model which applied loads and restraints to the structure, the AMRL substructure model only used applied displacement fields. These displacement fields were extracted from the equivalent reworked shape combined OEM/AMRL models described in Section 2.2. The applied boundary displacement region for the substructure models comprised: 1) the edge of the upper plate above and adjacent to Stiffener #2, Stiffener #4 and the Outer Chordwise Stiffener (see Figure 13); 2) the edge of the Chordwise Stiffener (see Figure 13); 3) the WPF hub section; and 4) Stiffener #3 bolt locations. Excluded from the boundary region was Stiffener #2, Stiffener #4 and the Outer Chordwise Stiffener. Figure 11 and Figure 12 show the mesh and boundary conditions applied to the structure for the -2.4g and the +7.33g loading conditions respectively.

3. FULL-SCALE WING TESTS

AMRL has conducted three full-scale wing strain surveys of the F-111 test wing, specifically to provide strain gauge data to correlate the three reworked shape FE models. The tests were conducted at ambient temperature and not at -40 deg C because the fracture toughness of D6ac steel was not considered an issue. The loading distribution and magnitude were representative of the CPLT.

CPLT consists of four different loading conditions:

1. - 2.4g at 56° sweep
2. +7.33g at 56° sweep
3. - 3.0g at 26° sweep
4. +7.33g at 26° sweep

Each loading condition is applied incrementally from zero to the maximum condition defined above, then back to zero, and the four conditions are applied sequentially in the order shown. The loading conditions were applied to the wing via actuators at discrete points on the wing (as layed out in [11]). The exact geometries of FFVH#13 tested, along with complete gauge location information and results can be found in the full test reports on each wing test [7, 8 and 9]. The Baseline test shape is shown in Figure 8 and the Intermediate and Large shapes are shown in Figure 9 and Figure 10 as well as in Figure 2 (shapes C and F).

The wing was fitted with strip gauges around the inside of FFVH#13 to record the hoop strain. Uniaxial gauges and strain gauge rosettes were fitted to various other points around the WPF to record the far-field strain distribution. Figure 13 to Figure 19 show the positions of all the relevant gauges on the WPF used to correlate the FE models. It should be noted that even though some FFVH#13 strip gauges have the same identifying number in successive wing tests they are not in exactly the same locations. All these gauges had to be removed in order to accommodate the Electro Discharge Machining (EDM) process for reworking.

With each rework of the FFVH#13 more strip gauges were installed around the hole to provide better strain gauge coverage and to avoid missing the peak strain location. The second wing test, however, missed the peak strain in the lower inboard corner. Data from Stiffener #3 and Titanium web strain gauge rosettes indicated that the Stiffener is under the influence of a complex out-of-plane bending field that causes some gauges to a exhibit non-linear response at very low strain levels. This issue is examined in greater detail in the final wing test report [14] and in the correlation Section 6 of this report.

4. ANALYSIS DESCRIPTION

4.1 INTRODUCTION

All FE analyses within this report utilised the PAFEC Finite Element Package, and the plasticity analyses of the AMRL Substructure models employed a unified constitutive material model of D6ac steel behaviour, which had previously been implemented in PAFEC. The analyses are underpinned by a large program of previous work ranging from the uniaxial experimental characterisation of D6ac steel to derive the constitutive material parameters[4], the implementation of the unified constitutive model into the PAFEC FE package [5], the biaxial experimental validation of the constitutive model and its PAFEC implementation for round and oval holes in coupon specimens [12 and 13], and finally to the full-scale wing test strain data[14] which was used for the correlations described in this report. The combination of all this work allowed AMRL to provided accurate cyclic and residual stress fields with a high level of confidence.

4.2 SOLUTION PROCESSING

All solutions were run on a Hewlett Packard 9000-800 K210 computer, running HP-UX 10.1 operating system. The PAFEC package and the unified constitutive code were optimised for this machine's configuration and CPU type. This optimisation provided a 64% reduction in the time the solution took to perform the displacement solution, and in the plasticity analyses, this saving was made on every plastic iteration. In order to confirm that the optimised code did not influence the results (by floating point truncation), the unoptimised and optimised solutions runs were compared for one typical analysis run and no measurable difference was detected.

All plasticity analyses were configured to run with the gaussian integration order reduced from 3x3x3 to 2x2x2 for the three dimensional (3D) bricks elements representing the upper wing skin. For the substructure models it was considered to be better to use reduced integration, as full integration results in an over-stiffening effect. This provided a significant run time saving when compared to a full integration run, with only a very slight softening effect as measured by the change in the solutions results. The plasticity analyses took approximately 30 to 40 CPU hours run time for a full CPLT cycle, depending upon the extent of plasticity encountered in the configuration being analysed.

4.3 APPLIED LOADING

The OEM Stub Wing FE model had two loading cases applied to it in a complex manner, but which correlated to the 56° wing sweep configuration at -2.4g and +7.33g. A comparison was made between the applied wing test forces [11] and the total applied shear forces in the original OEM Stub Wing FE model. This comparison

included the allowance for the total wing weight. It was clearly apparent that the loading in this model was Design Limit Load (DLL) condition, which is slightly different from the CPLT loading.

The DLL bending moment curves for all loading cases are shown in Figure 20 to Figure 23, and the location of FFVH#13 as a fractional distance outboard of the pivot is 0.04. Comparing the DLL and CPLT bending moment distributions, it is apparent that the CPLT loading needs to be reduced by 4% for both +7.33g cases, 22% for the -2.4g case and 6.5% for the -3.0g case. In all analyses of this report, the reaction distribution on the WPF hub region was kept the same for both wing sweep angles. This was justified after investigating the differences in between the two sets of +7.33g peak strain readings from the wing tests, where no significant difference existed in the WPF plate gauges.

4.4 PLASTICITY TECHNIQUE

All plasticity analyses were performed using the unified constitutive material model which is fully described in [4]. This material model was used because of difficulty in implementing an accurate classical plasticity representation of the inelastic cyclic response for D6ac steel under the non-symmetrical CPLT loading. The unified constitutive model allows the material to experience structural deformation on the micro scale during the cyclic loading which results in a more accurate characterisation of the structural behaviour.

The unified constitutive model is a time dependant material model which implied that the CPLT load cycle had to be applied as a load versus time curve. The material characterisation work showed that D6ac steel is strain rate independent and therefore an arbitrary time scale was chosen and kept consistent for all plasticity analyses. Figure 24 shows the applied CPLT load versus time curve for all plasticity analyses.

The plasticity solution progresses through the loading history in time steps that are controlled by parameters which are described in [5]. The structural convergence tolerance, used to determine if the solution was converged, was calculated via the energy of the residual forces scaled by the energy of currently applied loads each iteration. All solutions were analysed with a 0.05% tolerance value which was determined by processing various representative analyses with different values of the tolerance.

The structural solution utilised the Newton-Raphson solution technique. The material Jacobian for each gauss point within an element was updated each iteration. The technique used to calculate the structural tolerance caused the solution to iterate extensively when trying to obtain a global zero load (Points A, B, and C in Figure 24). In these circumstances the iterative process was terminated after 4 iterations even if the convergence tolerance had not been achieved and the solution was allowed to continue. The effect of terminating the solution early, by not allowing it to iterate until

convergence at each global zero load point (sometimes 15 iterations), was investigated and shown to have no marked effect on the converged total strains values.

4.5 FFVH#13 GEOMETRIES

The reworked geometries analysed for the correlation process can be seen in Figure 25 with the shapes labelled 'AMRL Baseline' for the initial geometry, 'C' for the intermediate rework and 'F' for the largest rework. The geometry used for the base DADTA analysis is labelled 'Original Profile' (Blueprint) and the variation from the original AMRL wing geometry can be seen in Figure 25. The other two shapes analysed were identical to the AMRL wing test geometries and are labelled 'C' and 'F' as seen in Figure 2 and Figure 25.

4.6 CORRELATION PROCEDURE

Correlation was performed by comparing the experimental wing test strain data with the strains generated by the FE models. Correlation was done as a two-stage process; firstly a far-field correlation and secondly a local correlation at FFVH#13. For the far-field correlation three areas of the WPF were examined in detail: 1) the upper plate top and bottom surfaces; 2) the Stiffener #3; and 3) the Titanium web. The far-field correlation was performed on the three combined OEM/AMRL FE models[3] for the -2.4g and +7.33g load cases for the areas 1 to 3 above. Finally, the FFVH#13 hoop strain distributions were correlated using the AMRL substructure plasticity FE models, as the +7.33g load case induced a high level plastic deformation in the local FFVH#13 region.

From the strain gauge location drawings (Figure 13 to Figure 19) the exact position on the structure of each individual gauge to be examined was obtained and then related to a position on the FE model. In most circumstances the gauge position was coincident with a node, however when a gauge was found to lie between nodes an average value was taken between the two adjacent nodes. In order to compare the strains from the wing test to the FE model, the strains were rotated into the local direction of the particular strain gauge element.

Line plots of strain were used to obtain an understanding of the distribution along the upper surface of the WPF directly above Stiffener #3 and along the lower edge of Stiffener #3. The global nodal strains were rotated into the element axis system which accounted for the curvature of the wing surface. Similar line plots were generated of FFVH#13 hoop strain, however here the global strain field at a node was rotated into the local hoop direction around the hole. This allowed an accurate comparison between strain gauge and FE results.

[3] The OEM Stub Wing FE model was not used to correlate any wing test experimental data and was only presented to indicate some of the problems associated with mesh density and structural representation.

All gauges used throughout the correlation process are presented in Table 4. Here details of relevant figure numbers are provided so that the gauge positions may be easily located. The FFVH#13 gauge numbering and locations changed between wing tests, and details of their physical locations were given in Section 3.

The Baseline, Intermediate and Large reworked geometries for FEA have been abbreviated to BASE, INTE and LARG respectively throughout all Tables presented in the correlation process, and the corresponding wing tests are referred to as Test 1, Test 2 and Test 3 respectively.

5. OEM/AMRL FE CORRELATION RESULTS

5.1 COMBINED OEM/AMRL FE RESULTS

The results of elastic analyses for the 3 wing test geometries inserted into the OEM FE model are presented in this section. All Tables presented have strain results, where possible, covering the Upper Wing Skin: outer and inner surfaces, Stiffener #'s 2, 3 and 4: fore and aft faces and the Titanium web: fore and aft faces. The FE results are for the DLL load condition which allowed AMRL to produce an overall correlation table. The detailed results for the -2.4g and +7.33g DLL cases are shown in Table 5 and Table 6 respectively and the percentage errors presented are relative to the particular wing test geometry.

Figure 26 shows plots of the strain distributions along the outside of the upper plate over Stiffener #3 and along the bottom edge of Stiffener #3 which were obtained from the FE analyses of the modified OEM model and the three variants of the combined OEM/AMRL model. Plots are shown for -2.4g and +7.33g load cases. On examination of the strain distributions along the outside of upper wing skin surface for the +7.33g and -2.4g load cases it is apparent that the modified OEM does not have sufficient detail to represent the effect of FFVH#13 (see Figure 26a and Figure 26b). In addition the strains along the under surface of Stiffener #3 (see Figure 26c and Figure 26d) show the effects of changing the shape of FFVH#13. In general, the OEM FE model, with its course meshing, appears to produced a weighted average result when compared to the much finer Combined OEM/AMRL FE models - hence the decision to discard the OEM FE model and use the combined OEM/AMRL FE model for the far-field correlation.

Table 5 and Table 6 indicate, for both load cases, a significant margin of error between the FE and the Wing Test. This level of error required AMRL to examine the far-field strain gauges in order to determine if the level of bending in the upper plate surface of the WPF was representative.

The far-field mid-bay plate gauges 91-1, 96-1, 92-1 and 97-1 were used to determine the level of strain and hence the bending load in the upper plate of the WPF. At these locations the loading was considered to be outside the local influence of the Stiffeners. All four gauges lie mid way between Stiffeners 2 and 3, or 3 and 4. These gauges were correlated against the equivalent positioned nodes in the FE models and then the differences between the wing test and FE were calculated and these values averaged to produce the Far-field Average Error (FFAE). Table 7 summarises these gauge results using data extracted from Table 5 and Table 6.

The calibration factor which can also be seen in Table 7 was produced by adding 100 to the FFAE and then taking the inverse. This is approximately the equivalent to summing the four test strains and dividing it by the sum of the four FE model strains. This factor is a measure of how much the FE model loading needed to be factored in order to obtain an averaged far-field calibration with respect to the particular wing test. Again it is important to note that this factor is relative to the DLL condition for each load case, and therefore encompasses not only the differences between analysis results and test data, but also the difference between CPLT and DLL loading.

5.2 DISCUSSION

The aim of this section of the correlation process was to ensure that the correct level of loading was applied to each reworked geometry substructure FE model. The Combined OEM/AMRL FE analyses showed that the reworked FFVH#13 shape had an important effect on the loading through Stiffener #3. This effect required the specific use of the reworked geometries in order to determine the boundary conditions and far-field loading factors which were to be applied to the substructure models.

As FFVH#13 became larger, the analysis was made more complicated by the proximity of the Titanium web so close to the reworked FFVH. As the rework shape is increased, the local bending field is changed due to the change in the centroid of the hole. This effect is shown in the deviation of the surface plate strains between reworks, in the region of 150mm to 200mm, as shown in Figure 26a and Figure 26b.

At this stage it should be mentioned that in the wing tests the Stiffener #3 surface strain rosettes 77 to 84 exhibited distinctly non-linear behaviour in the vertical direction at very low loads. Resolving these rosette results into their principle components indicated very scattered results between fore and aft gauges. The problems associated with the interpretation of these gauges are discussed in detail in Reference 14. Examination of only the horizontal (spanwise) direction of these rosettes, produced differences that were more meaningful with respect to the overall representation of these FE models. These results can be seen in detail in Table 5 and Table 6.

The rapidly varying strain distribution along the stiffeners, as shown in Figure 26 and caused by the fuel flow vent holes, makes correlation between strain data and FE

results very difficult. Any geometric differences between the FE model and the test wing then highly significant, as are any errors in strain gauge locations. Furthermore, the complex out-of-plane bending of the Titanium web and its influence on Stiffener #3, which are not well represented by the combined OEM/AMRL FE models, make correlation with the gauges in these areas very difficult. These considerations account for the large and varied percentage errors between the test data and FE results in Table 5 and Table 6. The mid-bay gauges are much less affected by the complex behaviour of the stiffeners and the web and Table 7 shows they provide a more consistent correlation with lesser percentage differences.

6. SUBSTRUCTURE FE CORRELATION RESULTS

6.1 FE RESULTS

The three AMRL substructure FE models utilised the calibrated boundary conditions developed in Section 5 and the correlation process was extended in this Section to look at the hoop strain levels around FFVH#13. Each reworked geometry FE model was required to have slightly different loading as a result of the previous far-field correlation/calibration. Also the DLL boundary conditions for each load case, ie. -2.4g, +7.33g, -3.0g and +7.33g, were individually scaled by the calibration factors presented in Table 7. The FE models were analysed plastically, with the Baseline analysis performed over 2 CPLT cycles and the Intermediate and Large analyses performed over 1 CPLT cycle.

The detailed FE results for the gauges used in the main far-field correlation are presented in Table 8 and Table 9 (which are essentially a representation of Table 5 and Table 6 but listing the substructure results rather than the combined OEM/AMRL FE results). Only the first -2.4g and 1st +7.33g loading conditions at 56 degrees sweep respectively have been extracted. These Tables do not have any Titanium web results due to this part of the structure not being represented in these models. These results show a much improved far-field correlation between the FE models and the wing tests, with a variation in the main regions of concern ranging from 0.4% to 12%. A summary of the correlation results for the mid-bay gauges for the all load cases is provided in Table 10. The good correlation results in Table 10 verify that the calibration factors derived from the correlation of the combined OEM/AMRL model translate well to the substructure model

An additional comparison was performed by examining the strain distributions along the outside of upper wing skin surface and the under surface of Stiffener #3 for just the Large reworked geometry. The wing test strain data, from test 3, was superimposed onto the FE results, see Figure 27. The FE analysis results show a variation in upper surface plate strains that is not as apparent in the wing test results but is compatible with them.

The focus of these FE models was directed towards the representation of the strain distributions around FFVH#13. The hoop strain distributions as a function of angle around FFVH#13 for the load cases: -2.4g, +7.33g, -3.0g, +7.33g and residual have been plotted for the Baseline, Intermediate and Large geometries. These can be seen in Figure 28, Figure 29 and Figure 30 respectively. The definition of the angle around FFVH#13 can be found in Figure 25 and the same origin was maintained throughout all the FE hoop strain plots.

As previously discussed in Section 3, the amount of detailed experimental strain data around FFVH#13 increased with each wing test. Comparing the FE results from one CPLT cycle to the wing test data has been performed by splitting the FE data into three groups. The first group incorporates the first -2.4g and +7.33g load cases, the second incorporates the -3.0g, +7.33g and the third group shows the predicted residual strain comparison. Figure 31, Figure 32 and Figure 33 cover the Baseline shape results, Figure 34, Figure 35 and Figure 36 cover the Intermediate rework results and Figure 37, Figure 38 and Figure 39 cover the Large rework results.

In order to fully understand the cyclic response of the FFVH#13 region in these analyses it was useful to examine the stress versus strain response of particular locations. In this instance the peak strain location in each of the geometries at the lower inboard corner was chosen and the hoop stress versus hoop strain plots were generated. These can be found in Figure 40 for 2 CPLT cycles for the Baseline analysis (see Section 6.2.2.1) and 1 CPLT cycle for the Intermediate and Large analyses.

6.2 DISCUSSION

6.2.1 Introduction

Careful interpretation of the results from both the wing test and the FE perspective is required so that a full understanding of the analyses can achieved.

Firstly, the interpretation of the raw wing test data for the first wing test was difficult due to the unknown prior history of the this wing. The AMRL wing had previously undergone at least one CPLT cycle and flight loads. This implies that yielding had previously occurred around FFVH#13 and that the material was cyclically saturated[4] prior to testing. Therefore, the initial residual strain at the start of the first wing test was undefinable and can only be estimated from FE analysis. All gauges placed in regions that had previously yielded would be offset by any pre-existing residual strain. In addition, the Intermediate and Large reworked geometry wing tests, which had the strain gauges re-installed around FFVH#13, would have an initial residual stress/strain state which was non-zero. This scenario is illustrated in Figure 41 where

[4] Cyclic Saturation: No change in stress/strain loop observed between subsequent cycles, see Reference 4.

schematically it can be seen that prior to reworking of the wing a residual strain state exists. Then on removal of the material, the plastic zone which had not been fully removed results in a small yielded region left at the boundary of the new rework. In a region where the material had previously being cyclically saturated and the initial strains unknown, such as the FFVH#13 in the first wing test, it is feasible to deduce that any strain measurements recorded would have to take into account the initial residual strain values for that location.

Secondly, comparing results for each geometry against each other requires great care and may be invalid for the following reason. Neuber's rule states that the product of the stress and strain is proportional to the stress concentration squared [15]. In the case of the FFVH#13 reworks, each geometry has a different stress concentration factor due to the changing shape. Also the load distribution variation, as a result of the geometric change, influences on the local stress and strain response in the region where a large degree of plastic deformation is occurring. This must be kept in mind when examining the effect of the reworks on FFVH#13.

Finally, the FE analyses results have been presented as if the material was 'virgin' unyielded material. For the Baseline analyses it is assumed that this is not the case and for the Intermediate and Large geometries it is assumed to be close to this condition.

6.2.2 FFVH#13 Correlation

6.2.2.1 Baseline Analysis

Interpreting the Baseline correlation was difficult. The FE results presented for FFVH#13 were relative to an initially unyielded material analysis, and therefore the analysis was re-run through two CPLT cycles in order to determine the relative change in residual strains from one CPLT cycle to the next. From this analysis, the difference in the residual strains at the end of the first and second CPLT cycle was compared to the wing test results and is shown in Figure 42. This provided a better correlation with the wing test data than the results presented in Figure 33. In addition it should be noted that the wing test data for this test [7] included an additional 70% load mid-CPLT cycle. The effect of this additional cycle on the plastic response was not taken into account in the FE analyses.

It should be noted that the effect on final residual stress is insignificant even though the residual strain shows changes between the first and second CPLT cycles (see the end points of the two CPLT cycles in Figure 40).

6.2.2.2 Intermediate and Large Analysis

The initial residual strain state in these analysis was not taken into account as discussed in Section 6.2.1 as the effect was expected to be minimal. The peak strain location around the lower inboard corner of FFVH#13 has shifted outboard from the

test data to the FE results by approximately 10 degrees as seen in Figure 34 and Figure 37 and the reasons for this are postulated in Section 6.2.3. The correlation of the +7.33g peaks show the FE analyses to be under predicting the absolute peak strain values, however the residual predictions were considered acceptable (see Figure 36 and Figure 39).

6.2.3 Factors Influencing Correlation

From the results presented in Figure 31 to Figure 39 it was apparent that additional external influences are affecting the level and distribution of load passing through the FFVH#13 region. The following sections discuss the effects of load, geometric representation, slippage between Stiffener #3 and the Titanium web and the lower boron doubler.

6.2.3.1 Load Sensitivity

In a plasticity analysis, a very small increase or decrease in local load will lead to a very large change in strain. This is directly related to the slope of the material stress strain curve which changes depending upon whether or not the material is cyclically saturated [4]. In the current plasticity analysis, at +7.33g peak load, a change of 1% load leads to a change of peak strain of approximately 1500 microstrain at the lower inboard corner of the FFVH#13. This indicates that any error in the applied load will result in large increase in strain, particularly when the material is saturated or close to it, ie. When small increases in stress correspond to large increases in strain, but the actual error in stress is small.

6.2.3.2 Geometry Representation

Several differences existed between the substructure FE model and the current wing test geometric configuration. Figure 19 shows the dimensional differences between the FE model and that of the AMRL wing, with the FE model dimensions in brackets. This occurred partly due to the original FE substructure model being established for a previous experimental test on a different wing, but also due to the fact that the original OEM Stub Wing FE model (from which the substructure FE model was derived) also had basic differences relative to the current test wing, such as the Stiffener #3 height.

6.2.3.3 Slippage

The FE model represents the loads being transferred through the Titanium web and into the Stiffener solely via the bolt displacements. In the wing, this transfer also involves the clamp-up friction of the bolted structure. Slippage that may occur in this area would involve a slight redistribution of the loading. This phenomenon is not taken into account in the FE model and may actually be occurring [14].

6.2.3.4 *Lower Boron Doubler*

As previously discussed in Section 2.1.1 the lower boron doubler, which is present in the wing test, is not accounted for in the FE models. It is assumed that the doubler would lower the neutral axis of the WPF section, thereby having an additional unquantified effect on the stresses in the upper plate.

6.2.3.5 *2D Stiffener #3 Representation*

The substructure FE model is a 2D/3D FE model with the Stiffener being represented via semi Loof shell elements. These elements were formulated in plane stress and yet the Stiffener thickness varied from 5.0mm to approximately 10.0mm as it approached the plate. Even though the FE model included a step wise increment in thickness approaching the plate this representation caused the outboard upper corner to exhibit dramatic changes in strain from one thickness layer to the next.

The upper outboard corner results show a distorted hoop strain distribution around the surface of the FFVH#13 in the plastic analyses. This is a direct result of the piece wise stepping representing the thickness change as the Stiffener approaches the upper wing skin. The elastic analysis stress distributions, which are presented in Section 7 for this region, show a much more even transition in stress between layers. When conducting the plastic analysis, the increase in load in one layer results in that layer having a larger plasticity zone than the thicker layer directly above.

6.2.4 Summary

The results presented for the elastic response of the substructure FE models agree very well with the experimental wing test data. In addition, the plastic analyses also agree quite well, except in isolated locations in the upper outboard corner, where discrete FE points have excessive over prediction due to the piece wise thickness representation discussed in Section 6.2.3.5. Overall, the residual strain representation for all reworked geometries show close agreement with the results from the experimental wing test. The correlation discrepancies seen at intermediate points in the CPLT cycle can be accounted for by the variation in the FE models structural representation and the factors explained in Section 6.2.3.

7. DADTA INPUT RESULTS

7.1 INTRODUCTION

From the correlation of the FE analyses previously described, it was established that the generic shape (Baseline) required 2 CPLT cycles in order to correlate with the wing test results. The RAAF are currently at III SIP and this implies that any F-111 wing with the original FFVH#13 geometry would have been through three CPLT cycles. This now requires the Blueprint geometry analysis to be analysed through three CPLT cycles for it to be representative of the current in-service RAAF F-111 aircraft. The Intermediate and Large DADTA analysis geometries were assumed to have had the residual plastic zone removed and therefore only one CPLT cycle analysis was performed. The load levels for each analysis were taken to be those determined by the correlation process (see Section 6.1 and Table 7).

7.2 DADTA INPUT

The elastic and residual stress distribution FE results will be sent to LMTAS for use in the calculation of the inspection interval for DADTA control points 90a (lower inboard corner of FFVH#13) and 90b (upper outboard corner of FFVH#13). The stress tensor and equivalent Von Mises Stress value, for each point in the local FFVH#13 region, were extracted from the PAFEC data base and stored in a separate computer file.

7.3 ELASTIC/RESIDUAL STRESS RESULTS

The Blueprint, Intermediate and Large plasticity analyses were processed in the same manner as the correlation FE analyses, and the elastic and residual stresses were extracted for the FFVH#13 region. The elastic Von-Mises stress distributions at -3.0g and +7.33g corresponding to the Blueprint, Intermediate and Large analyses can be seen as contour plots in Figure 43 to Figure 48 and these have been ranged from zero to a yield stress value of 1410 MPa [4]. The detailed Von-Mises stress distributions at -2.4g, 1st +7.33g, -3.0g and 2nd +7.33g loading points, for the 1st CPLT cycle, for the Blueprint geometry only, can be seen in Figure 49 to Figure 52. The residual Von-Mises stress distribution contour plots for the three geometric configurations can be seen in Figure 53 to Figure 55.

7.4 DISCUSSION

As discussed for the correlation analysis in Section 6.2.3.5, the upper outboard corner of FFVH#13 has discrete peaks in strain due to the two dimensional representation of Stiffener #3. The stress distributions shown in Figure 53 to Figure 55 indicate that the

distribution internal to the Stiffener changes over this varying thickness section. A smoothing algorithm could be applied in this region to reduce the effect of the thickness change. The problem of discrete thickness changes, which is inherent in a 2D FE representation, can only be avoided by performing a three dimensional analysis, which LMTAS is currently doing under a contract as part of a United States Air Force and RAAF co-operative agreement.

The residual stress distribution (see Figure 53) at the lower inboard corner of FFVH#13 shows an interesting internal peak stress region left after CPLT. This region was caused by the non-symmetrical nature of the CPLT loading. After the first +7.33g cycle has completed, the stress field (see Figure 50) produces a defined yielded region. On unloading to -3.0g (see Figure 51) only a limited area of the initially yielded region experiences reverse yielding. This has the effect of blunting the peak strains as seen in the hoop strain plot at this point for the similar Baseline FE analysis (see Figure 32). The Large reworked wing test strain gauge results also demonstrate this effect (see Figure 29 and Figure 30). On reload there are internal regions which have different states of yield and it is interesting to note that the 2nd +7.33g cycle does not totally remove and smooth out the yielding region (see Figure 52).

8. CONCLUSIONS

This report describes in detail the work performed in modelling the F-111 Wing Pivot Fitting in the region of the Fuel Flow Vent Hole Number 13 and in correlating the Finite Element Analyses to the AMRL full-scale wing tests. Many of the influencing factors were considered and investigated. The correlation of the FE analyses to the full-scale wing test was successful and the results for the three geometric configurations are to be used in the determination of inspection intervals for this critical region. The elastic and residual stress fields were calculated so that the Durability And Damage Tolerance Analysis could fully incorporate the effects of the residual plastic zone left after the application of the Cold Proof Load Test.

ACKNOWLEDGMENTS

The authors wish to acknowledge the efforts of many AMRL and RAAF personnel ranging from the collection and processing of the experimental data from the three wing tests and the F-111 aircraft to the development of the analysis technique and computer code used to perform the analyses. All contributions have been gratefully accepted.

REFERENCES

1. 'Analysis of Fuel Flow Hole 13, Wing Pivot Fitting', Report FZS-12-324, General Dynamics, Fort Worth, Texas, USA, March 1971.
2. R. H. Keays, L. Molent, A. D. Graham, 'F-111 Wing Pivot Fitting: Finite Element Analysis of Rework of Fuel Flow Hole #13', ARL-STRUCT-TM-557, Melbourne, Australia, July 1992.
3. 'Improved Electrical Discharge Machining Procedures for Re-work of Fuel Flow Vent Hole No 13 in F-111 Wing Pivot Fitting', Structures Laboratory Report No. 9/96, AMRL File: SE5/52/5/1/04, Melbourne, Australia, September 1996.
4. A. Searl and J. Paul, 'Characterisation of D6AC Steel Using A Unified Constitutive Model', AMRL File: M1/8/982, Melbourne, Australia, (In Press).
5. J. Paul, 'Final Report on the Implementation of a Unified Constitutive Model into the PAFEC Finite Element Package', AMRL File: M1/8/992, (In Press).
6. R. H. Keays, 'F-111 Wing Pivot Fitting: Finite Element Analysis of Overall Effect of Upper Plate Boron/Epoxy Doubler', ARL-STRUC-TM-444, Melbourne, Australia, July 1986.
7. K. Lillingston, 'F-111 Wing Variable Sweep Strain Survey', AMRL Structures Laboratory Report No. 8/95, AMRL File: B2/03/101, Melbourne, Australia, October 1995.
8. G. Swanton, 'F-111 FFVH#13 Intermediate Re-Work Strain Survey', AMRL Structures Laboratory Report No. 6/96, Melbourne, Australia, October 1995.
9. K. Watters, 'F-111 Large Rework Strain Survey', AMRL Structures Laboratory Report No. 7/96, AMRL File: B2/03/101, Melbourne, Australia, October 1995.
10. L. Molent and R. Jones, 'Stress Analysis of a Boron/Epoxy Reinforcement for the F-111C Wing Pivot Fitting', ARL-STRUC-R-426, Melbourne, Australia, May 1987.
11. 'Test loads and general test procedures for F-111 proof testing phase III structural inspection program', Report FZS-12-360A, General Dynamics, Fort Worth, Texas, USA, November, 1985.
12. R. B. Allan, 'Elastic-plastic analysis of a plate of strain hardening material with a central circular hole - Comparison of experiment with finite element analysis containing the unified constitutive material model', AMRL File No M1/9/165, Melbourne, Australia, (In Press).
13. R. B. Allan, 'Elastic-plastic analysis of a plate with a central elongated hole - Comparison of experiment with finite element analysis containing the unified constitutive material model', Melbourne, Australia, (In press).

14. K. Watters, 'Strain Surveys of Fuel Flow Vent Hole Number 13 and Stiffener Runout Number 2 in the F-111 Wing Pivot Fitting for a Range of Rework Shapes', Melbourne, Australia, (In Press).

15. H. Neuber, 'Theory of stress concentration for shear-strained prismatic bodies with arbitrary nonlinear stress-strain law', J. Applied Mechanics 28, 544-551, 1961.

TABLES

Table 1: Finite Element Types and Number used in Original OEM FE Model.

ELEMENT DESCRIPTION	NUMBER
8 noded isoparametric brick element	800
6 noded triangular prism element	60
4 noded facet shell element	1658
3 noded flat facet shell element	529
Tension bar element	223
3 noded isoparametric curvilinear quadrilateral	102
4 noded isoparametric curvilinear quadrilateral	62
Simple beam element	203
Stiffness element	72

Table 2: Structural Information for Combined OEM/AMRL FE Models.

COMBINED OEM/AMRL FE MODELS	NODES	ELEMENTS	DEGREES OF FREEDOMS
BASELINE	12613	5994	51273
INTERMEDIATE	13200	6170	54137
LARGE	12956	6072	51512

Table 3: Structural Information for AMRL Substructure FE Models.

AMRL SUBSTRUCTURE FE MODEL	NODES	ELEMENTS	DEGREES OF FREEDOMS
BASELINE	10169	2877	37727
INTERMEDIATE	9873	2759	36439
LARGE	9629	2661	34267

Table 4: Correlation Strain Gauge Description.

LOCATION	Figure #	Gauge No.	Type	Orientation[5]		Direction
				Combined FE Models (°)	Substructure Models (°)	
Upper Wing Skin						
Outer Surface						
Stiffener 2	14	285	Uniaxial	0	19.8	
	↑	34	Uniaxial	0	19.8	
	|	286	Uniaxial	0	19.8	
	↓	35	Uniaxial	-16.6	3.2	
	14	36/37-1 to 5	Strip	-16.6	3.2	
Stiffener 3	14	287	Uniaxial	-19.8	0	
	↑	38	Uniaxial	-19.8	0	
	|	288	Uniaxial	-19.8	0	
	|	39	Uniaxial	-19.8	0	
	|	289	Uniaxial	-19.8	0	
	|	40	Uniaxial	-19.8	0	
	↓	290	Uniaxial	-19.8	0	
	14	41-1 to 5	Strip	-19.8	0	
Stiffener 4	14	291	Uniaxial	-37.6	-17.8	
	↑	42	Uniaxial	-37.6	-17.8	
	|	292	Uniaxial	-37.6	-17.8	
	↓	43	Uniaxial	-22.5	-2.7	
	14	44/45-1 to 5	Strip	-22.5	-2.7	
Inner Surface						
Stiffener 3	14	71	Uniaxial	-19.8	0	
	14	74	Uniaxial	-19.8	0	
Between Stiffener 2&3	15	91-1	Rosette	-19.8	0	spanwise
	↑	91-2				
	|	91-3				chordwise
	|	96-1	Rosette	-19.8	0	spanwise
	|	96-2				
	|	96-3				chordwise
Between Stiffener 3&4	|	92-1	Rosette	-19.8	0	spanwise
	|	92-2				
	|	92-3				chordwise
	|	97-1	Rosette	-19.8	0	spanwise
	↓	97-2				
	15	97-3				chordwise
Stiffener 3 - Surface						
Average between Forward Side and Aft Side	14	77/81-h	Rosette	-19.8	0	spanwise
	↑	77/81-v				vertical
	|	77/81-d				
	|	78/82-h	Rosette	-19.8	0	spanwise
	|	78/82-v				vertical
	|	78/82-d				
	|	79/83-h	Rosette	-19.8	0	spanwise
	|	79/83-v				vertical
	|	79/83-d				
	|	80/84-h	Rosette	-19.8	0	spanwise
	↓	80/84-v				vertical
	14	80/84-d				

[5] The orientation angle provided in these columns represents the angle of the strain gauge relative to the global axis of the FE model.

Table 4: Correlation Strain Gauge Description. (continued)

LOCATION	Figure #	Gauge No.	Type	Orientation[5]		Direction
				Combined FE Models (°)	Substructure Models (°)	
Stiffener Underside Edge						
Stiffener 2	15	277	Uniaxial	0		
	↑	57	Uniaxial	0		
	|	276	Uniaxial	0		
	↓	58	Uniaxial	-16.6		
	15	59/60-1to 5	Strip	-16.6		
Stiffener 3	14	275	Uniaxial	-19.8	0	
	↑	274	Uniaxial	-19.8	0	
	|	273	Uniaxial	-19.8	0	
	|	272	Uniaxial	-19.8	0	
	|	263	Uniaxial	-19.8	0	
	↓	262	Uniaxial	-19.8	0	
	14	261	Uniaxial	-19.8	0	
Stiffener 4	15	283	Uniaxial	-37.6		
	↑	61	Uniaxial	-37.6		
	|	284	Uniaxial	-37.6		
	↓	62	Uniaxial	-22.5		
	15	63/64-1 to 5	Strip	-22.5		
Web						
Top Edge						
	17	282	Uniaxial	-19.8		
	↑	281	Uniaxial	-19.8		
	|	280	Uniaxial	-19.8		
	|	279	Uniaxial	-19.8		
Far-field						
Fwd Face	|	264-1	Rosette	-19.8		spanwise
	|	264-2				
	|	264-3				vertical
	|	265-1	Rosette	-19.8		spanwise
	|	265-2				
	|	265-3				vertical
	|	266-1	Rosette	-19.8		spanwise
	|	266-2				
	|	266-3				vertical
	|	267-1	Rosette	-19.8		spanwise
	|	267-2				
	|	267-3				vertical
Aft Face	|	25-1	Rosette	-19.8		vertical
	|	25-2				
	|	25-3				spanwise
	|	26-1	Rosette	-19.8		vertical
	|	26-2				
	|	26-3				spanwise
	|	278-1	Rosette	-19.8		vertical
	|	278-2				
	|	278-3				spanwise
	|	27-1	Rosette	-19.8		vertical
	↓	27-2				
	17	27-3				spanwise

Table 4: Correlation Strain Gauge Description. (continued)

LOCATION	Figure #	Gauge No.	Type	Orientation[5]		Direction
				Combined FE Models (°)	Substructure Models (°)	
Lower Wing Skin						
Inner Surface						
Between	16	139-1	Rosette	-19.8		chordwise
Stiffener 2&3	↑	139-2				
	|	139-3				spanwise
	|	144-1	Rosette	-16.6		chordwise
	|	144-2				
	|	144-3				spanwise
Between	|	140-1	Rosette	-19.8		chordwise
Stiffener 3&4	|	140-2				
	|	140-3				spanwise
	|	145-1	Rosette	-19.8		chordwise
	|	145-2				
	↓	145-3				spanwise
	16					
FFVH#13				Description		
BASELINE	14	73	Strip	Outboard Upper Corner		
	14	72	Strip	Inboard Lower Corner		
INTERMEDIATE	18	73	Strip	Outboard Upper Corner		
	↑	260	Strip	Outboard Upper Corner		
	|	258	Strip	Inboard Lower Corner		
	↓	259	Strip	Inboard Lower Corner		
	18	72	Strip	Inboard Lower Corner		
LARGE	19	303	Strip	Outboard Upper Corner		
	↑	73	Strip	Outboard Upper Corner		
	|	260	Strip	Outboard Upper Corner		
	|	302	Strip	Inboard Lower Corner		
	|	301	Strip	Inboard Lower Corner		
	|	300	Strip	Inboard Lower Corner		
	|	258	Strip	Inboard Lower Corner		
	↓	259	Strip	Inboard Lower Corner		
	19	72	Strip	Inboard Lower Corner		

Table 5: Combined OEM/AMRL FE Model -2.4g Results: FE at 100% DLL.

POSITION	Gauge	-2.4g @ 56° Sweep								
		Test Results (microstrain)			FEA Results (microstrain)					
		Test 1	Test 2	Test 3	BASE	% Error	INTE	% Error	LARG	Error
Upper Wing Skin										
Outer Surface										
Stiffener 2	285	N/G	1318	1234	1422	***	1431	8.6%	1439	16.6%
	34	1266	1347	1262	1547	22.2%	1552	15.2%	1552	22.9%
	286	N/G	1272	1193	1594	***	1601	25.9%	1601	34.2%
	35	1504	1590	1500	1724	14.6%	1727	8.6%	1729	15.3%
Stiffener 3	287	N/G	1449	1510	1429	***	1522	5.0%	1690	11.9%
	38	1288	1412	1317	1615	25.4%	1646	16.6%	1639	24.5%
	288	N/G	1562	1440	1675	***	1675	7.2%	1679	16.6%
	39	1440	1536	1467	1741	20.9%	1809	17.8%	1839	25.3%
	289	N/G	1788	1683	2006	***	2000	11.9%	1999	18.7%
	40	1516	1622	1514	1730	14.1%	1731	6.7%	1728	14.2%
	290	N/G	1565	1432	1502	***	1552	-0.8%	1505	5.1%
Stiffener 4	291	N/G	1132	1067	1322	***	1328	17.3%	1335	25.2%
	42	1315	1403	1314	1517	15.4%	1524	8.6%	1526	16.2%
	292	N/G	1451	1359	1579	***	1589	9.5%	1591	17.1%
	43	1671	1767	1670	1759	5.3%	1761	-0.3%	1763	5.6%
Inner Surface										
Stiffener 3	71	1475	1409	1308	1696	15.0%	1697	20.4%	1798	37.5%
	74	1904	1974	1846	1738	-8.7%	1745	-11.6%	1739	-5.8%
Between	91-1	1145	1189	1124	1443	26.0%	1449	21.9%	1459	29.8%
Stiffener 2&3	91-2	482	487	441	N/R	***	N/R	***	N/R	***
	91-3	-395	-419	-396	-423	7.1%	-422	0.7%	-423	6.7%
	96-1	1464	1538	1453	1750	19.5%	1741	13.2%	1742	19.9%
	96-2	260	269	257	N/R	***	N/R	***	N/R	***
	96-3	B/G	-566	-537	-568	***	-554	-2.1%	-556	3.5%
Between	92-1	1244	1303	1160	1454	16.9%	1465	12.4%	1481	27.6%
Stiffener 3&4	92-2	296	346	347	N/R	***	N/R	***	N/R	***
	92-3	-442	-469	-446	-519	17.4%	-530	13.0%	-535	20.1%
	97-1	1466	1536	1457	1635	11.5%	1632	6.3%	1633	12.1%
	97-2	351	348	335	N/R	***	N/R	***	N/R	***
	97-3	-427	-467	-435	-566	32.6%	-571	22.3%	-572	31.4%
Stiffener 3 - Surface										
Average	77/81-h	911	1029	936	1437	57.7%	1528	48.6%	N/R	***
between	77/81-v	-249	-330	-349	-443	78.3%	-501	51.8%	N/R	***
Fwd Side	77/81-d	1103	1317	1438	N/R	***	N/R	***	N/R	***
and	78/82-h	1089	1453	N/G	1538	41.3%	N/R	***	N/R	***
Aft Side	78/82-v	-287	-358	N/G	-496	72.8%	N/R	***	N/R	***
	78/82-d	956	851	N/G	N/R	***	N/R	***	N/R	***
	79/83-h	915	787	556	1416	54.8%	1313	66.9%	N/R	***
	79/83-v	-357	-384	-336	-537	50.4%	-601	56.7%	N/R	***
	79/83-d	584	407	254	N/R	***	N/R	***	N/R	***
	80/84-h	964	911	802	1437	49.1%	1448	58.9%	1342	67.4%
	80/84-v	-133	-126	-95	-506	282%	-463	269%	-424	347%
	80/84-d	953	924	878	N/R	***	N/R	***	N/R	***

Table 5: Combined OEM/AMRL FE Model -2.4g Results: FE at 100% DLL. (continued)

POSITION	Gauge	-2.4g @ 56° Sweep								
		Test Results (microstrain)			FEA Results (microstrain)					
		Test 1	Test 2	Test 3	BASE	% Error	INTE	% Error	LARG	% Error
Stiffener Underside Edge										
Stiffener 2	277	N/G	57	59	496	***	481	744%	472	697%
	57	1297	1347	1300	992	-23.5%	992	-26.4%	1001	-23.0%
	276	N/G	1168	1129	1065	***	1076	-7.9%	1087	-3.7%
	58	644	668	638	715	11.0%	700	4.8%	704	10.4%
Stiffener 3	275	N/G	350	291	840	***	800	129%	771	165%
	274	N/G	328	515	1027	***	1037	216%	1134	120%
	273	N/G	912	1027	1130	***	1199	31.5%	1265	23.2%
	272	N/G	764	730	1223	***	1187	55.4%	1139	56.0%
	263	N/G	640	735	683	***	680	6.3%	667	-9.2%
	262	N/G	603	551	301	***	297	-50.7%	289	-47.5%
	261	N/G	706	536	615	***	610	-13.6%	606	13.0%
Stiffener 4	283	N/G	764	717	1052	***	1055	38.1%	1050	46.5%
	61	645	628	638	695	7.8%	692	10.2%	701	9.8%
	284	N/G	-218	-160	456	***	455	-309%	462	-389%
	62	-108	-176	-128	22	-120%	14	-108%	31	-124%
Web										
Top Edge										
	282	N/G	1105	1168	1276	***	1348	22.0%	1462	25.2%
	281	N/G	1190	905	1400	***	1426	19.8%	1466	62.0%
	280	N/G	B/G	990	1410	***	1376	***	1342	35.6%
	279	N/G	888	764	1396	***	1351	52.1%	1305	70.9%
Far-field										
Fwd Face	264-1	N/G	162	230	460	***	444	174%	438	90.5%
	264-2	N/G	1833	1801	N/R	***	N/R	***	N/R	***
	264-3	N/G	62	84	0	***	3	-95.2%	6	-92.9%
	265-1	N/G	-252	-288	-231	***	-224	-11.1%	-227	-21.3%
	265-2	N/G	1306	1228	N/R	***	N/R	***	N/R	***
	265-3	N/G	-260	-252	4	***	-2	-99.2%	0	-100%
	266-1	N/G	-385	-389	-797	***	-797	107%	-799	105%
	266-2	N/G	1531	1446	N/R	***	N/R	***	N/R	***
	266-3	N/G	7	14	341	***	334	4671%	331	2334%
	267-1	N/G	-283	-278	-744	***	-737	160%	728	-362%
	267-2	N/G	1152	1091	N/R	***	N/R	***	N/R	***
	267-3	N/G	-56	-59	117	***	108	-293%	93	-257%
Aft Face	25-1	-318	-330	-314	N/R	***	N/R	***	N/R	***
	25-2	1722	1787	1702	N/R	***	N/R	***	N/R	***
	25-3	161	126	148	460	186%	444	252%	438	196%
	26-1	99	102	106	4	-96.0%	-2	-102%	0	-100%
	26-2	1545	1613	1516	N/R	***	N/R	***	N/R	***
	26-3	139	178	135	-231	-266%	-224	-226%	-227	-268%
	278-1	N/G	114	133	341	***	334	193%	331	148%
	278-2	N/G	1497	1409	N/R	***	N/R	***	N/R	***
	278-3	N/G	-712	-702	-797	***	-797	11.9%	-799	13.9%
	27-1	-133	-153	-150	117	-188%	108	-171%	93	-162%
	27-2	1364	1393	1310	N/R	***	N/R	***	N/R	***
	27-3	-569	-589	-566	-744	30.8%	-737	25.1%	728	-229%

N/G = No Gauge B/G = Bad Gauge *** = Result Could Not Be Calculated N/R = No Result

Table 6: Combined OEM/AMRL FE Model +7.33g Results: FE at 100% DLL.

POSITION	Gauge	+7.33g @ 56° Sweep								
		Test Results (microstrain)			FEA Results (microstrain)					
		Test 1	Test 2	Test 3	BASE	% Error	INTE	% Error	LARG	% Error
Upper Wing Skin										
Outer Surface										
Stiffener 2	285	N/G	-6784	-6551	-5043	***	-5062	-25.4%	-5083	-22.4%
	34	-4272	-4508	-4265	-4166	-2.5%	-4173	-7.4%	-4176	-2.1%
	286	N/G	-3737	-3551	-4078	***	-4087	9.4%	-4089	15.1%
	35	-4281	-4520	-4298	-4256	-0.6%	-4263	-5.7%	-4266	-0.7%
Stiffener 3	287	N/G	-6021	-6415	-4418	***	-4647	-22.8%	-5091	-20.6%
	38	-4802	-5322	-5046	-4557	-5.1%	-4641	-12.8%	-4647	-7.9%
	288	N/G	-4960	-4569	-4392	***	-4384	-11.6%	-4380	-4.1%
	39	-4460	-4754	-4552	-4436	-0.5%	-4585	-3.6%	-4657	2.3%
	289	N/G	-5027	-4800	-4919	***	-4903	-2.5%	-4897	2.0%
	40	-4359	-4633	-4383	-4287	-1.7%	-4286	-7.5%	-4279	-2.4%
	290	N/G	-4269	-4053	-3789	***	-3797	-11.1%	-3791	-6.5%
Stiffener 4	291	N/G	-4902	-4765	-4608	***	-4620	-5.8%	-4639	-2.6%
	42	-3975	-4207	-4005	-3972	-0.1%	-3985	-5.3%	-3990	-0.4%
	292	N/G	-4046	-3862	-4043	***	-4060	0.3%	-4065	5.3%
	43	-4653	-4931	-4691	-4417	-5.1%	-4422	-10.3%	-4426	-5.6%
Inner Surface										
Stiffener 3	71	-5553	-5264	-4966	-4773	-14.0%	-4775	-9.3%	-5030	1.3%
	74	-6253	-6493	-6161	-4493	-28.1%	-4506	-30.6%	-4494	-27.1%
Between	91-1	-4388	-4506	-4236	-4023	-8.3%	-4032	-10.5%	-4053	-4.3%
Stiffener 2&3	91-2	-657	-593	-430	N/R	***	N/R	***	N/R	***
	91-3	2389	2496	2367	2145	-10.2%	2139	-14.3%	2141	-9.6%
	96-1	-4171	-4378	-4164	-4321	3.6%	-4299	-1.8%	-4300	3.3%
	96-2	-417	-433	-410	N/R	***	N/R	***	N/R	***
	96-3	B/G	2081	1985	1464	***	1426	-31.5%	1431	-27.9%
Between	92-1	-4203	-4387	-4239	-4125	-1.9%	-4147	-5.5%	-4184	-1.3%
Stiffener 3&4	92-2	-1672	-1846	-1868	N/R	***	N/R	***	N/R	***
	92-3	2204	2327	2248	2344	6.4%	2370	1.8%	2382	5.9%
	97-1	-4060	-4264	-4061	-4082	0.5%	-4074	-4.5%	-4076	0.4%
	97-2	-892	-874	-816	N/R	***	N/R	***	N/R	***
	97-3	1625	1738	1659	1499	-7.8%	1511	-13.1%	1511	-8.9%
Stiffener 3 - Surface										
Average	77/81-h	-3627	-3899	-3145	-4029	11.1%	-4243	8.8%	N/R	***
between	77/81-v	25	57	-185	936	3720%	1070	1794%	N/R	***
Fwd Side	77/81-d	-5025	-6007	-6322	N/R	***	N/R	***	N/R	***
and	78/82-h	-4106	-5060	N/G	-4169	1.5%	N/R	***	N/R	***
Aft Side	78/82-v	1037	1338	N/G	1247	20.3%	N/R	***	N/R	***
	78/82-d	-3532	-2919	N/G	N/R	***	N/R	***	N/R	***
	79/83-h	-3073	-2611	-1645	-3655	19.0%	-3370	29.1%	N/R	***
	79/83-v	878	920	615	1288	46.8%	1422	54.6%	N/R	***
	79/83-d	-2104	-1460	-948	N/R	***	N/R	***	N/R	***
	80/84-h	-3253	-3130	-2692	-4005	23.1%	-3691	17.9%	-3413	26.8%
	80/84-v	411	354	252	1210	195%	1099	211%	993	295%
	80/84-d	-2714	-2700	-2491	N/R	***	N/R	***	N/R	***

Table 6: Combined OEM/AMRL FE Model +7.33g Results: FE at 100% DLL. (continued)

POSITION	Gauge	+7.33g @ 56° Sweep								
		Test Results (microstrain)			FEA Results (microstrain)					
		Test 1	Test 2	Test 3	BASE	% Error	INTE	% Error	LARG	% Error
Stiffener Underside Edge										
Stiffener 2	277	N/G	2018	1980	-1220	***	-1187	-159%	-1163	-159%
	57	-4161	-4364	-4221	-2723	-34.6%	-2723	-37.6%	-2746	-34.9%
	276	N/G	-4500	-4357	-3065	***	-3082	-31.5%	-3111	-28.6%
	58	-2278	-2366	-2268	-2035	-10.7%	-2001	-15.4%	-2011	-11.3%
Stiffener 3	275	N/G	-409	B/G	-2007	***	-1897	364%	-1790	***
	274	N/G	-2016	-2633	-2802	***	-2848	41.3%	-3150	19.6%
	273	N/G	-3668	-3746	-2950	***	-3118	-15.0%	-3275	-12.6%
	272	N/G	-1665	-1408	-3022	***	-2923	75.6%	-2789	98.1%
	263	N/G	-2682	-2454	-1821	***	-1809	-32.6%	-1774	-27.7%
	262	N/G	-2032	-1892	-1021	***	-1003	-50.6%	-980	-48.2%
	261	N/G	-2030	-1927	-1582	***	-1567	-22.8%	-1558	-19.2%
Stiffener 4	283	N/G	-1781	-1638	-3354	***	-3345	87.8%	-3330	103%
	61	-2301	-2389	-2354	-1943	-15.6%	-1935	-19.0%	-1958	-16.8%
	284	N/G	-78	-131	-1268	***	-1261	1517%	-1282	876%
	62	1133	1273	1177	-90	-108%	-84	-107%	-97	-108%
Web										
Top Edge										
	282	N/G	-3328	-3471	-3339	***	-3521	5.8%	-3828	10.3%
	281	N/G	-2088	-1829	-3480	***	-3538	69.4%	-3627	98.3%
	280	N/G	B/G	-1749	-3477	***	-3383	***	-3286	87.9%
	279	N/G	-2459	-2247	-3447	***	-3328	35.3%	-3207	42.7%
Far-field										
Fwd Face	264-1	N/G	-493	L/D	-1166	***	-1127	129%	-1113	***
	264-2	N/G	-4441	L/D	N/R	***	N/R	***	N/R	***
	264-3	N/G	120	L/D	30	***	28	-76.7%	20	***
	265-1	N/G	664	L/D	612	***	599	-9.8%	608	***
	265-2	N/G	-3284	L/D	N/R	***	N/R	***	N/R	***
	265-3	N/G	602	L/D	2	***	14	-97.7%	8	***
	266-1	N/G	967	L/D	1910	***	1916	98.1%	192	***
	266-2	N/G	-3854	L/D	N/R	***	N/R	***	N/R	***
	266-3	N/G	79	71	-797	***	-781	-1089%	-773	-1196%
	267-1	N/G	1095	1025	1747	***	1734	58.4%	1709	66.7%
	267-2	N/G	-2580	-2438	N/R	***	N/R	***	N/R	***
	267-3	N/G	-685	-604	-490	***	-467	-31.8%	-429	-29.0%
Aft Face	25-1	514	537	L/D	30	-94.2%	28	-94.8%	20	***
	25-2	-4656	-4827	L/D	N/R	***	N/R	***	N/R	***
	25-3	-886	-877	L/D	-1166	31.6%	-1127	28.5%	-1113	***
	26-1	97	81	L/D	2	-97.9%	14	-82.7%	8	***
	26-2	-3753	-3907	L/D	N/R	***	N/R	***	N/R	***
	26-3	-214	-234	L/D	612	-386%	599	-356%	608	***
	278-1	N/G	-898	L/D	-797	***	-781	-13.0%	-773	***
	278-2	N/G	-4211	L/D	N/R	***	N/R	***	N/R	***
	278-3	N/G	1545	L/D	1910	***	1916	24.0%	192	***
	27-1	-717	-719	L/D	-490	-31.7%	-467	-35.0%	-429	***
	27-2	-3879	-3998	L/D	N/R	***	N/R	***	N/R	***
	27-3	1243	1318	L/D	1747	40.5%	1734	31.6%	1709	***

N/G = No Gauge N/G = Bad Gauge *** = Result Could Not Be Calculated N/R = No Result
L/D = Lost Strain Gauge Data

Table 7: Summary of Correlation Results for Combined OEM/AMRL FE Models.

Load Case	Gauge	Test Results (microstrain)			FEA Results (microstrain)					
		Test 1	Test 2	Test 3	BASE	% Error	INTE	% Error	LARG	% Error
1	91-1	1145	1189	1124	1443	26.0%	1449	21.9%	1459	29.8%
(-2.4 g)	96-1	1464	1538	1453	1750	19.5%	1741	13.2%	1742	19.9%
	92-1	1244	1303	1160	1454	16.9%	1465	12.4%	1481	27.6%
	97-1	1466	1536	1457	1635	11.5%	1632	6.3%	1633	12.1%
					average	18.5%		13.4%		22.3%
					calibration factor	0.844		0.882		0.817
2	91-1	-4388	-4506	-4236	-4023	-8.3%	-4032	-10.5%	-4053	-4.3%
(1st +7.33 g)	96-1	-4171	-4378	-4164	-4321	3.6%	-4299	-1.8%	-4300	3.3%
	92-1	-4203	-4387	-4239	-4125	-1.9%	-4147	-5.5%	-4184	-1.3%
	97-1	-4060	-4264	-4061	-4082	0.5%	-4074	-4.5%	-4076	0.4%
					average	-1.5%		-5.6%		-0.5%
					calibration factor	1.015		1.059		1.005
3	91-1	1446	1492	1413	1443	-0.2%	1449	-2.9%	1459	3.3%
(-3.0 g)	96-1	1842	1926	1824	1750	-5.0%	1741	-9.6%	1742	-4.5%
	92-1	1578	1652	1493	1454	-7.9%	1465	-11.3%	1481	-0.8%
	97-1	1830	1914	1813	1635	-10.7%	1632	-14.7%	1633	-9.9%
					average	-5.9%		-9.6%		-3.0%
					calibration factor	1.063		1.107		1.031
4	91-1	-4476	-4592	-4316	-4023	-10.1%	-4032	-12.2%	-4053	-6.1%
(2nd +7.33 g)	96-1	-4209	-4401	-4193	-4321	2.7%	-4299	-2.3%	-4300	2.6%
	92-1	-4248	-4423	-4244	-4125	-2.9%	-4147	-6.2%	-4184	-1.4%
	97-1	-4085	-4273	-4078	-4082	-0.1%	-4074	-4.7%	-4076	0.0%
					average	-2.6%		-6.4%		-1.3%
					calibration factor	1.027		1.068		1.013

Note: The FEA results for the -2.4g and -3.0g load cases and the two 7.33g load cases are identical because -2.4g and +7.33g DLL load cases were used as the basis for correlation. Hence the calibration factors derived are relative to the -2.4g and +7.33g DLL load cases.

Table 8: Substructure FE Model Results: -2.4g Load Case, Correlated Load.

POSITION	Gauge	-2.4g @ 56° Sweep								
		Test Results (microstrain)			Substructure FEA Results (microstrain)					
		Test No.	Test 2	Test 3	BASE	% Error	INTI	% Error	LARG	% Error
Upper Wing Skin										
Outer Surface										
Stiffener 2	285	N/G	1318	1234	1200	***	1262	-4.2%	1175	-4.8%
	34	1266	1347	1262	1302	2.8%	1366	1.4%	1266	0.3%
	286	N/G	1272	1193	1344	***	1409	10.8%	1306	9.5%
	35	1504	1590	1500	1458	-3.1%	1527	-4.0%	1416	-5.6%
Stiffener 3	287	N/G	1449	1510	1160	***	1291	-10.9%	1312	-13.1%
	38	1288	1412	1317	1353	5.0%	1437	1.8%	1332	1.2%
	288	N/G	1562	1440	1465	***	1539	-1.5%	1420	-1.4%
	39	1440	1536	1467	1637	13.7%	1731	12.7%	1621	10.5%
	289	N/G	1788	1683	1643	***	1715	-4.1%	1590	-5.5%
	40	1516	1622	1514	1423	-6.1%	1488	-8.3%	1377	-9.0%
	290	N/G	1565	1432	1225	***	1287	-17.8%	1191	-16.8%
Stiffener 4	291	N/G	1132	1067	1117	***	1172	3.5%	1091	2.3%
	42	1315	1403	1314	1280	-2.7%	1345	-4.1%	1247	-5.1%
	292	N/G	1451	1359	1333	***	1402	-3.4%	1300	-4.3%
	43	1671	1767	1670	1486	-11.1%	1554	-12.1%	1441	-13.7%
Inner Surface										
Stiffener 3	71	1475	1409	1308	1448	-1.8%	1496	6.2%	1458	11.5%
	74	1904	1974	1846	1659	-12.9%	1721	-12.8%	1586	-14.1%
Between	91-1	1145	1189	1124	1219	6.5%	1274	7.1%	1187	5.6%
Stiffener 2&3	91-2	482	487	441	N/R	***	N/R	***	N/R	***
	91-3	-395	-419	-396	-366	-7.3%	-381	-9.1%	-354	-10.7%
	96-1	1464	1538	1453	1435	-2.0%	1499	-2.5%	1390	-4.3%
	96-2	260	269	257	N/R	***	N/R	***	N/R	***
	96-3	B/G	-566	-537	-500	***	-520	-8.1%	-483	-10.1%
Between	92-1	1244	1303	1160	1255	0.9%	1317	1.1%	1233	6.3%
Stiffener 3&4	92-2	296	346	347	N/R	***	N/R	***	N/R	***
	92-3	-442	-469	-446	-440	-0.5%	-465	-0.9%	-434	-2.6%
	97-1	1466	1536	1457	1367	-6.8%	1433	-6.7%	1328	-8.9%
	97-2	351	348	335	N/R	***	N/R	***	N/R	***
	97-3	-427	-467	-435	-463	8.4%	-491	5.1%	-455	4.5%
Stiffener 3 - Surface										
Average	77/81-h	911	1029	936	1186	30.2%	1303	26.7%	N/R	***
between	77/81-v	-249	-330	-349	-363	46.1%	-418	26.7%	N/R	***
Fwd Side	77/81-d	1103	1317	1438	N/R	***	N/R	***	N/R	***
and	78/82-h	1089	1453	N/G	1264	16.1%	N/R	***	N/R	***
Aft Side	78/82-v	-287	-358	N/G	-397	38.3%	N/R	***	N/R	***
	78/82-d	956	851	N/G	N/R	***	N/R	***	N/R	***
	79/83-h	915	787	556	1126	23.1%	1107	40.8%	N/R	***
	79/83-v	-357	-384	-336	-399	11.8%	-479	24.9%	N/R	***
	79/83-d	584	407	254	N/R	***	N/R	***	N/R	***
	80/84-h	964	911	802	1084	12.5%	1057	16.0%	900	12.3%
	80/84-v	-133	-126	-95	-228	72.1%	-220	75.3%	-178	87.6%
	80/84-d	953	924	878	N/R	***	N/R	***	N/R	***
Stiffener Underside Edge										
Stiffener 3	275	N/G	350	291	724	***	722	106%	642	121%
	274	N/G	328	515	969	***	1023	212%	1021	98.4%
	273	N/G	912	1027	923	***	1031	13.0%	1017	-0.9%
	272	N/G	764	730	1005	***	1025	34.2%	912	24.9%
	263	N/G	640	735	586	***	609	-4.8%	554	-24.6%
	262	N/G	603	551	262	***	271	-55.1%	244	-55.7%
	261	N/G	706	536	525	***	545	-22.8%	502	-6.4%

N/G = No Gauge N/G = Bad Gauge *** = Result Could Not Be Calculated N/R = No Result

Table 9: Substructure FE Model Results: +7.33g Load Case, Correlated Load.

POSITION	Gauge	+7.33g @ 56° Sweep								
		Test Results (microstrain)			Substructure FEA Results (microstrain)					
		Test 1	Test 2	Test 3	BASE	% Error	INTE	% Error	LARG	% Error
Upper Wing Skin										
Outer Surface										
Stiffener 2	285	N/G	-6784	-6551	-5134	***	-5377	-20.7%	-5123	-21.8%
	34	-4272	-4508	-4265	-4223	-1.1%	-4415	-2.1%	-4193	-1.7%
	286	N/G	-3737	-3551	-4134	***	-4322	15.7%	-4104	15.6%
	35	-4281	-4520	-4298	-4327	1.1%	-4523	0.1%	-4296	0.0%
Stiffener 3	287	N/G	-6021	-6415	-4237	***	-4645	-22.9%	-4776	-25.5%
	38	-4802	-5322	-5046	-4550	-5.2%	-4813	-9.6%	-4584	-9.2%
	288	N/G	-4960	-4569	-4568	***	-4774	-3.8%	-4508	-1.3%
	39	-4460	-4754	-4552	-4961	11.2%	-5228	10.0%	-5014	10.1%
	289	N/G	-5027	-4800	-4807	***	-5009	-0.4%	-4758	-0.9%
	40	-4359	-4633	-4383	-4239	-2.8%	-4420	-4.6%	-4189	-4.4%
	290	N/G	-4269	-4053	-3719	***	-3893	-8.8%	-3690	-9.0%
Stiffener 4	291	N/G	-4902	-4765	-4694	***	-4910	0.2%	-4678	-1.8%
	42	-3975	-4207	-4005	-4036	1.5%	-4226	0.5%	-4015	0.2%
	292	N/G	-4046	-3862	-4106	***	-4302	6.3%	-4088	5.9%
	43	-4653	-4931	-4691	-4488	-3.5%	-4686	-5.0%	-4451	-5.1%
Inner Surface										
Stiffener 3	71	-5553	-5264	-4966	-4704	-15.3%	-4893	-7.0%	-4855	-2.2%
	74	-6253	-6493	-6161	-5093	-18.6%	-5270	-18.8%	-4976	-19.2%
Between	91-1	-4388	-4506	-4236	-4055	-7.6%	-4223	-6.3%	-4028	-4.9%
Stiffener 2&3	91-2	-657	-593	-430	N/R	***	N/R	***	N/R	***
	91-3	2389	2496	2367	2179	-8.8%	2272	-9.0%	2159	-8.8%
	96-1	-4171	-4378	-4164	-4271	2.4%	-4449	1.6%	-4225	1.5%
	96-2	-417	-433	-410	N/R	***	N/R	***	N/R	***
	96-3	B/G	2081	1985	1540	***	1596	-23.3%	1520	-23.4%
Between	92-1	-4203	-4387	-4239	-4218	0.4%	-4413	0.6%	-4223	-0.4%
Stiffener 3&4	92-2	-1672	-1846	-1868	N/R	***	N/R	***	N/R	***
	92-3	2204	2327	2248	2351	6.7%	2466	6.0%	2349	4.5%
	97-1	-4060	-4264	-4061	-4093	0.8%	-4281	0.4%	-4065	0.1%
	97-2	-892	-874	-816	N/R	***	N/R	***	N/R	***
	97-3	1625	1738	1659	1480	-8.9%	1556	-10.5%	1478	-10.9%
Stiffener 3 - Surface										
Average	77/81-h	-3627	-3899	-3145	-3954	9.0%	-4207	7.9%	N/R	***
between	77/81-v	25	57	-185	898	3565%	977	1629%	N/R	***
Fwd Side	77/81-d	-5025	-6007	-6322	N/R	***	N/R	***	N/R	***
and	78/82-h	-4106	-5060	N/G	-4110	0.1%	N/R	***	N/R	***
Aft Side	78/82-v	1037	1338	N/G	1279	23.3%	N/R	***	N/R	***
	78/82-d	-3532	-2919	N/G	N/R	***	N/R	***	N/R	***
	79/83-h	-3073	-2611	-1645	-3479	13.2%	-3391	29.9%	N/R	***
	79/83-v	878	920	615	1158	32.0%	1365	48.4%	N/R	***
	79/83-d	-2104	-1460	-948	N/R	***	N/R	***	N/R	***
	80/84-h	-3253	-3130	-2692	-3344	2.8%	-3251	3.9%	-2835	5.3%
	80/84-v	411	354	252	651	58.6%	620	75.4%	505	
	80/84-d	-2714	-2700	-2491	N/R	***	N/R	***	N/R	***
Stiffener Underside Edge										
Stiffener 3	275	N/G	-409	B/G	-2077	***	-2051	401%	-1847	***
	274	N/G	-2016	-2633	-3224	***	-3426	69.9%	-3527	33.9%
	273	N/G	-3668	-3746	-2896	***	-3213	-12.4%	-3226	-13.9%
	272	N/G	-1665	-1408	-2964	***	-3005	80.5%	-2726	93.6%
	263	N/G	-2682	-2454	-1875	***	-1940	-27.7%	-1806	-26.4%
	262	N/G	-2032	-1892	-1056	***	-1085	-46.6%	-1007	-46.8%
	261	N/G	-2030	-1927	-1622	***	-1677	-17.4%	-1583	-17.9%

N/G = No Gauge N/G = Bad Gauge *** = Result Could Not Be Calculated N/R = No Result

Table 10: Summary of Correlated Results of AMRL Substructure FE Model.

Load Case	Gauge	Test Results (microstrain)			Substructure FEA Results (microstrain)					
		Test 1	Test 2	Test 3	BASE	%Error	INTE	% Error	LARG	% Error
1 (-2.4 g)	91-1	1145	1189	1124	1219	6.5%	1274	7.1%	1187	5.6%
	96-1	1464	1538	1453	1435	-2.0%	1499	-2.5%	1390	-4.3%
	92-1	1244	1303	1160	1255	0.9%	1317	1.1%	1233	6.3%
	97-1	1466	1536	1457	1367	-6.8%	1433	-6.7%	1328	-8.9%
					average	-0.3%		-0.3%		-0.3%
2 (1st +7.33 g)	91-1	-4388	-4506	-4236	-4055	-7.6%	-4223	-6.3%	-4028	-4.9%
	96-1	-4171	-4378	-4164	-4271	2.4%	-4449	1.6%	-4225	1.5%
	92-1	-4203	-4387	-4239	-4218	0.4%	-4413	0.6%	-4223	-0.4%
	97-1	-4060	-4264	-4061	-4093	0.8%	-4281	0.4%	-4065	0.1%
					average	-1.0%		-0.9%		-0.9%
3 (-3.0 g)	91-1	1446	1492	1413	1537	6.3%	1601	7.3%	1501	6.2%
	96-1	1842	1926	1824	1807	-1.9%	1881	-2.3%	1753	-3.9%
	92-1	1578	1652	1493	1582	0.3%	1656	0.2%	1558	4.4%
	97-1	1830	1914	1813	1722	-5.9%	1798	-6.1%	1676	-7.6%
					average	-0.3%		-0.2%		-0.2%
4 (2nd +7.33 g)	91-1	-4476	-4592	-4316	-4102	-8.4%	-4259	-7.3%	-4060	-5.9%
	96-1	-4209	-4401	-4193	-4322	2.7%	-4487	2.0%	-4259	1.6%
	92-1	-4248	-4423	-4244	-4268	0.5%	-4450	0.6%	-4256	0.3%
	97-1	-4085	-4273	-4078	-4141	1.4%	-4317	1.0%	-4097	0.5%
					average	-1.0%		-0.9%		-0.9%

FIGURES

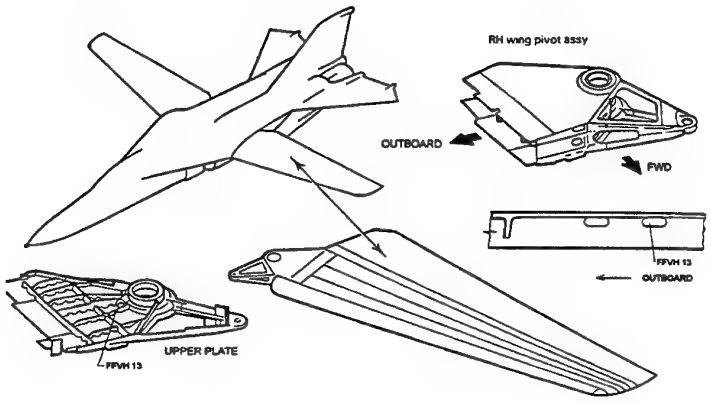

Figure 1: Location of FFVH#13 in the F-111 Aircraft.

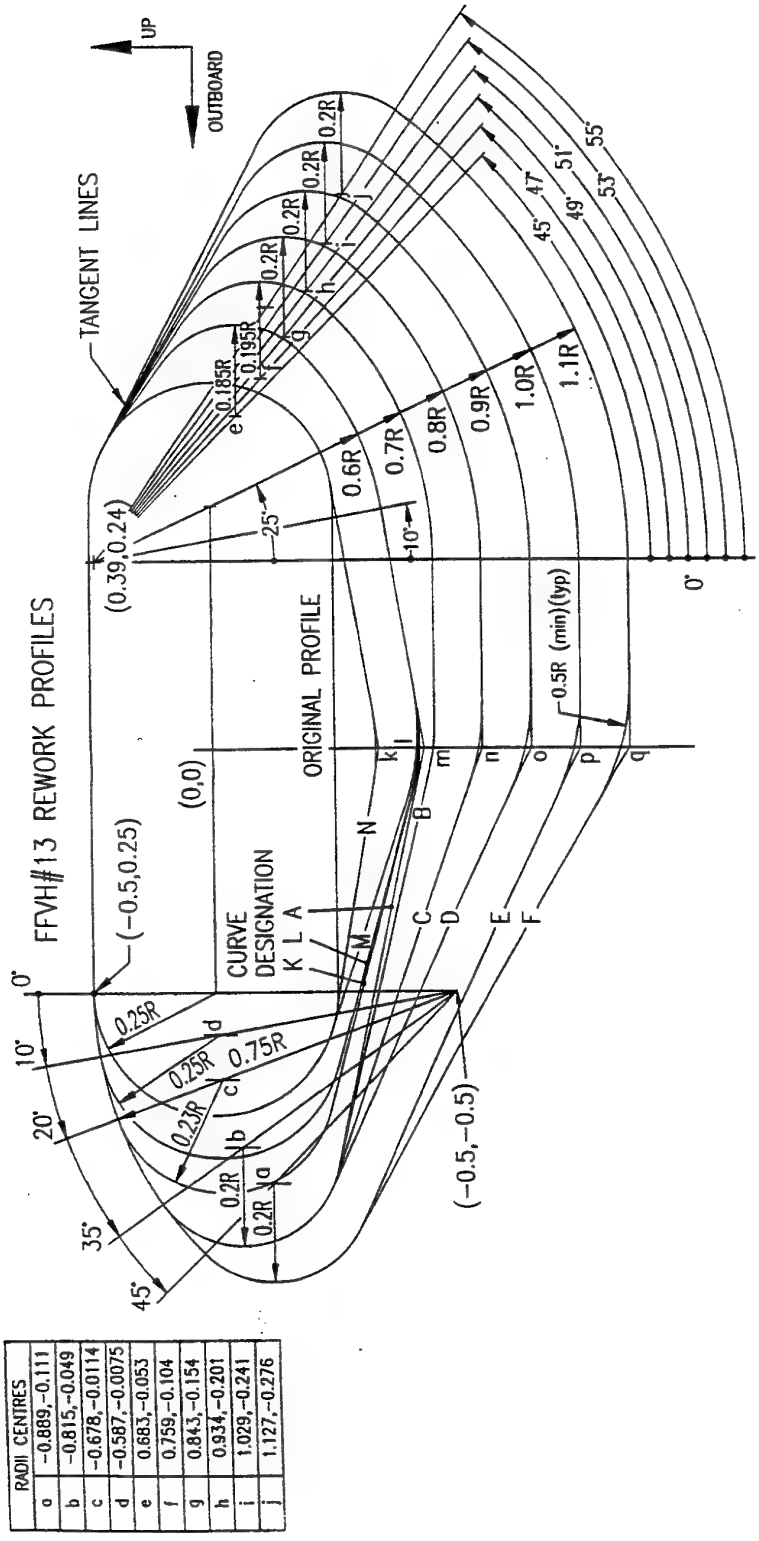

RADII CENTRES	
a	-0.889,-0.111
b	-0.815,-0.049
c	-0.678,-0.0114
d	-0.587,-0.0075
e	0.683,-0.053
f	0.759,-0.104
g	0.843,-0.154
h	0.934,-0.201
i	1.029,-0.241
j	1.127,-0.276

Figure 2: FFVH#13 Re-Work Profile Configurations.

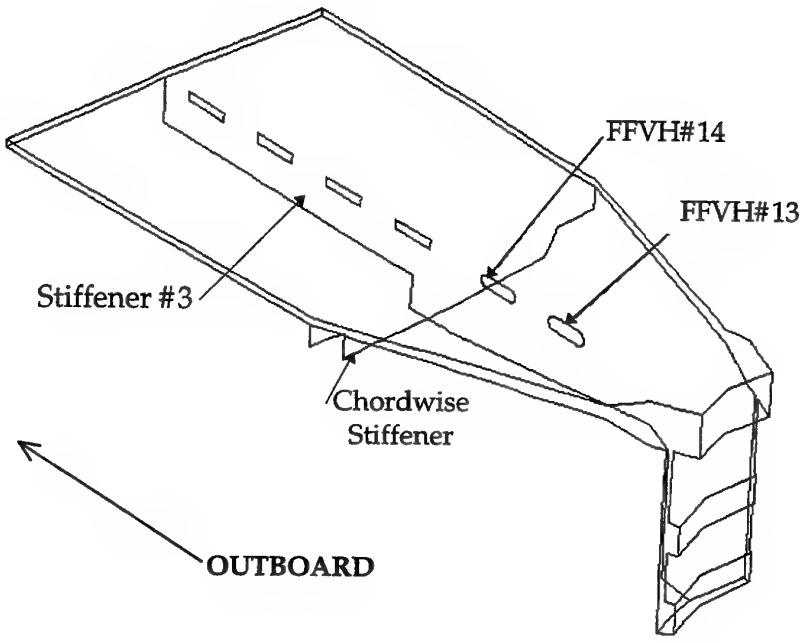

Figure 3: AMRL FE Substructure Region.

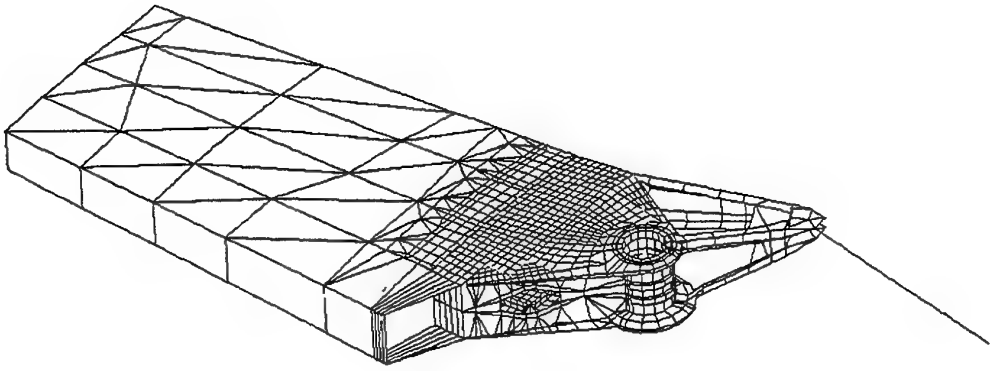

Figure 4: View of OEM Original Wing Stub FE Model.

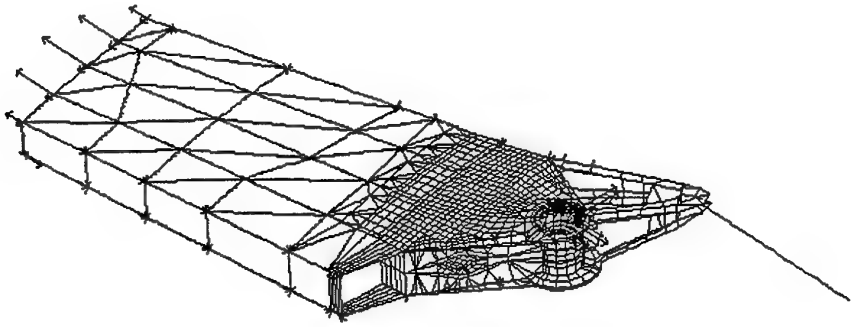

Figure 5: Load Distribution for OEM FE Model: -2.4g Load Case.

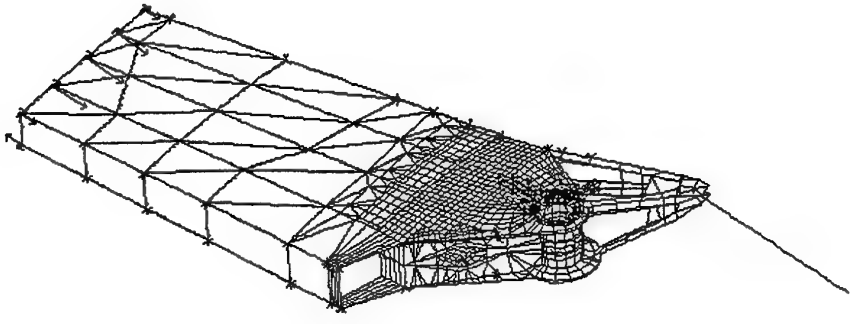

Figure 6: Load Distribution for OEM FE Model: +7.33g Load Case.

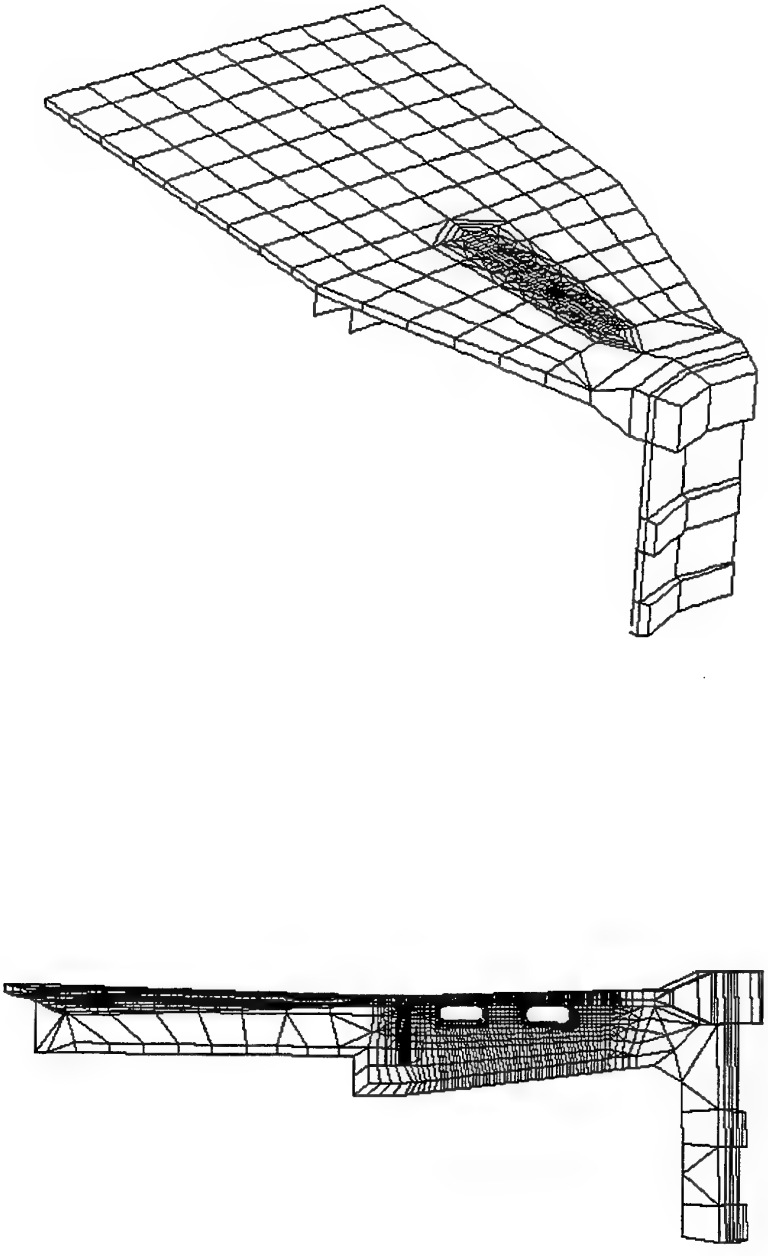

Figure 7: Views of AMRL Substructure FE Model Mesh.

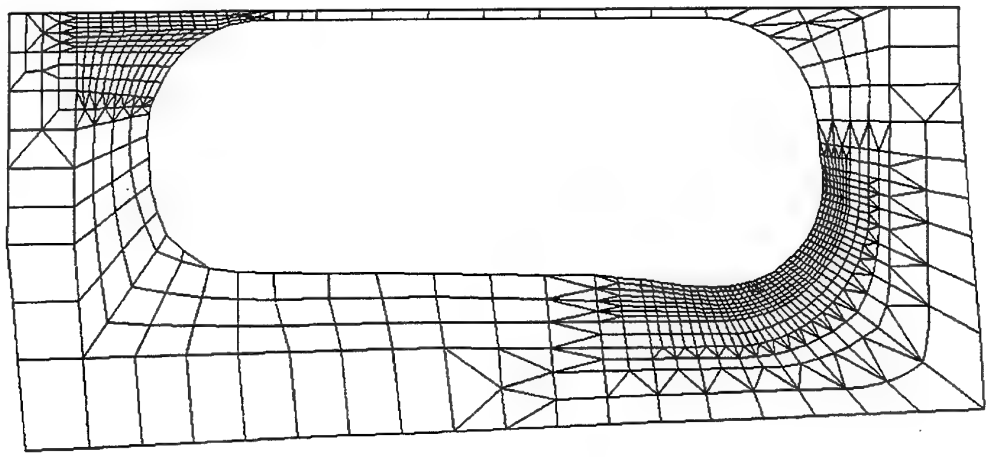

Figure 8: FFVH#13 Baseline FE Model Mesh.

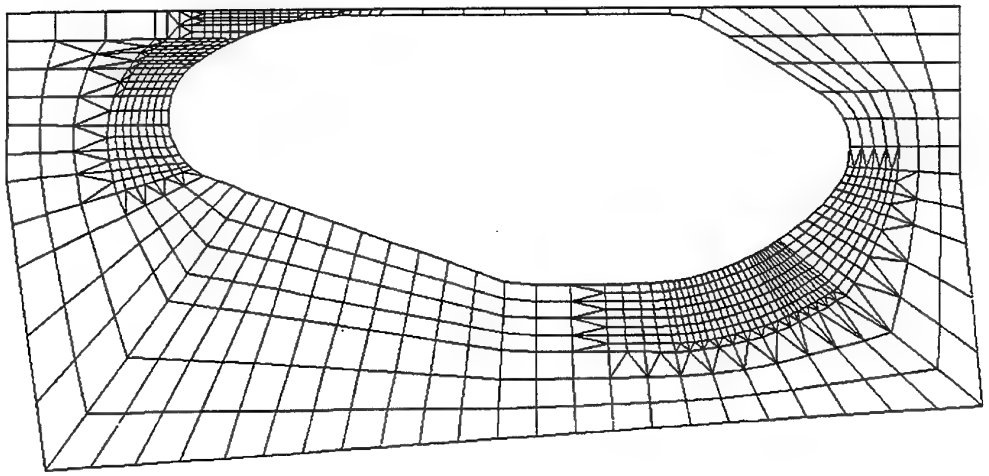

Figure 9: FFVH#13 Intermediate Reworked FE Model Mesh.

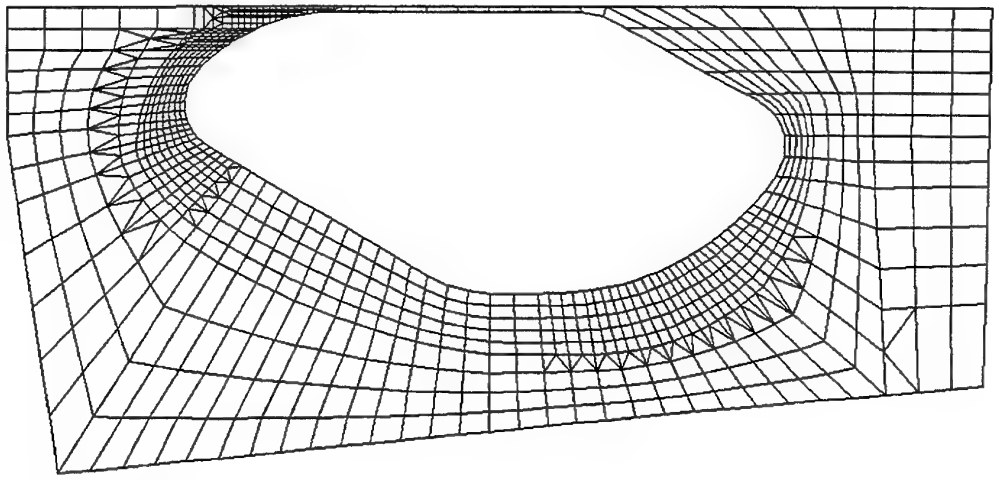

Figure 10: FFVH#13 Large Reworked FE Model Mesh.

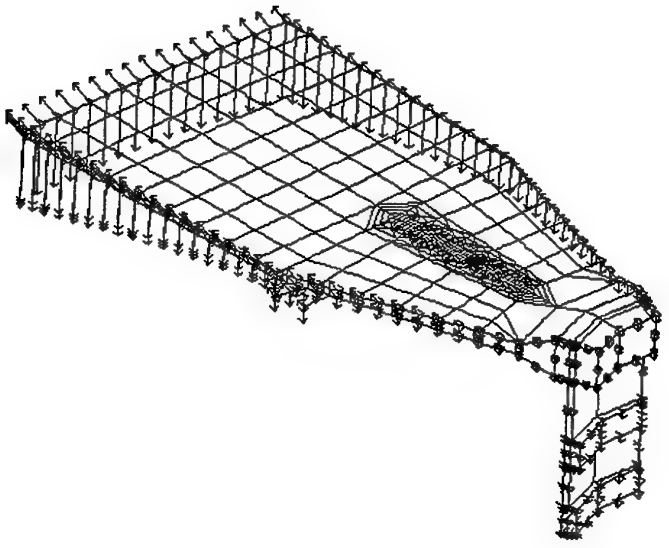

Figure 11: Boundary Loading on Substructure FE Model: -2.4g Load Case.

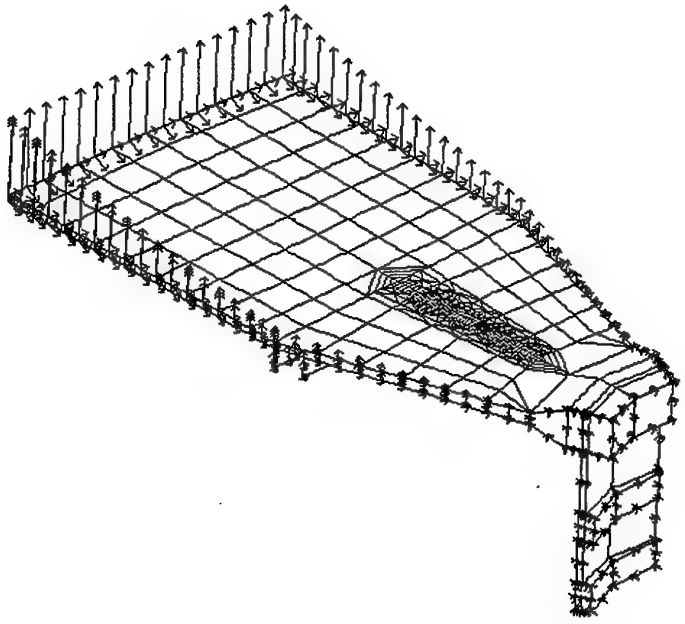

Figure 12: Boundary Loading on Substructure FE Model: +7.33g Load Case.

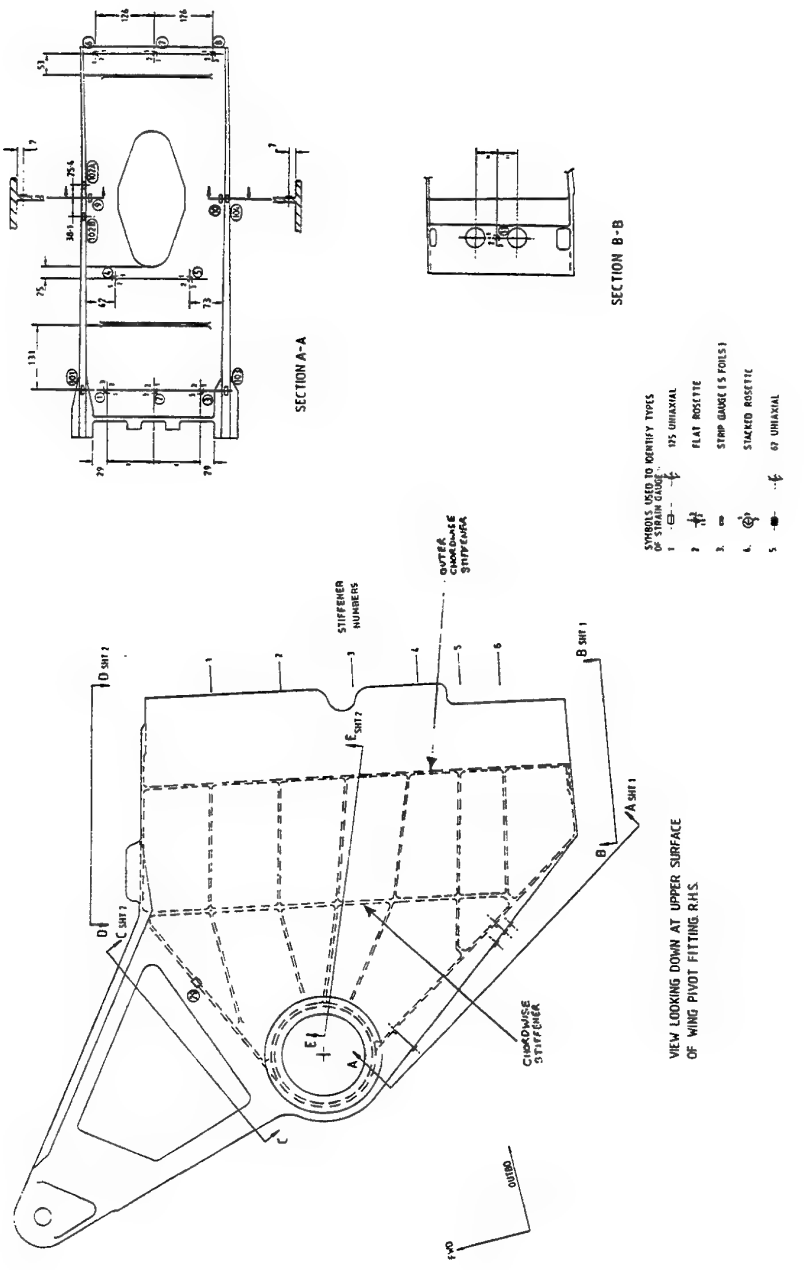

Figure 13: Stiffener Locations.

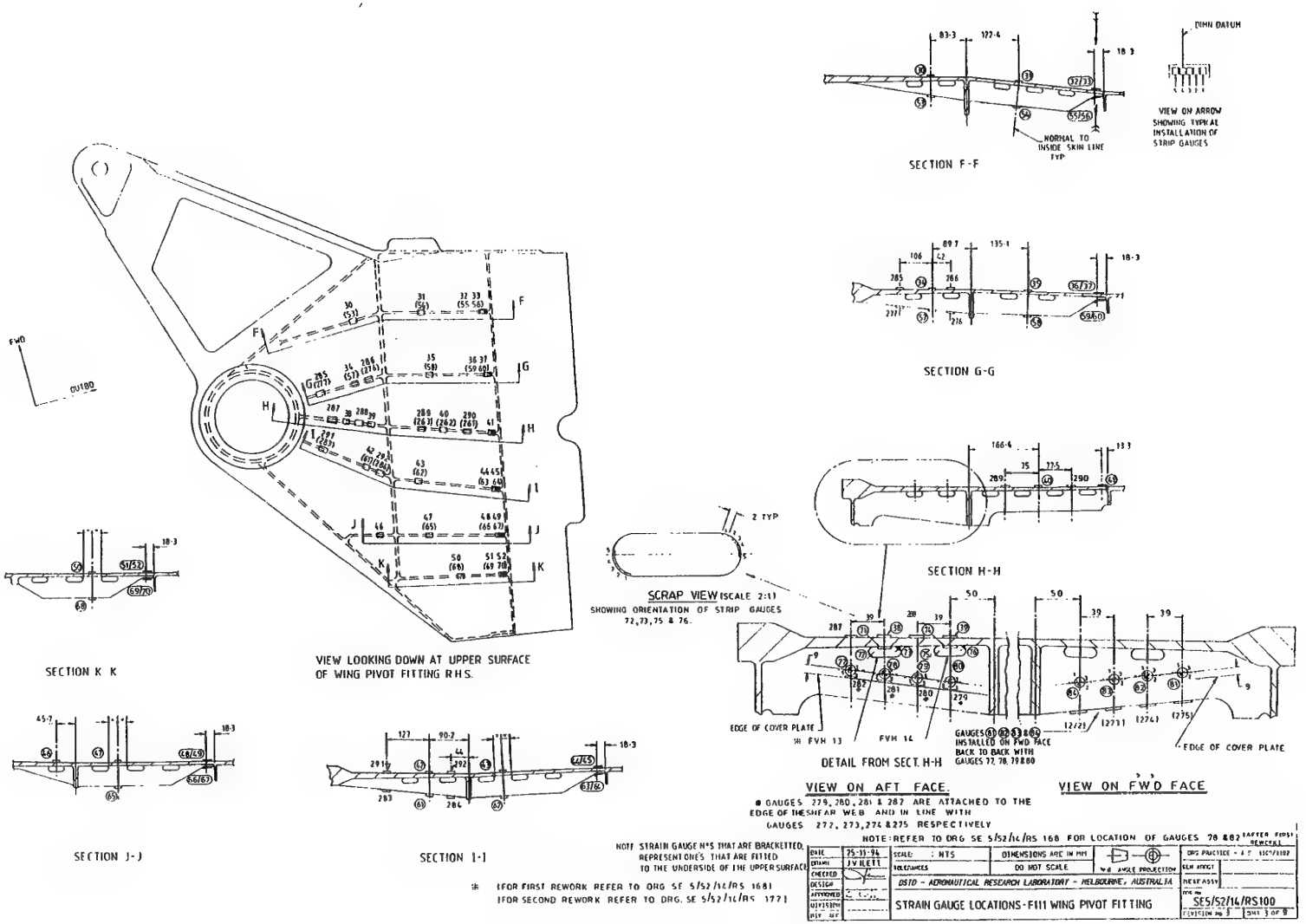

Figure 14: Strain Gauge Locations: Outer Surface Upper Plate.

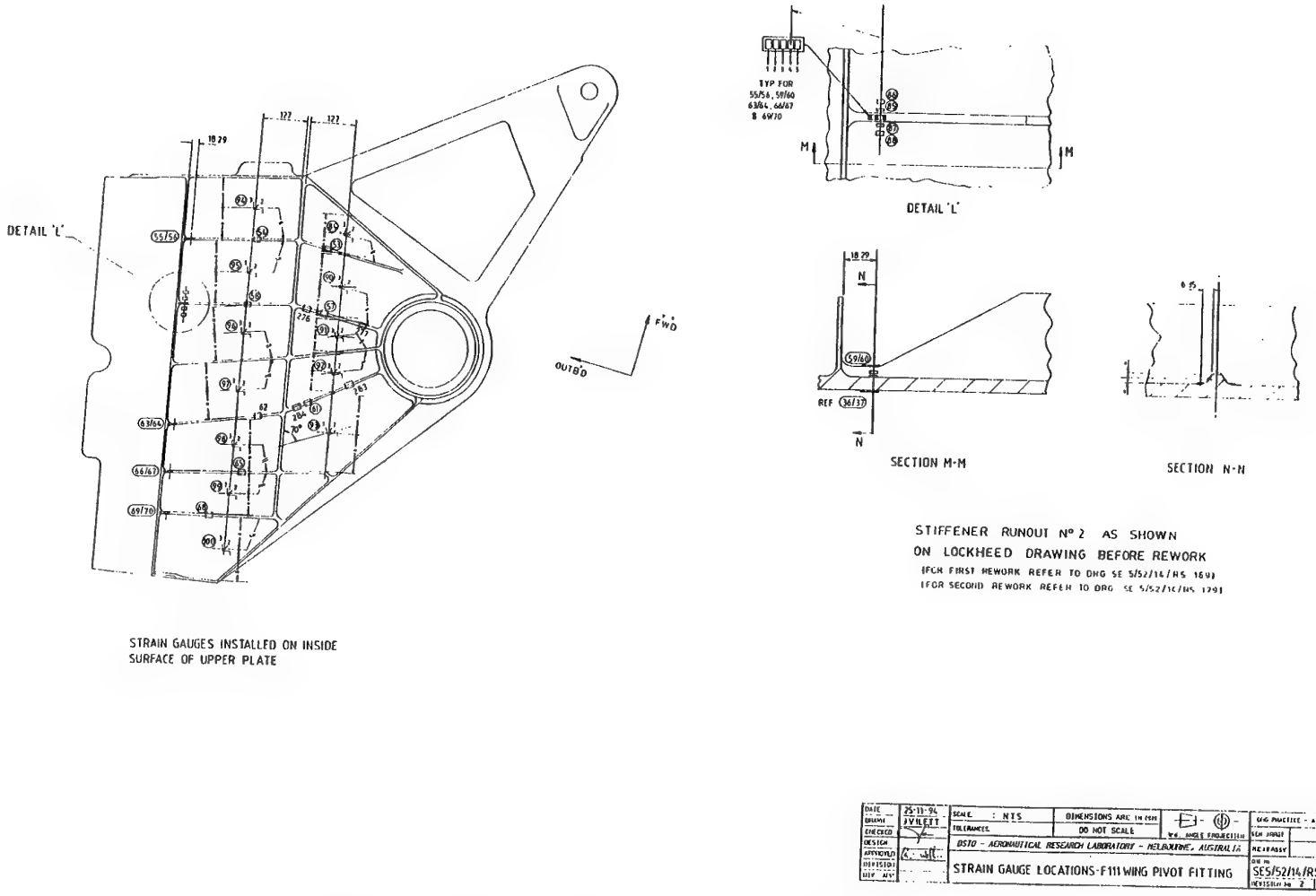

Figure 15: Strain Gauge Locations: Inside Surface Upper Plate.

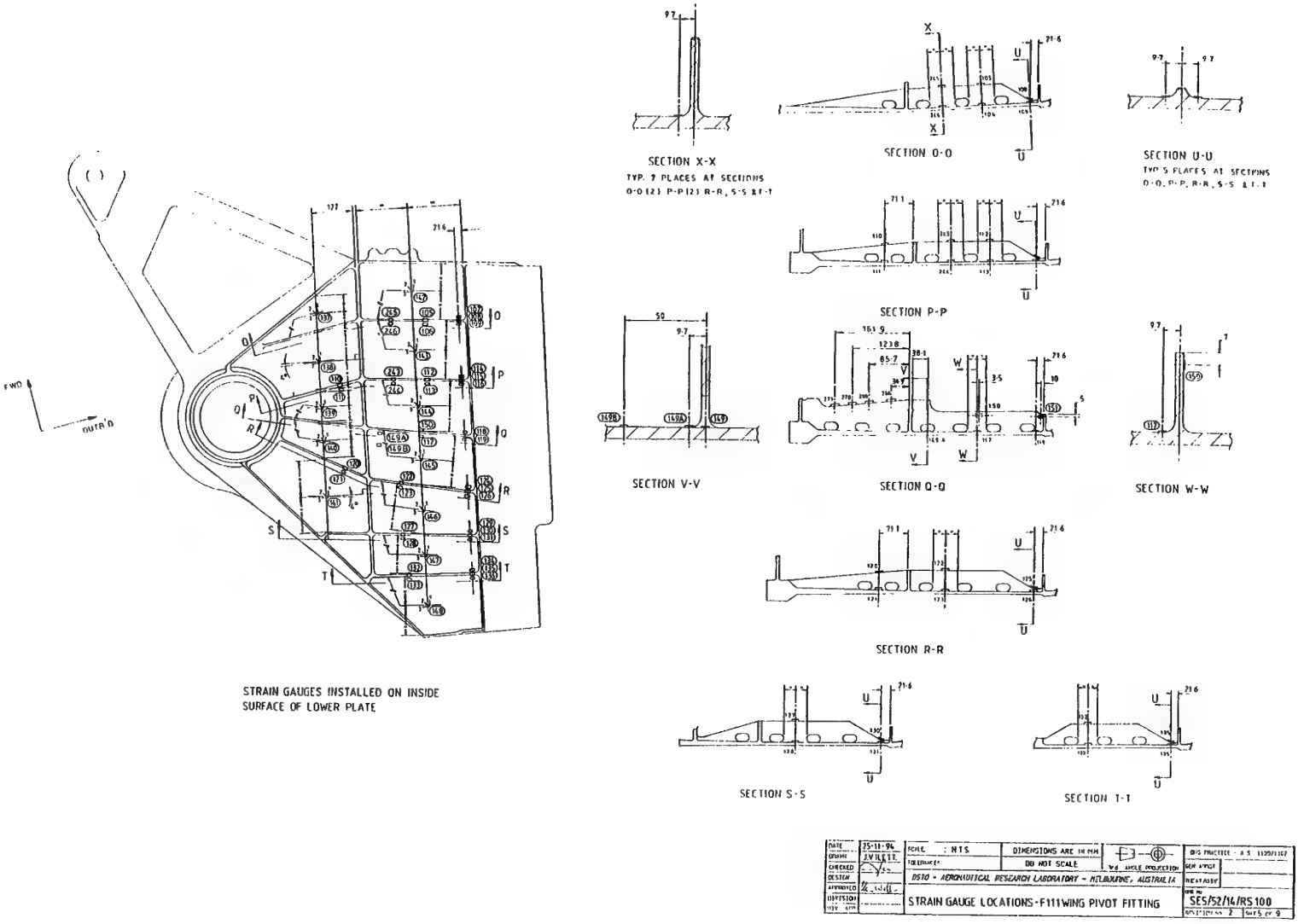

Figure 16: Strain Gauge Locations: Inside Surface Lower Plate.

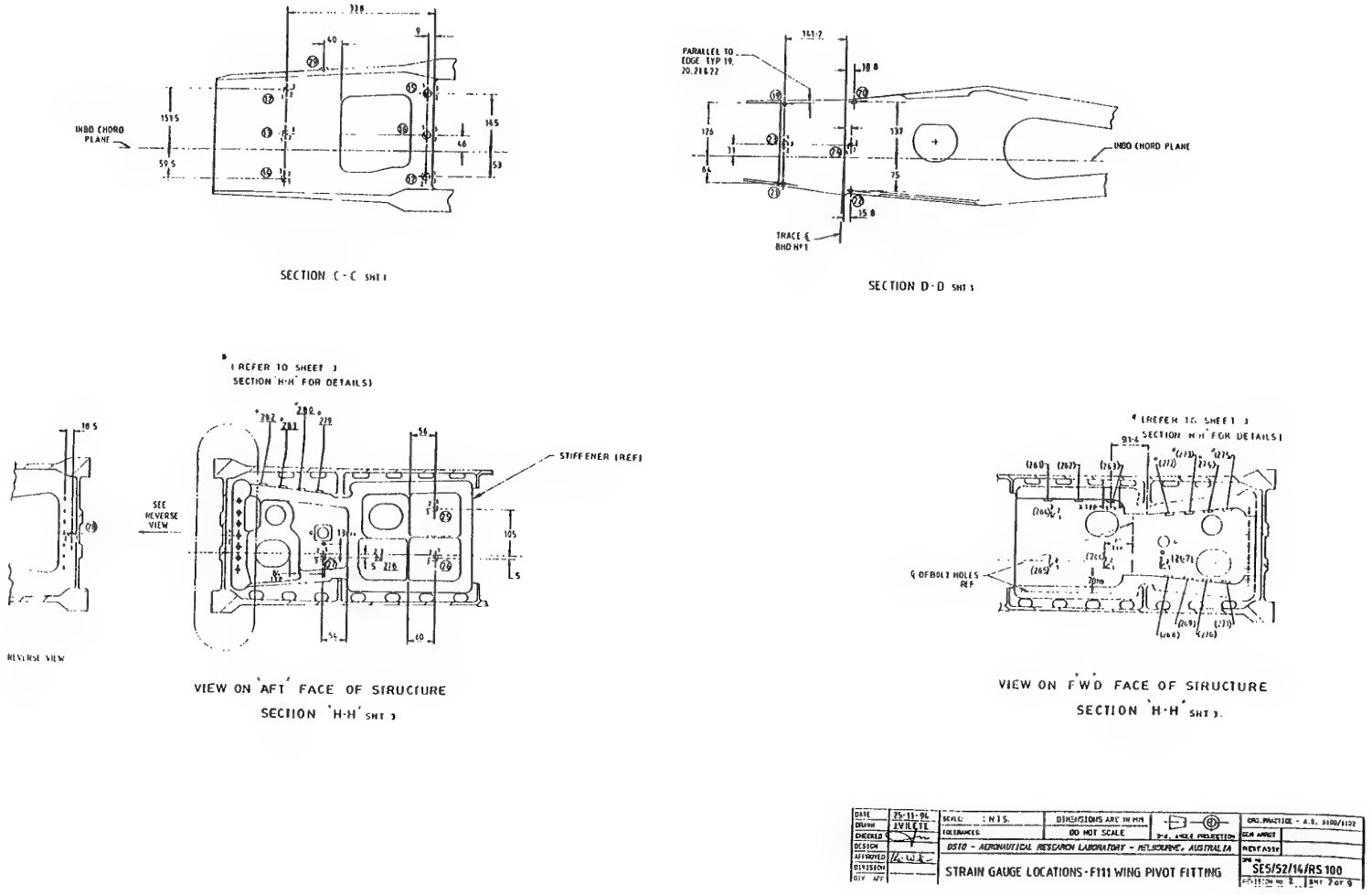

Figure 17: Strain Gauge Locations: Titanium Web.

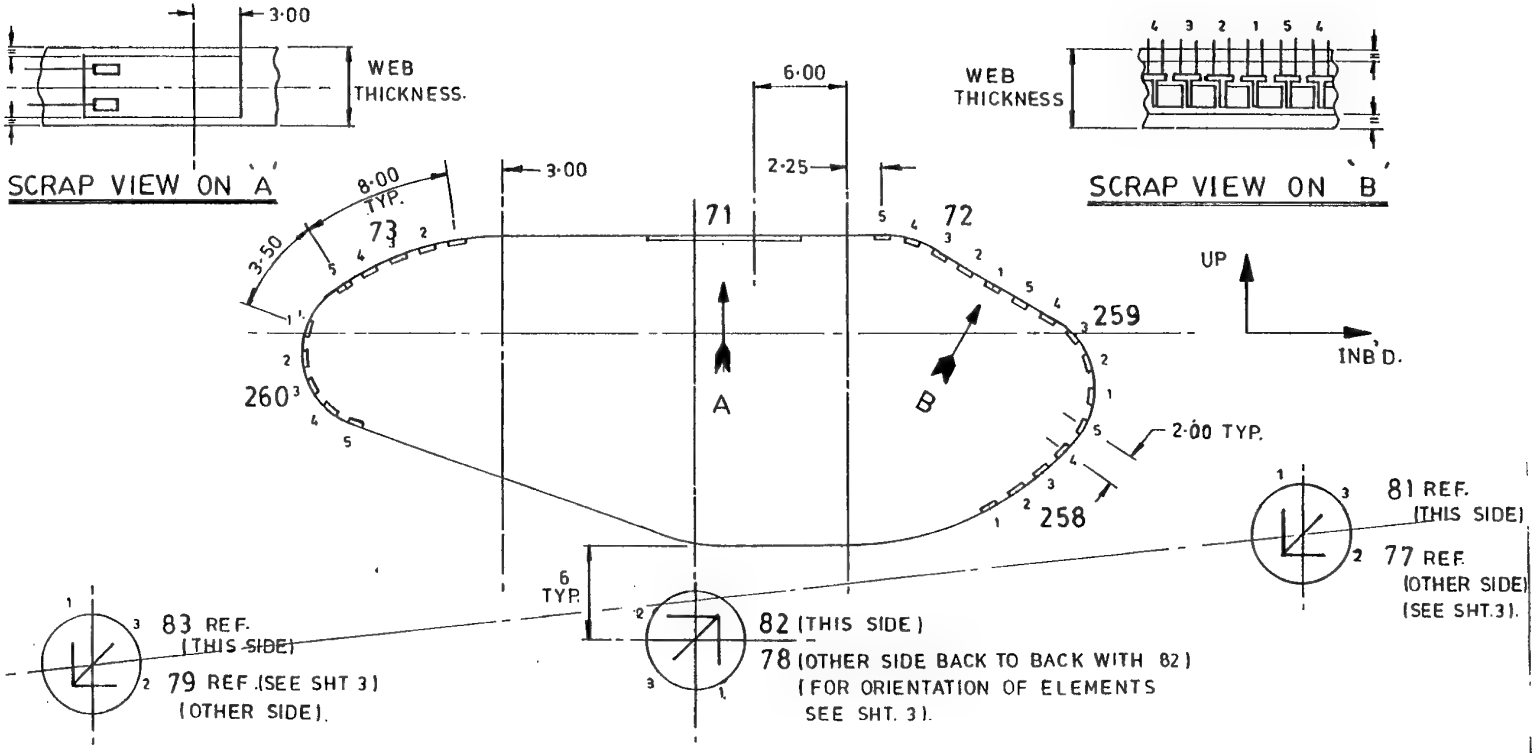

DATE	29-2-96	SCALE: 4:1	DIMENSIONS ARE IN MM	3rd. ANGLE PROJECTION	DRG.PRACTICE - A.S. 1100/1102
DRAWN	P.TIKTIKAKIS	TOLERANCES:	DO NOT SCALE		GEN ARRGT
CHECKED		DSTO - AERONAUTICAL RESEARCH LABORATORY - MELBOURNE, AUSTRALIA			NEXT ASSY
DESIGN		F111-MOUSE HOLE FVH 13-FIRST REWORK.			DRG.No SE 5/52/14/RS 168
APPROVED					REVISION No. 1 SHT OF
DIVISION					
DIV. APP					

Figure 18: Strain Gauge Locations: FFVH#13 Intermediate Rework.

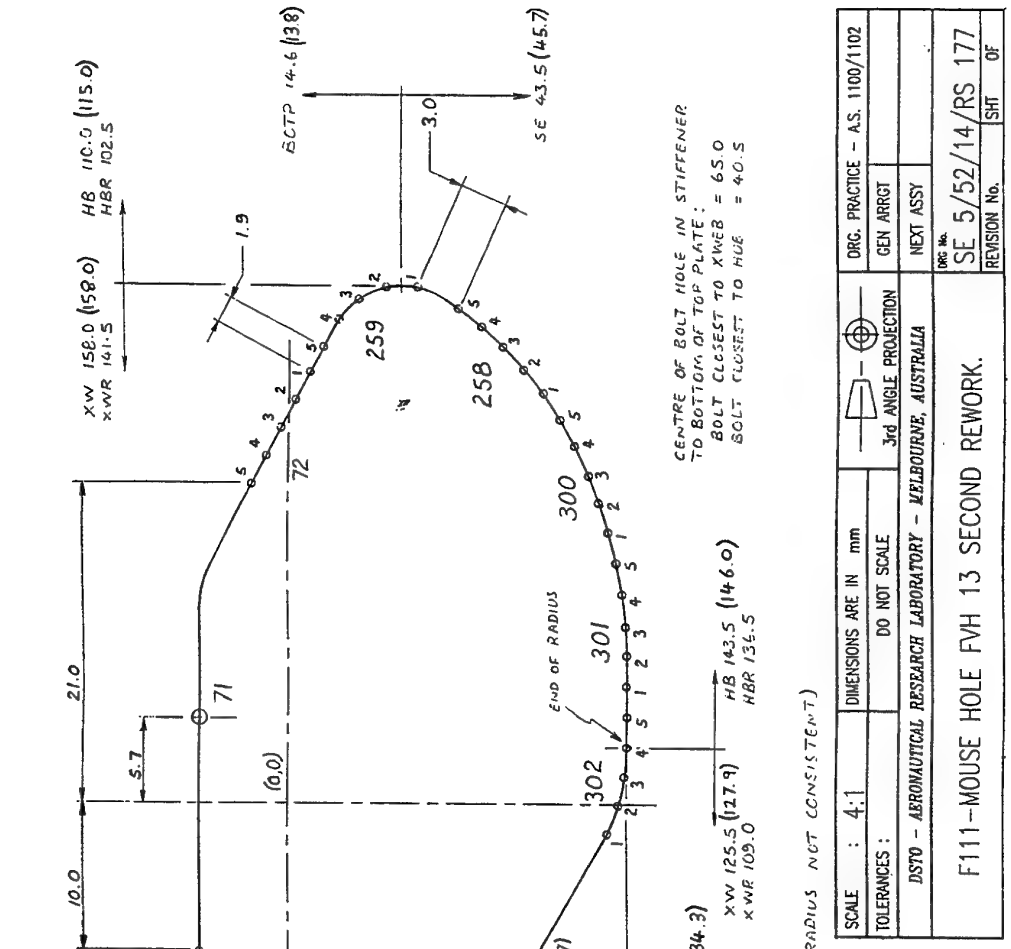

Figure 19: Strain Gauge Locations: FFVH#13 Large Rework.

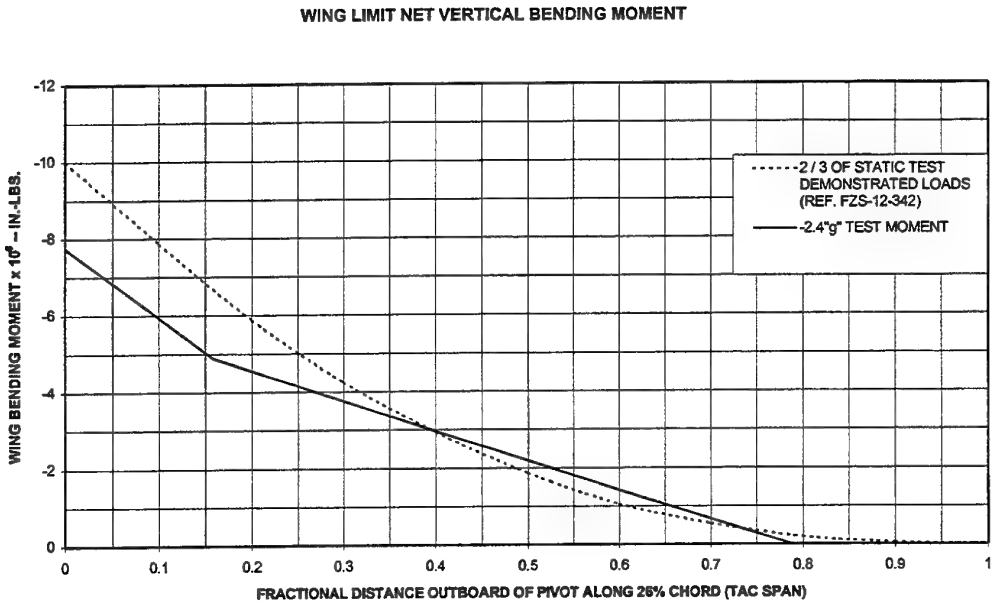

Figure 20: CPLT Wing Root Bending Moment: -2.4g Load Case.

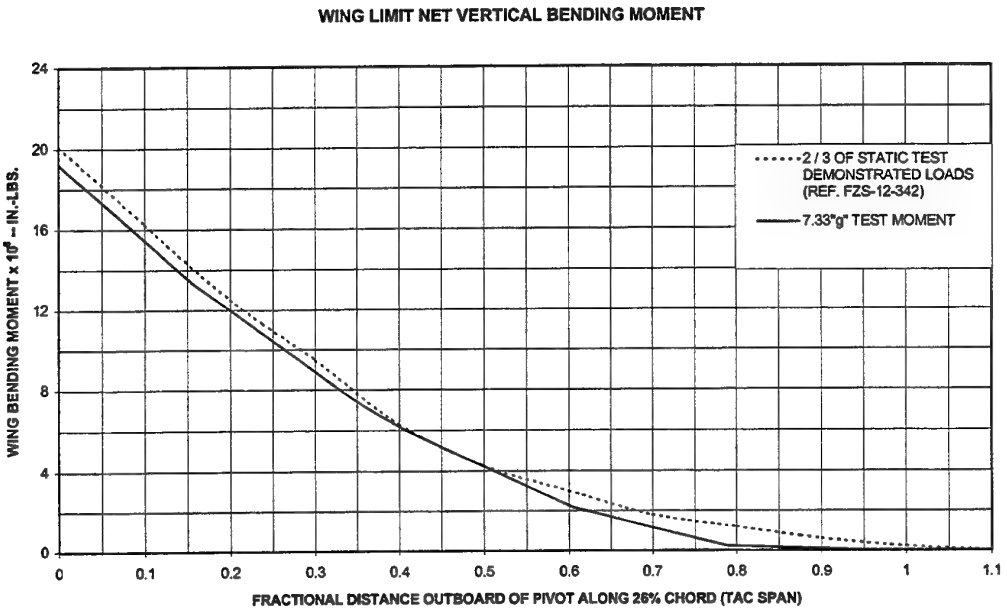

Figure 21: CPLT Wing Root Bending Moment: 1st +7.33g Load Case.

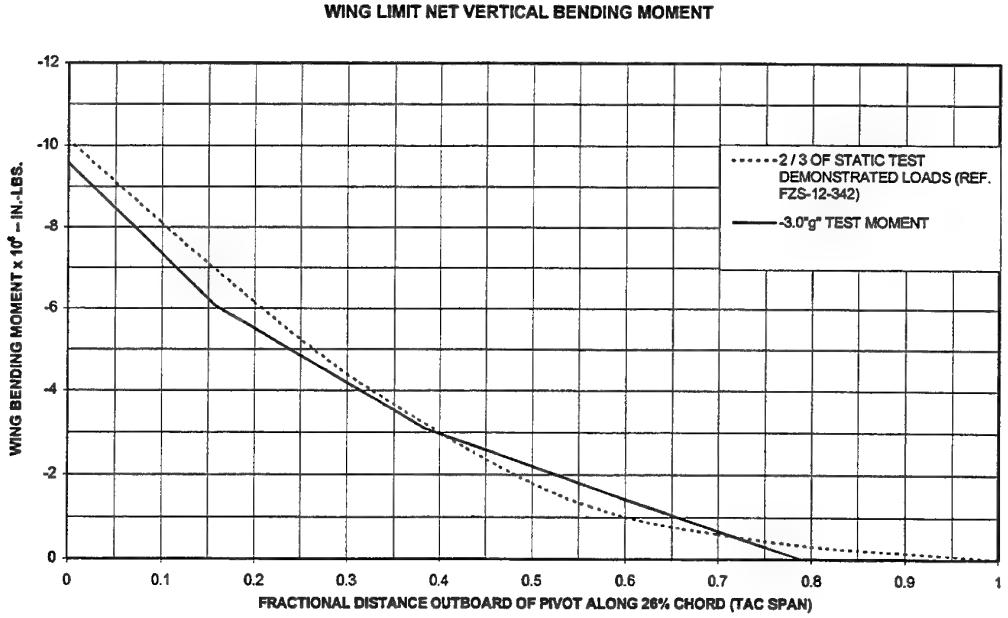

Figure 22: CPLT Wing Root Bending Moment: -3.0g Load Case.

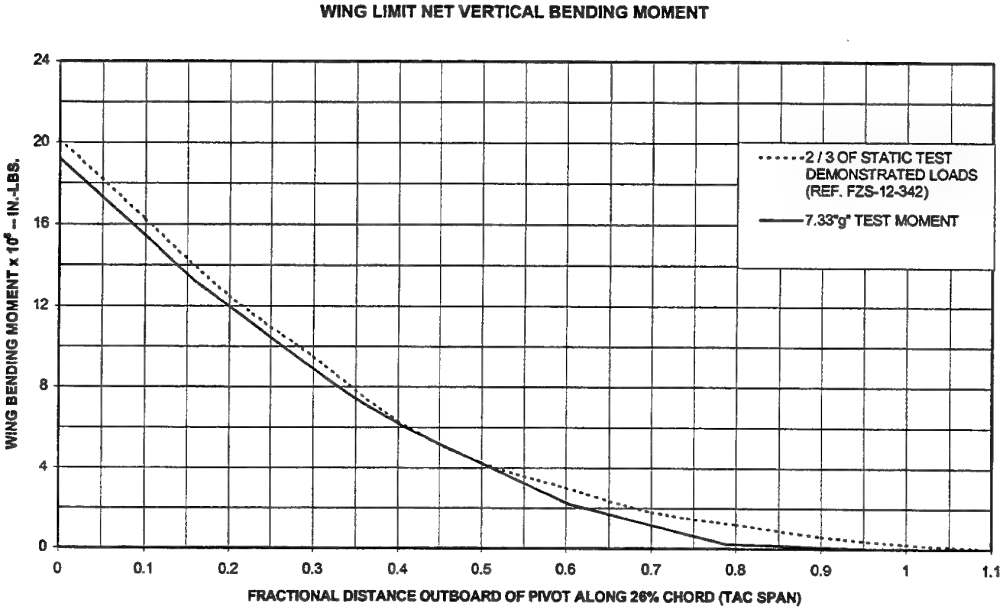

Figure 23: CPLT Wing Root Bending Moment: 2nd +7.33g Load Case.

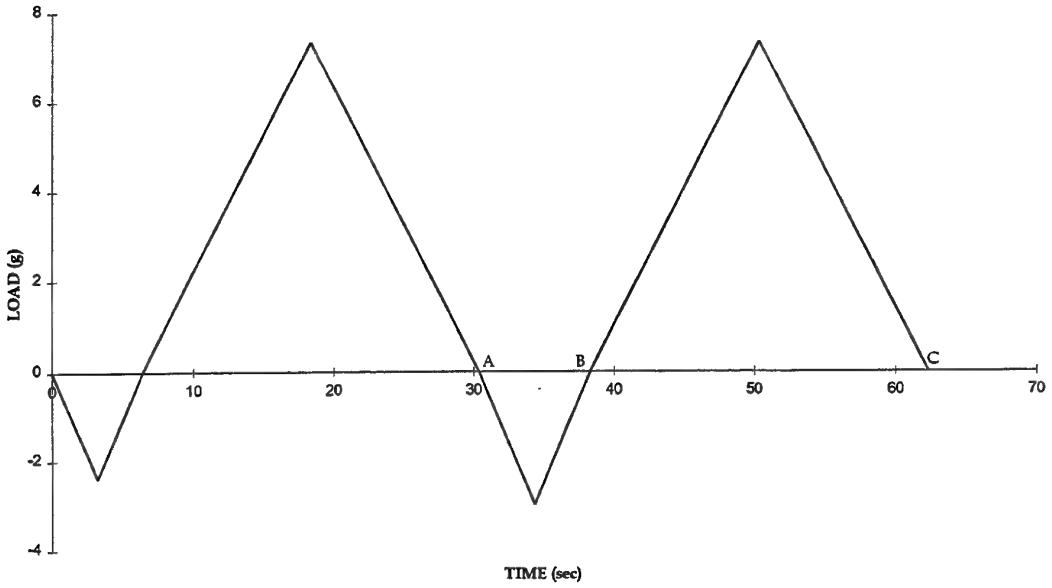

Figure 24: Single CPLT cycle Definition: Load versus Time Sequence.

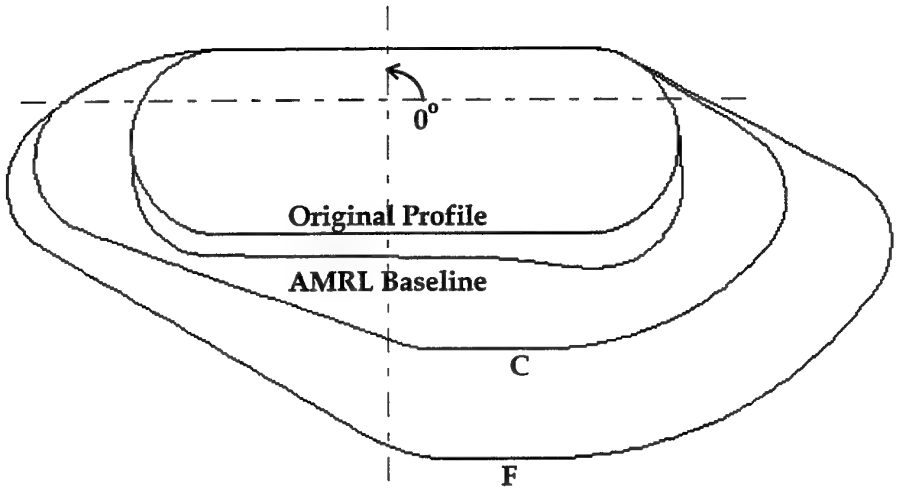

Figure 25: FFVH#13 Original, Baseline, Intermediate and Large Profiles.

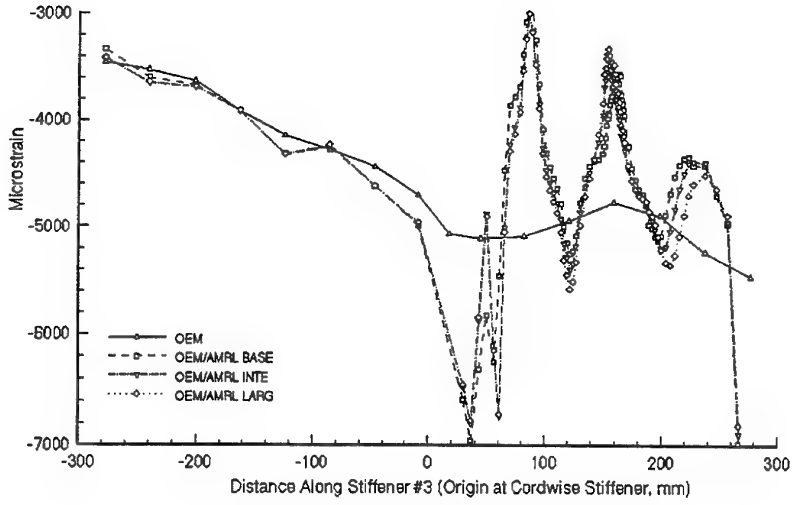

a) Upper Plate: +7.33g Load Case.

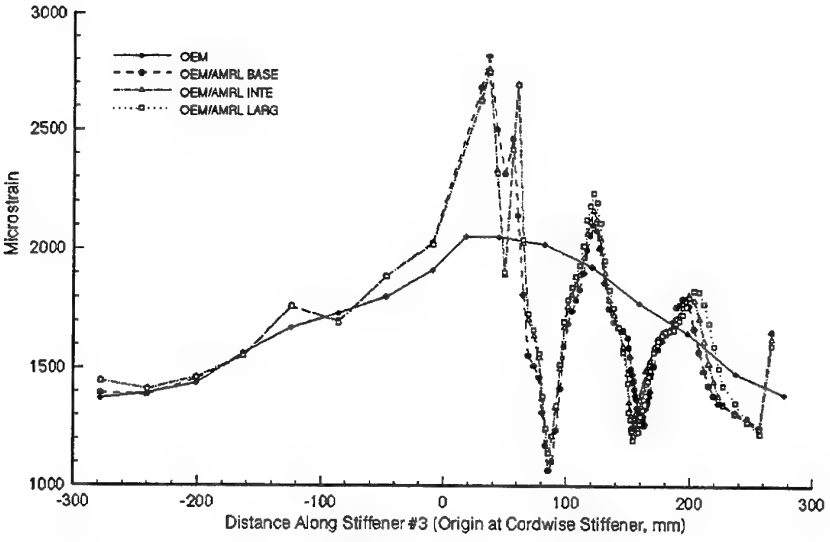

b) Upper Plate: -2.4g Load Case.

Figure 26: Strain Distributions along Upper Plate and Under Surface of Stiffener #3 for Modified OEM and OEM/AMRL FE Models.

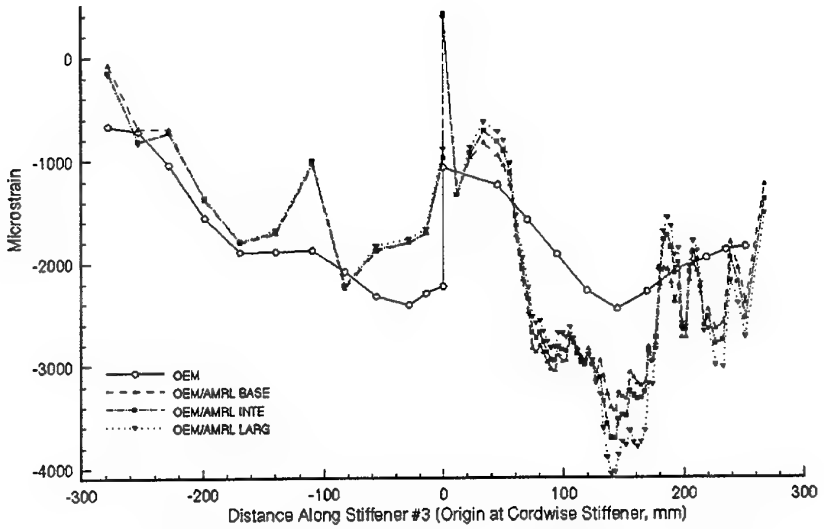

c) Under Surface Stiffener #3: +7.33g Load Case.

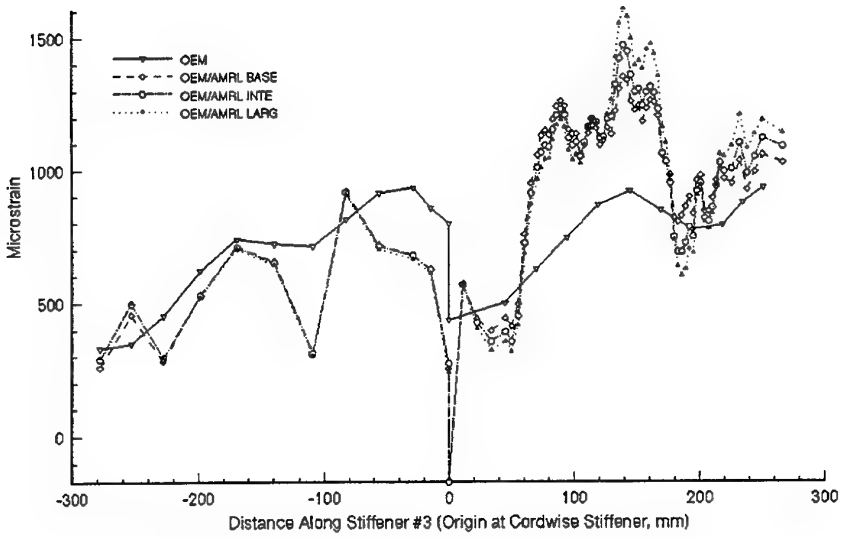

d) Under Surface Stiffener #3: -2.4g Load Case

Figure 26: Strain Distributions along Upper Plate and Under Surface of Stiffener #3 for Modified OEM and OEM/AMRL FE Models (continued).

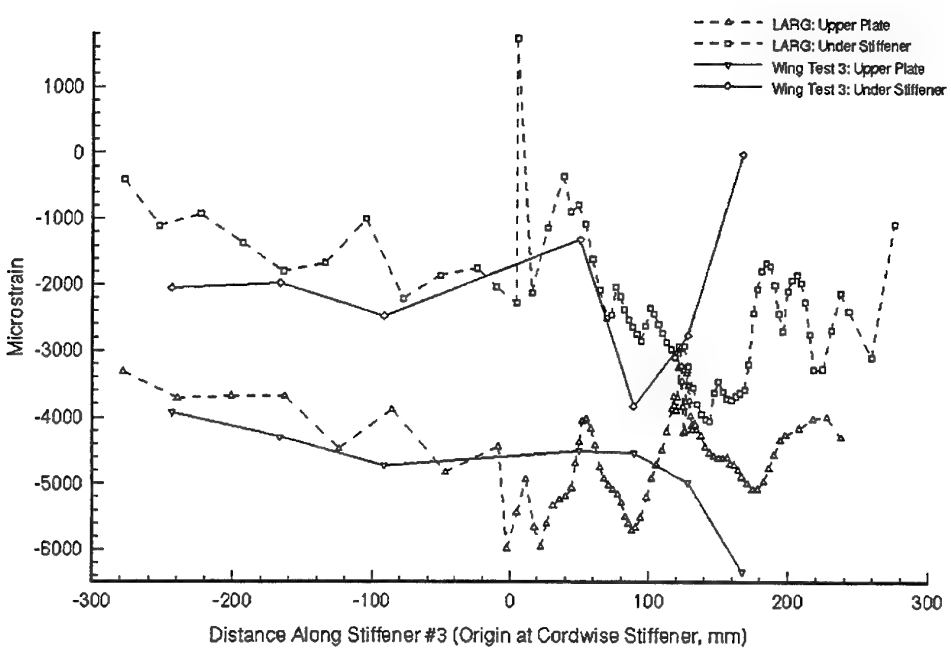

a) +7.33g Load Case.

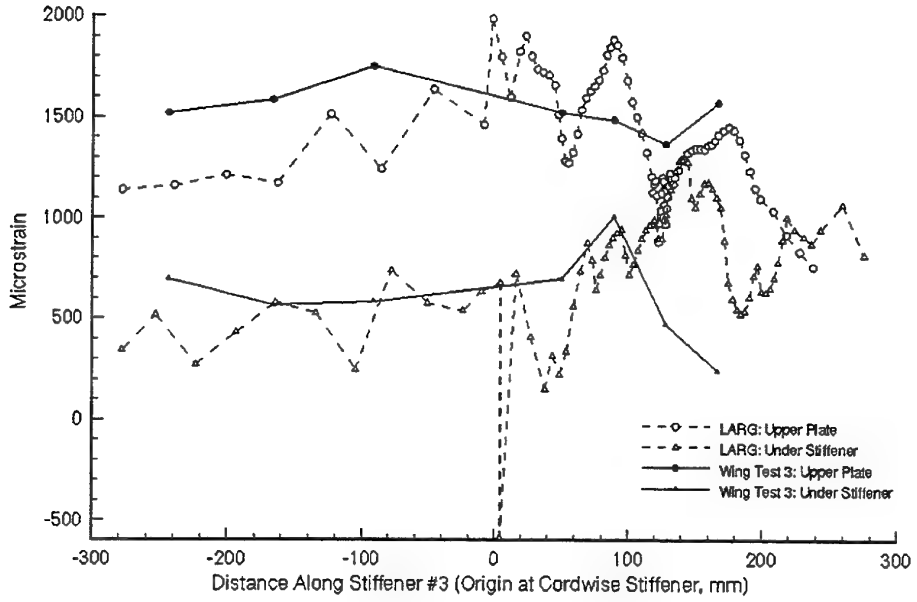

b) -2.4g Load Case.

Figure 27: Strain Distributions along Upper Plate and Under Surface of Stiffener #3 Comparison between Wing Test 3 and LARGE Rework FE Analysis.

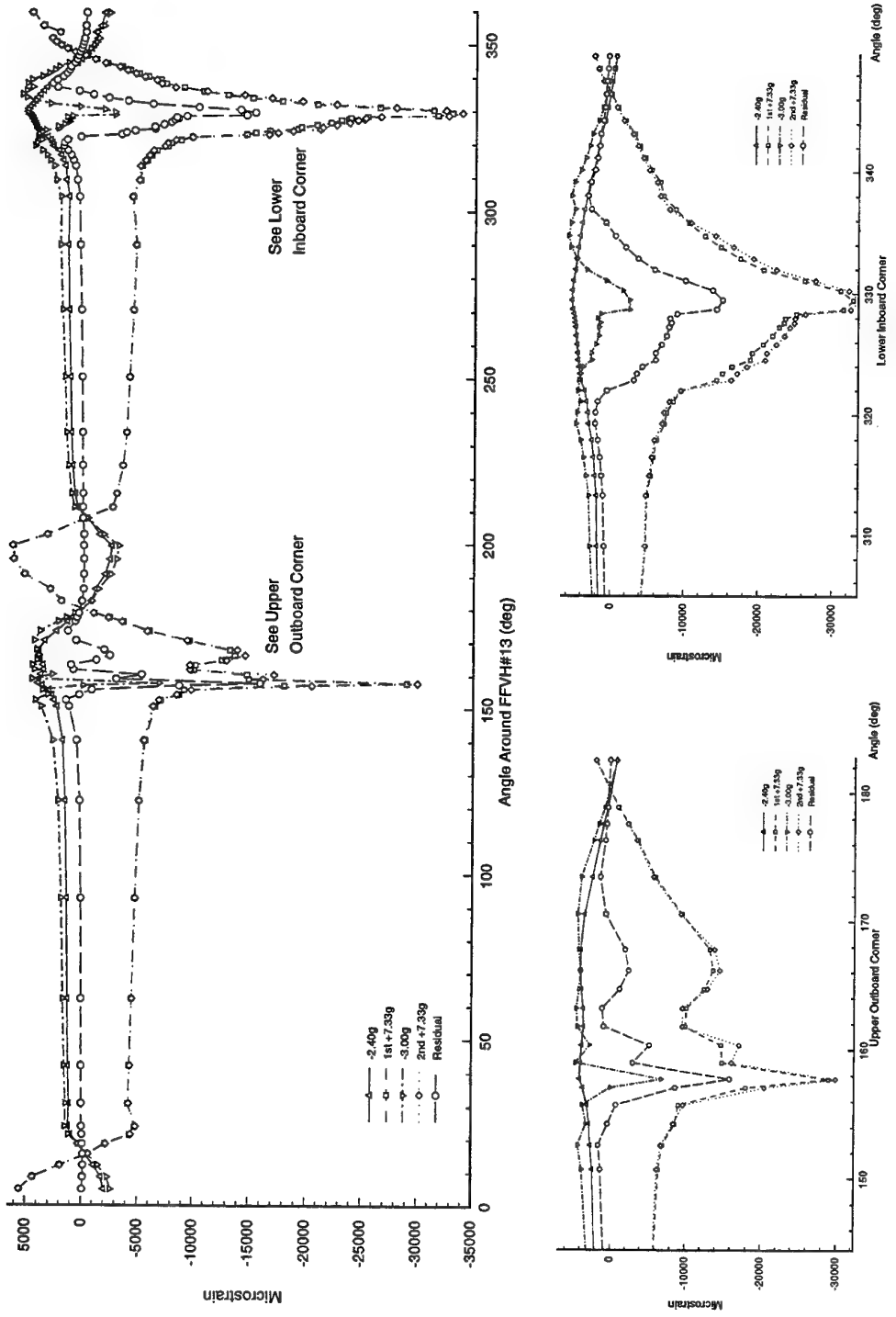

Figure 28: Hoop Strain Distribution around FFVH#13 for Baseline Analysis.

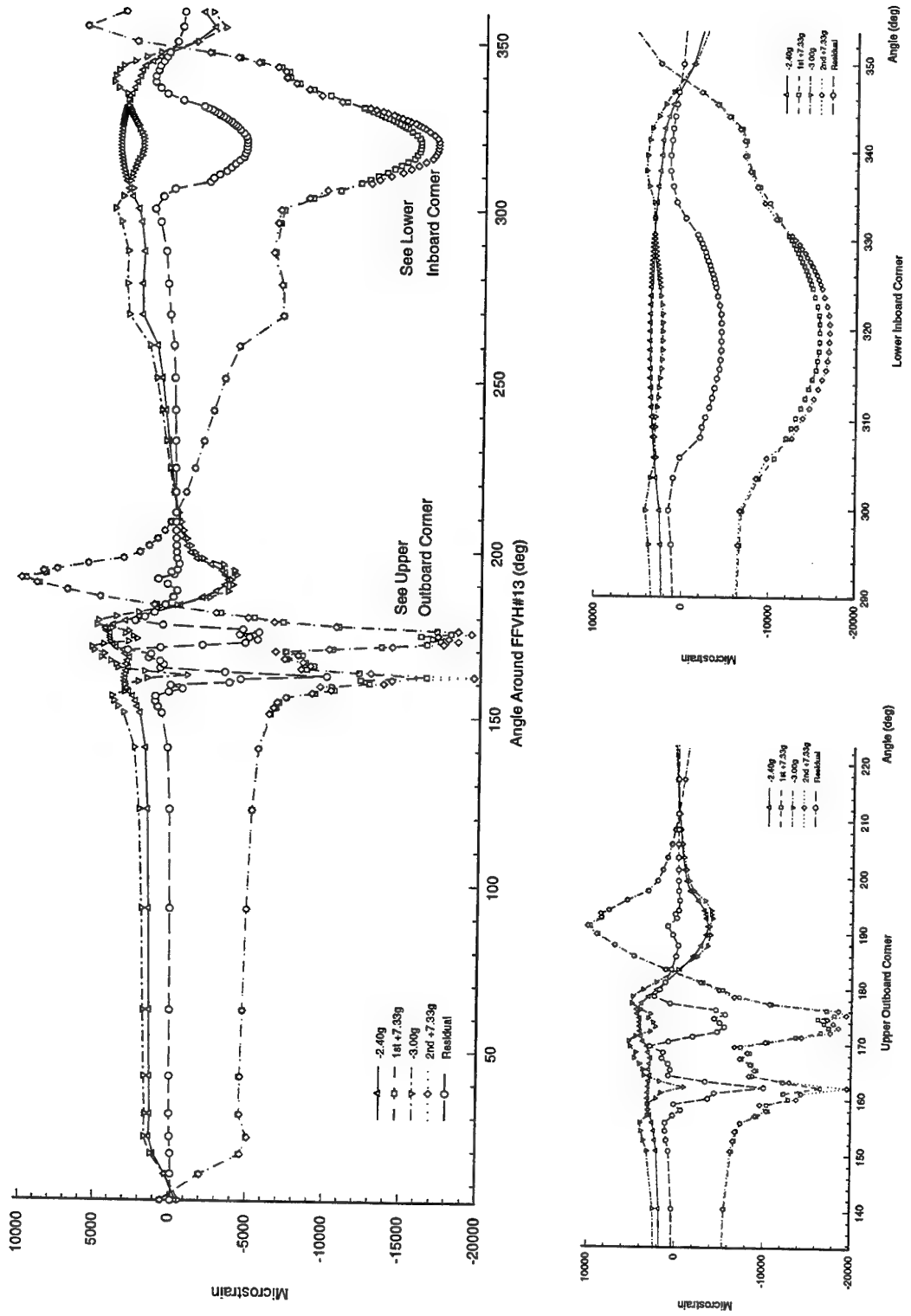

Figure 29: Hoop Strain Distribution around FFVH#13 for Intermediate Analysis.

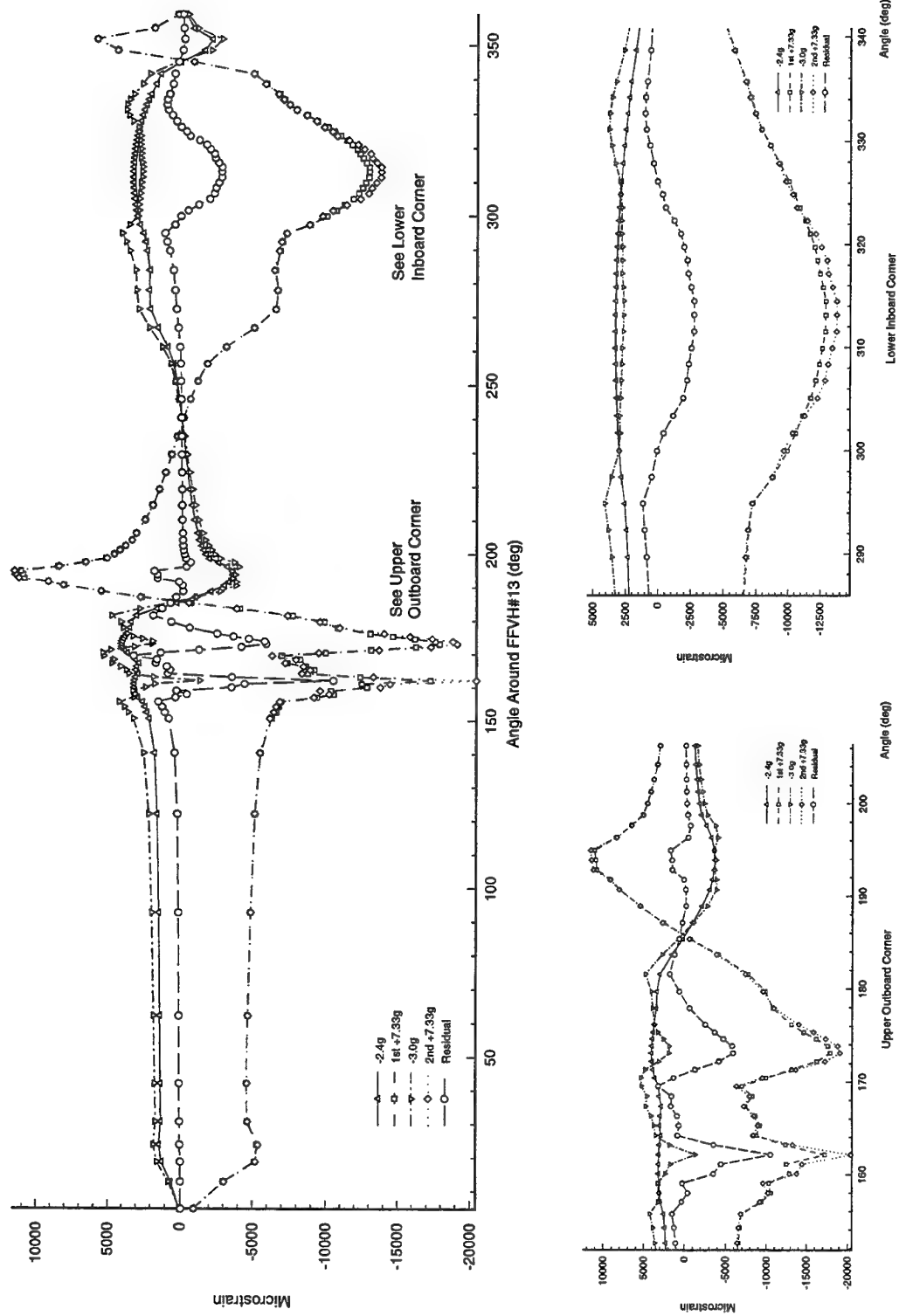

Figure 30: Hoop Strain Distribution around FFVH#13 for Large Analysis.

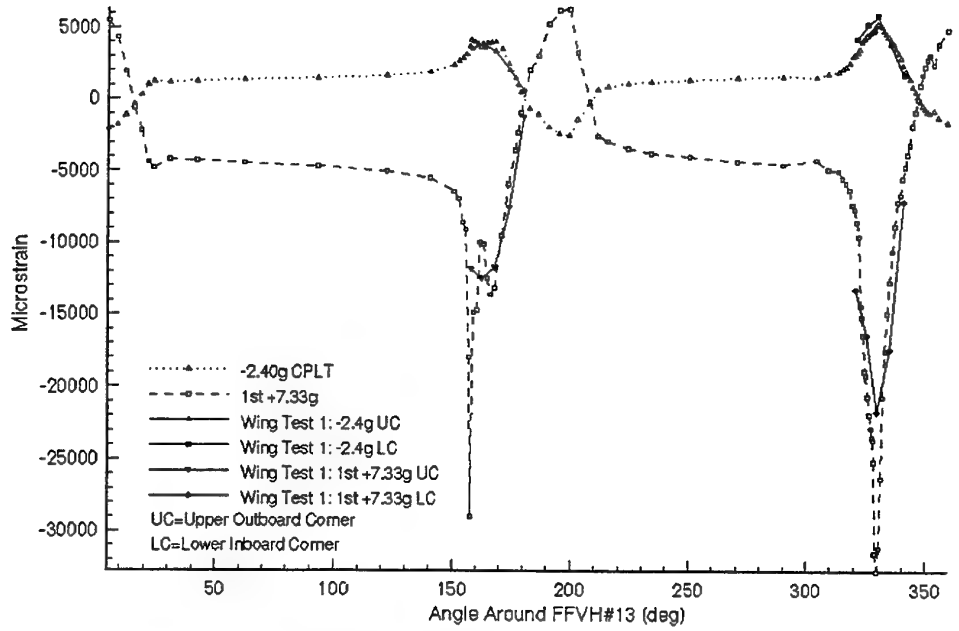

Figure 31: Comparision between Wing Test 1 results and FE results for Baseline Analysis: -2.4g and 1st +7.33g Load Case.

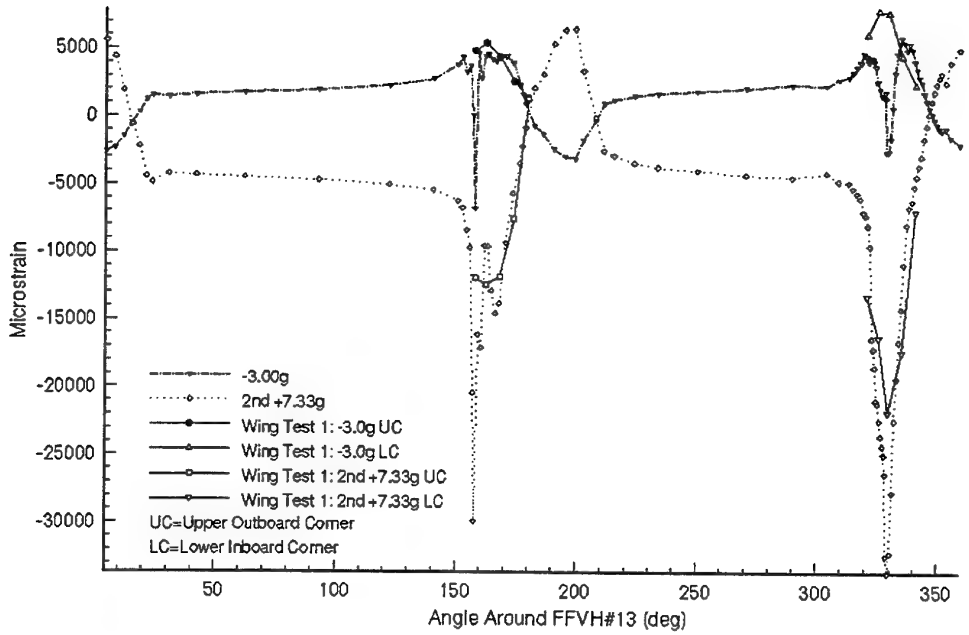

Figure 32: Comparision between Wing Test 1 results and FE results for Baseline Analysis: -3.0g and 2nd +7.33g Load Case.

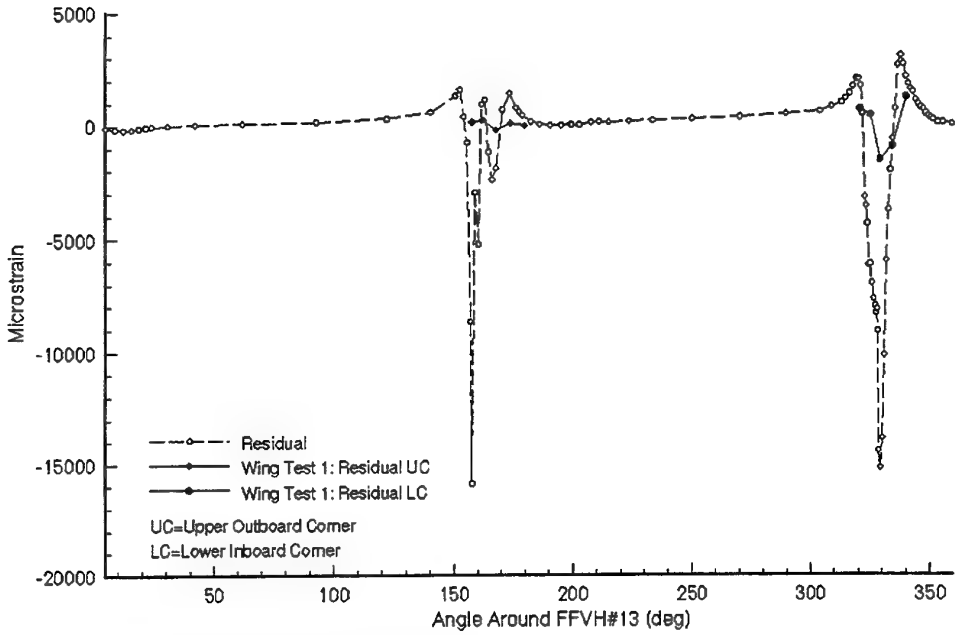

Figure 33: Comparision between Wing Test 1 results and FE results for Baseline Analysis: Residual after 1 CPLT cycle.

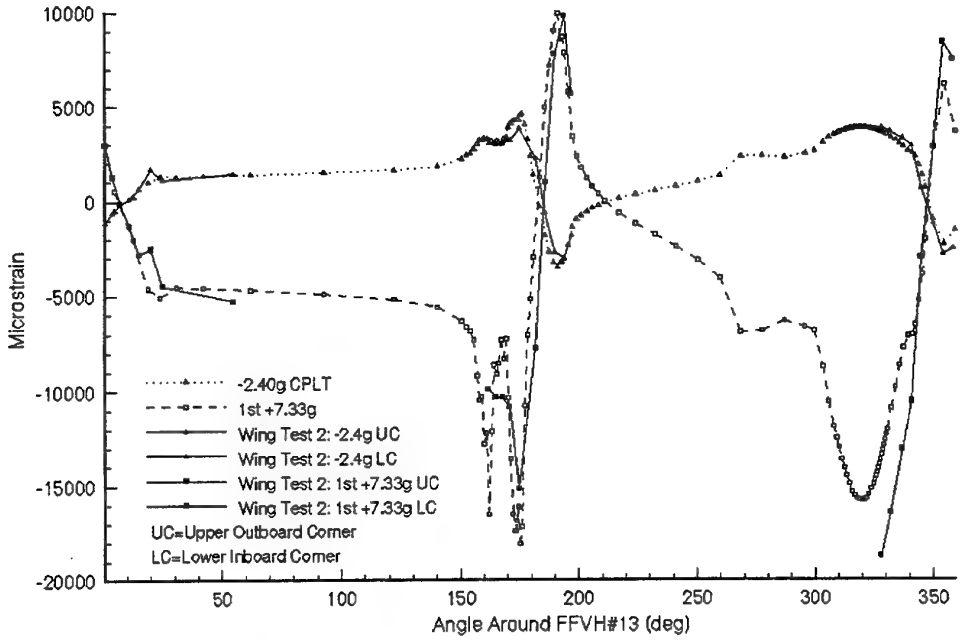

Figure 34: Comparision between Wing Test 2 results and FE results for Intermediate Analysis: -2.4g and 1st +7.33g Load Case.

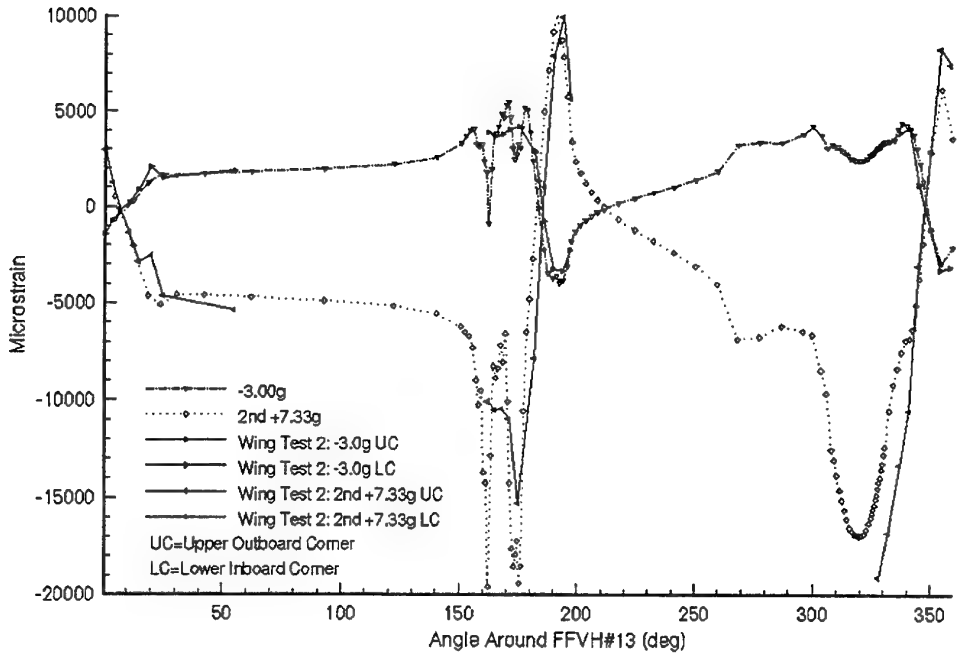

Figure 35: Comparision between Wing Test 2 results and FE results for Intermediate Analysis: -3.0g and 2nd +7.33g Load Case.

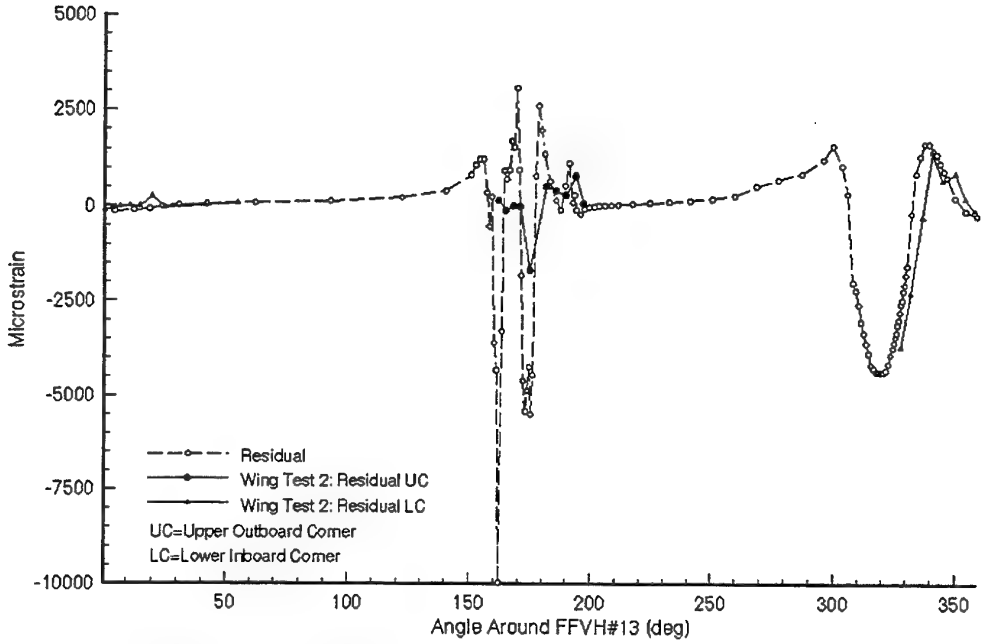

Figure 36: Comparision between Wing Test 2 results and FE results for Intermediate Analysis: Residual after 1 CPLT cycle.

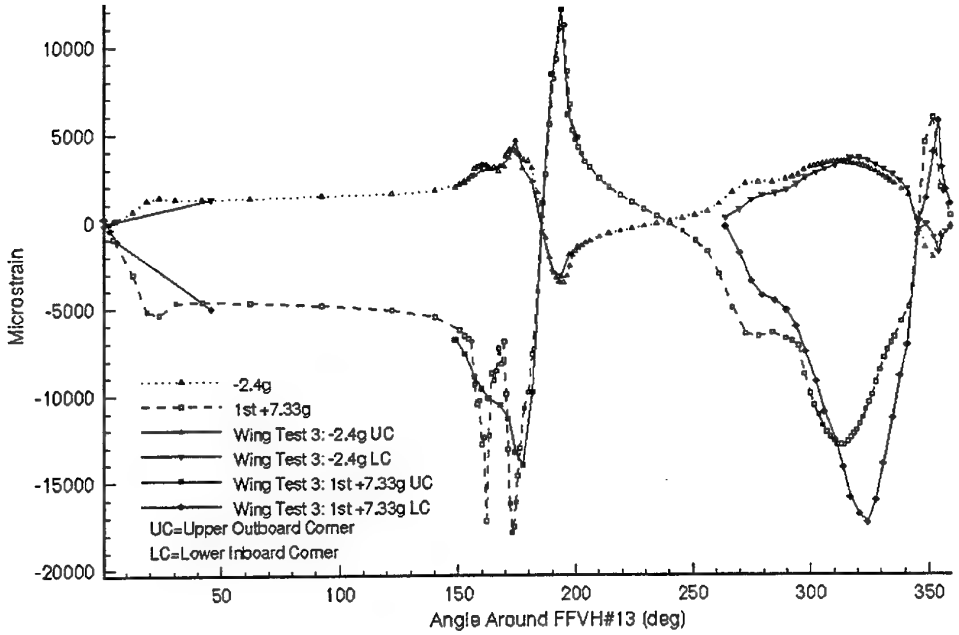

Figure 37: Comparision between Wing Test 3 results and FE results for Large Analysis: -2.4g and 1st +7.33g Load Case.

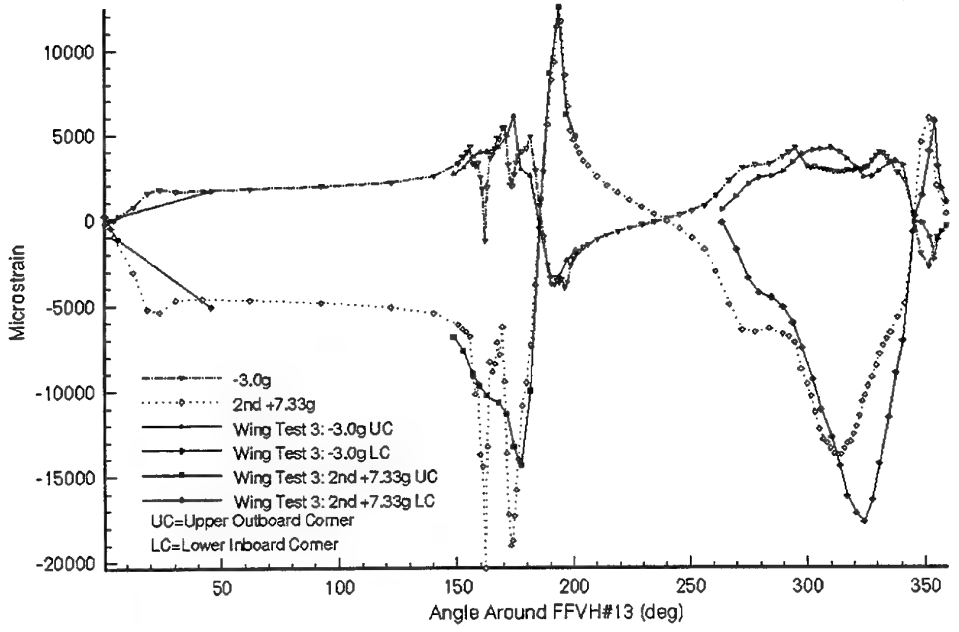

Figure 38: Comparision between Wing Test 3 results and FE results for Large Analysis: -3.0g and 2nd +7.33g Load Case.

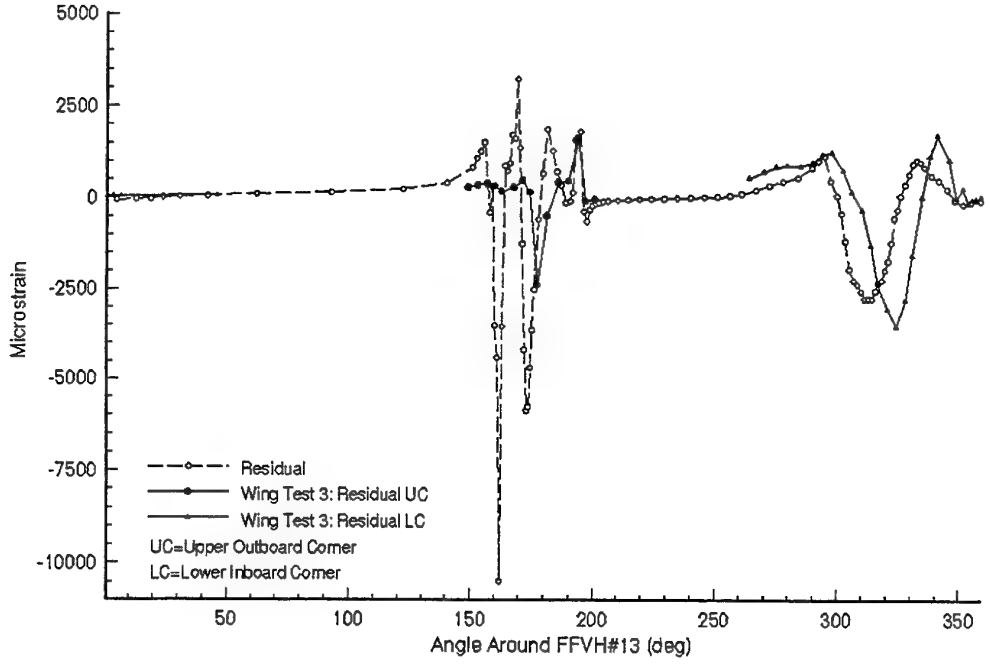

Figure 39: Comparision between Wing Test 3 results and FE results for Large Analysis: Residual after 1 CPLT cycle.

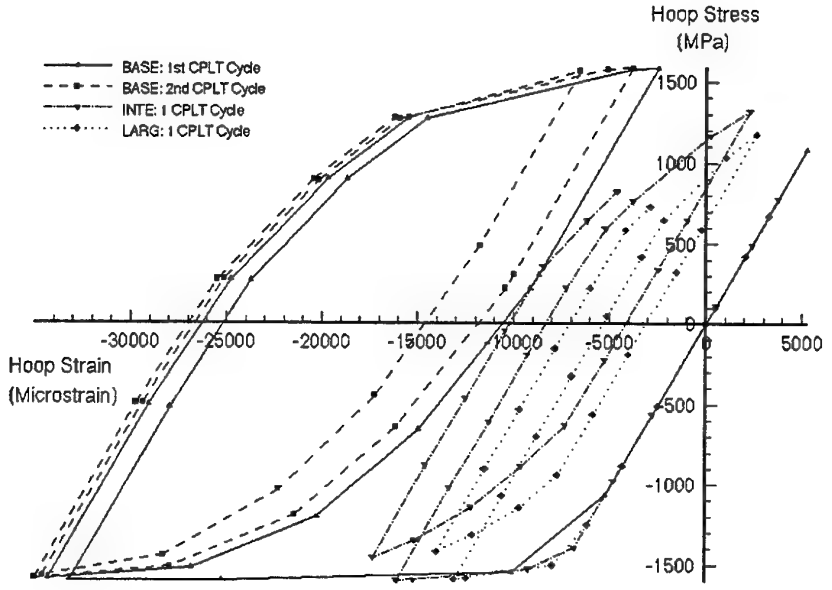

Figure 40: Hoop Stress versus Hoop Strain plot for Baseline, Intermediate and Large FE Analyses.

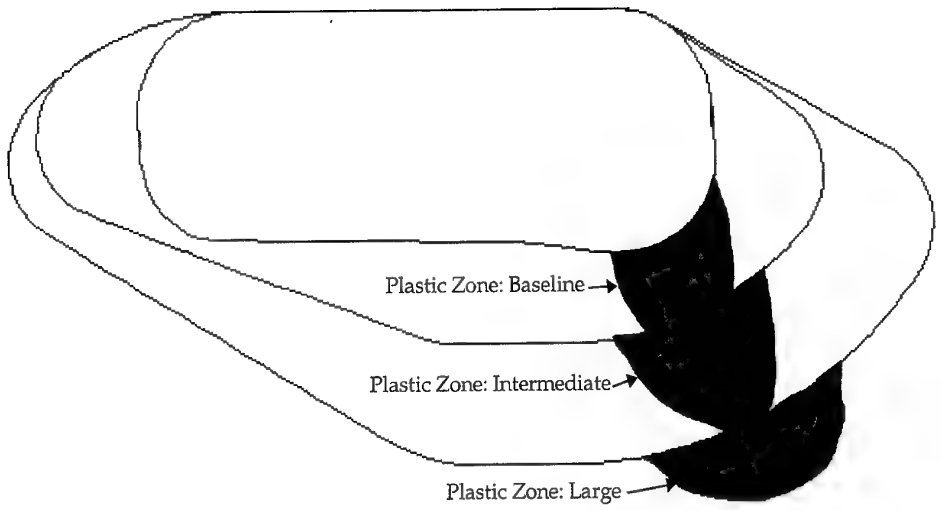

Figure 41: Schematic of residual strain residue between FFVH#13 Reworks.

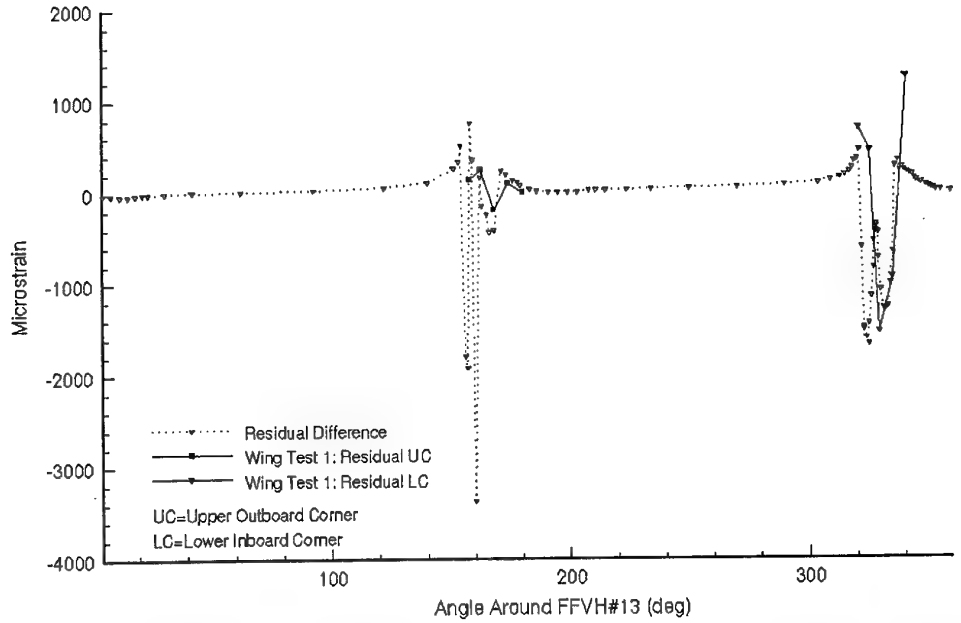

Figure 42: Comparision between Wing Test 1 results and FE results for Baseline Analysis: Difference in Residual strains between 1st CPLT and 2nd CPLT. CPLT cycle.

Figure 43: Von-Mises Stress Distribution: Baseline, Elastic FE, -3.0g Load Case.

Figure 44: Von-Mises Stress Distribution: Baseline, Elastic FE, +7.33g Load Case.

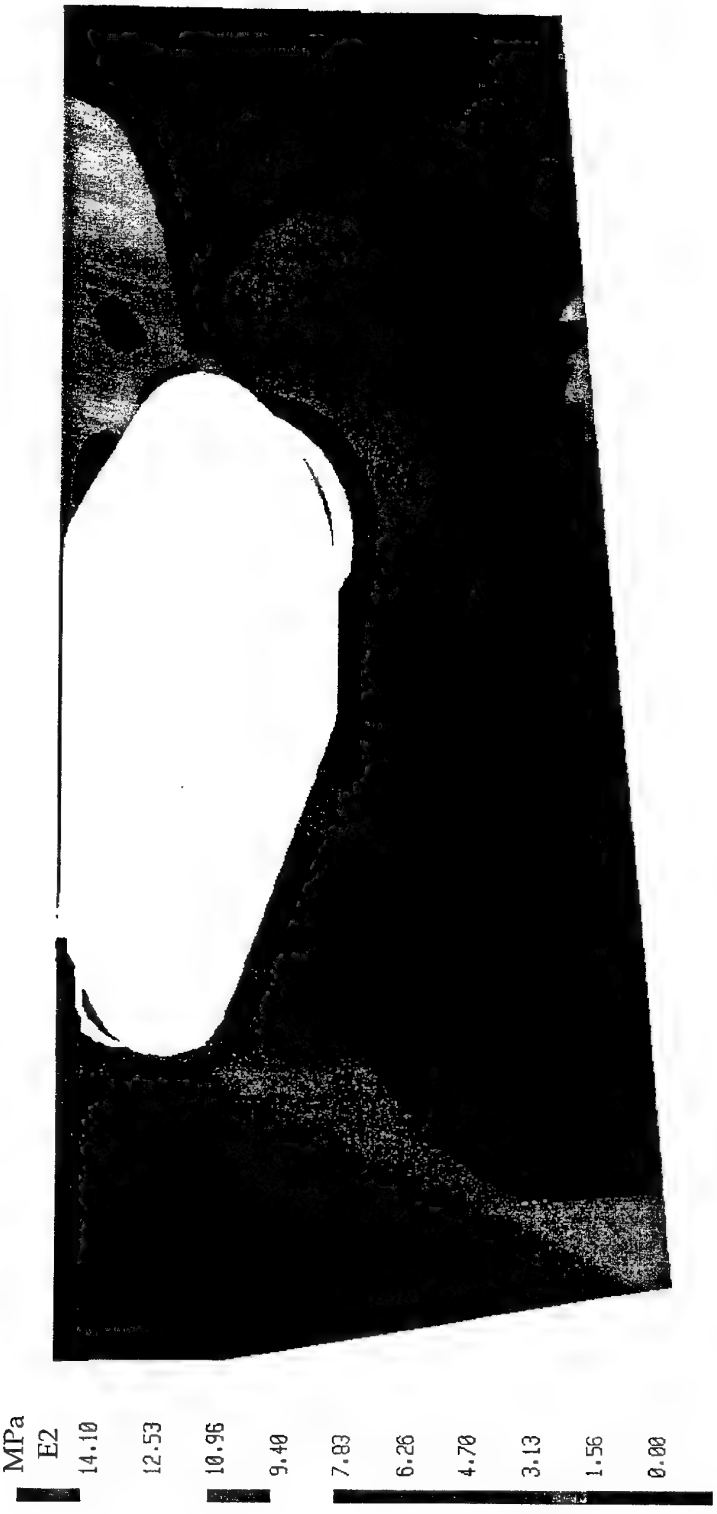

Figure 45: Von-Mises Stress Distribution: Intermediate, Elastic FE, -3.0g Load Case.

Figure 46: Von-Mises Stress Distribution: Intermediate, Elastic FE, +7.33g Load Case.

Figure 47: Von-Mises Stress Distribution: Large, Elastic FE, -3.0g Load Case.

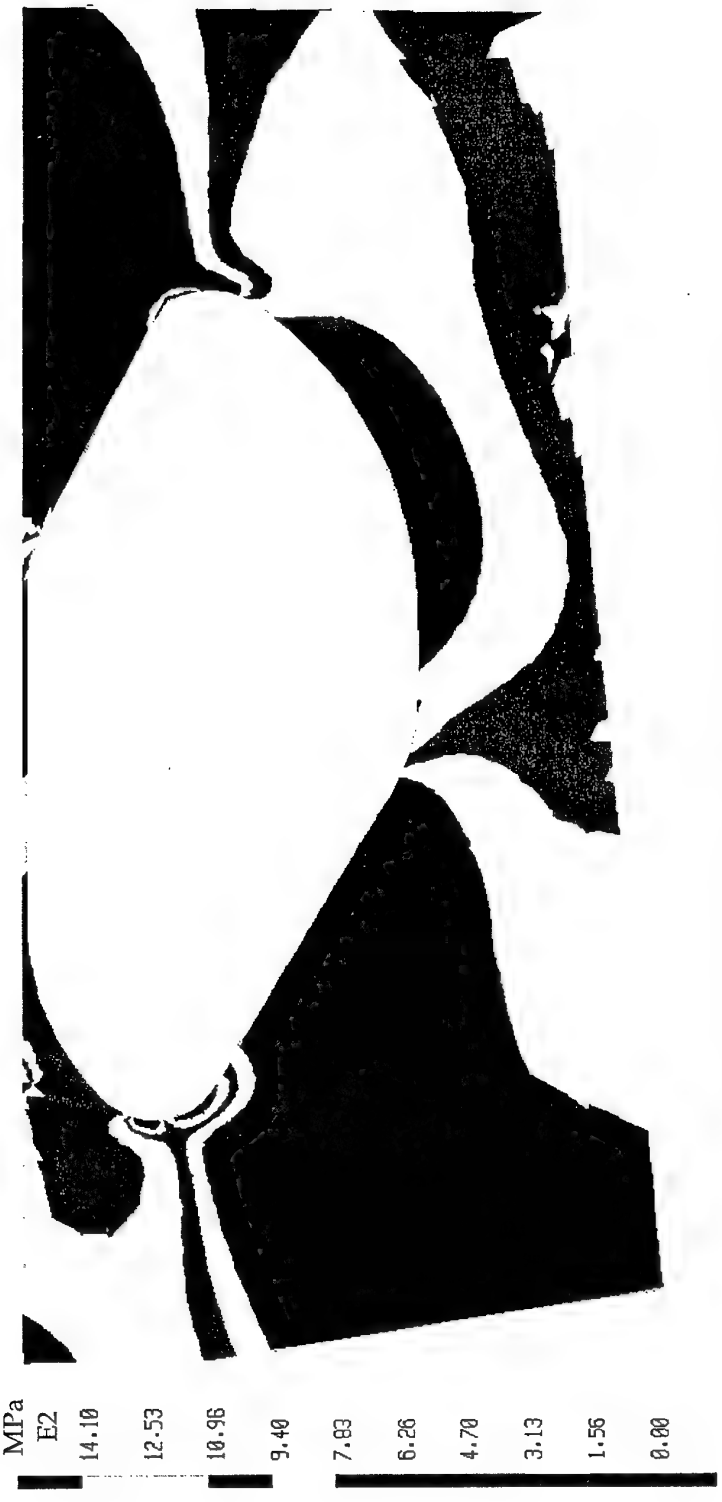

Figure 48: Von-Mises Stress Distribution: Large, Elastic FE, +7.33g Load Case.

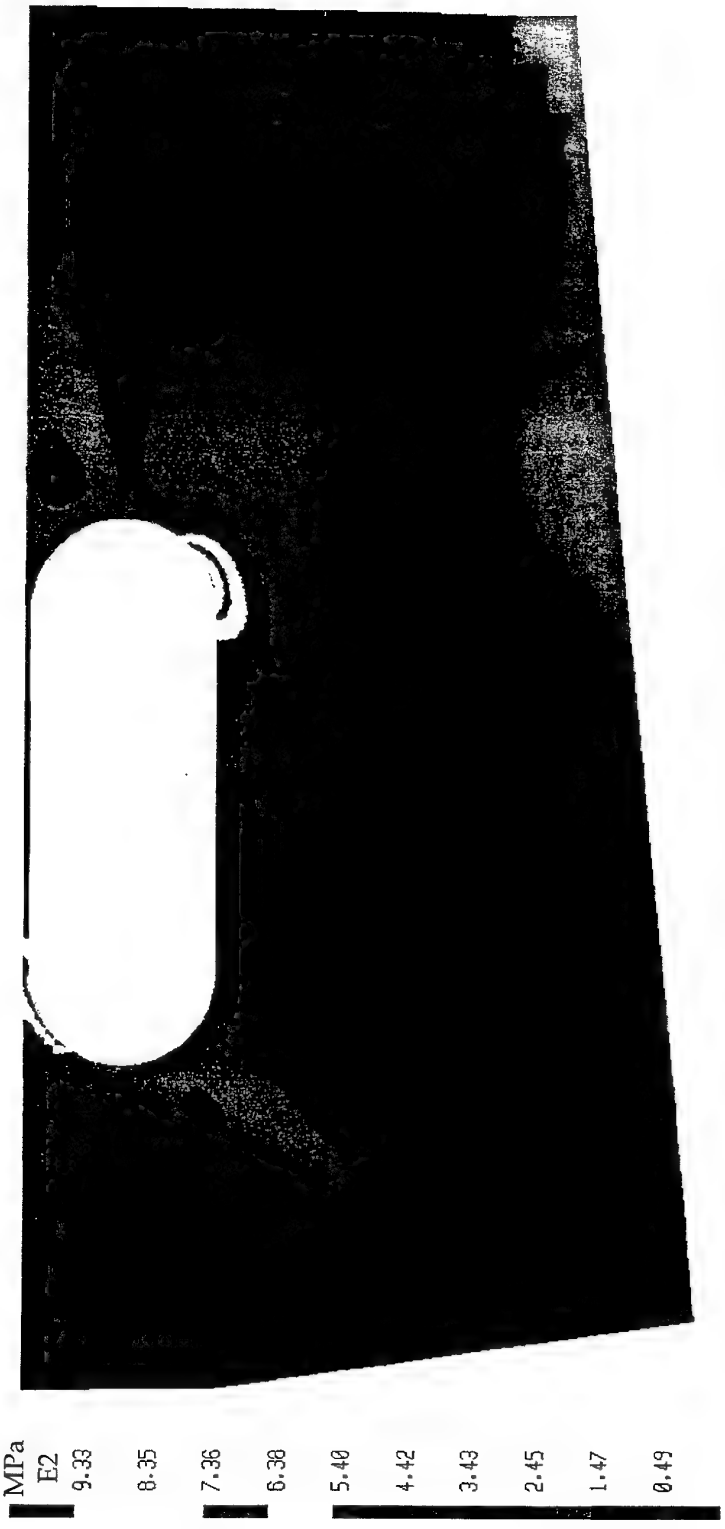

Figure 49: Von-Mises Stress Distribution: Blueprint, Plastic FE, 1st CPLT cycle, -2.4g Load Case.

Figure 50: Von-Mises Stress Distribution: Blueprint, Plastic FE, 1st CPLT cycle, 1st +7.33g Load Case.

Figure 51: Von-Mises Stress Distribution: Blueprint, Plastic FE, 1st CPLT cycle, -3.0g Load Case.

Figure 52: Von-Mises Stress Distribution: Blueprint, Plastic FE, 1st CPLT cycle, 2nd +7.33g Load Case.

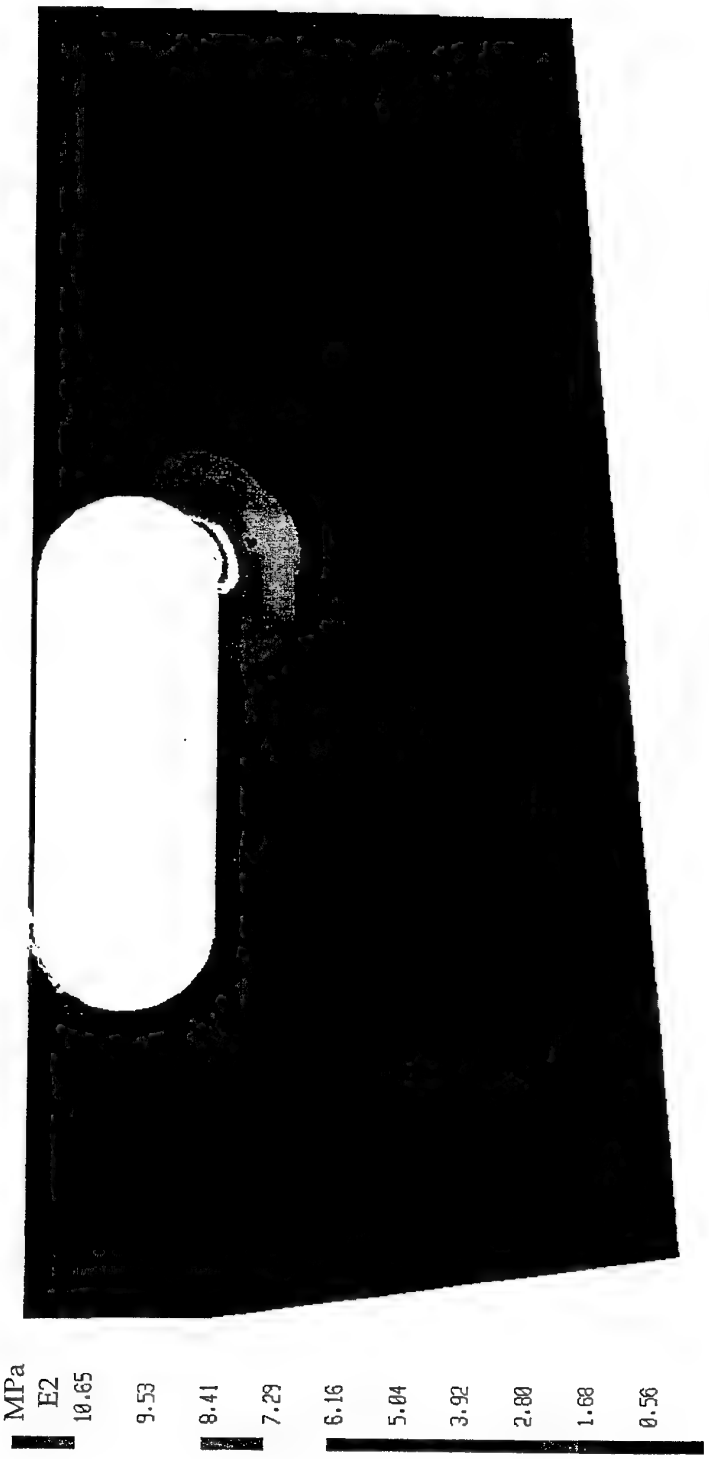

Figure 53: Von-Mises Stress Distribution: Blueprint, Plastic FE, 3rd CPLT cycle, Residual.

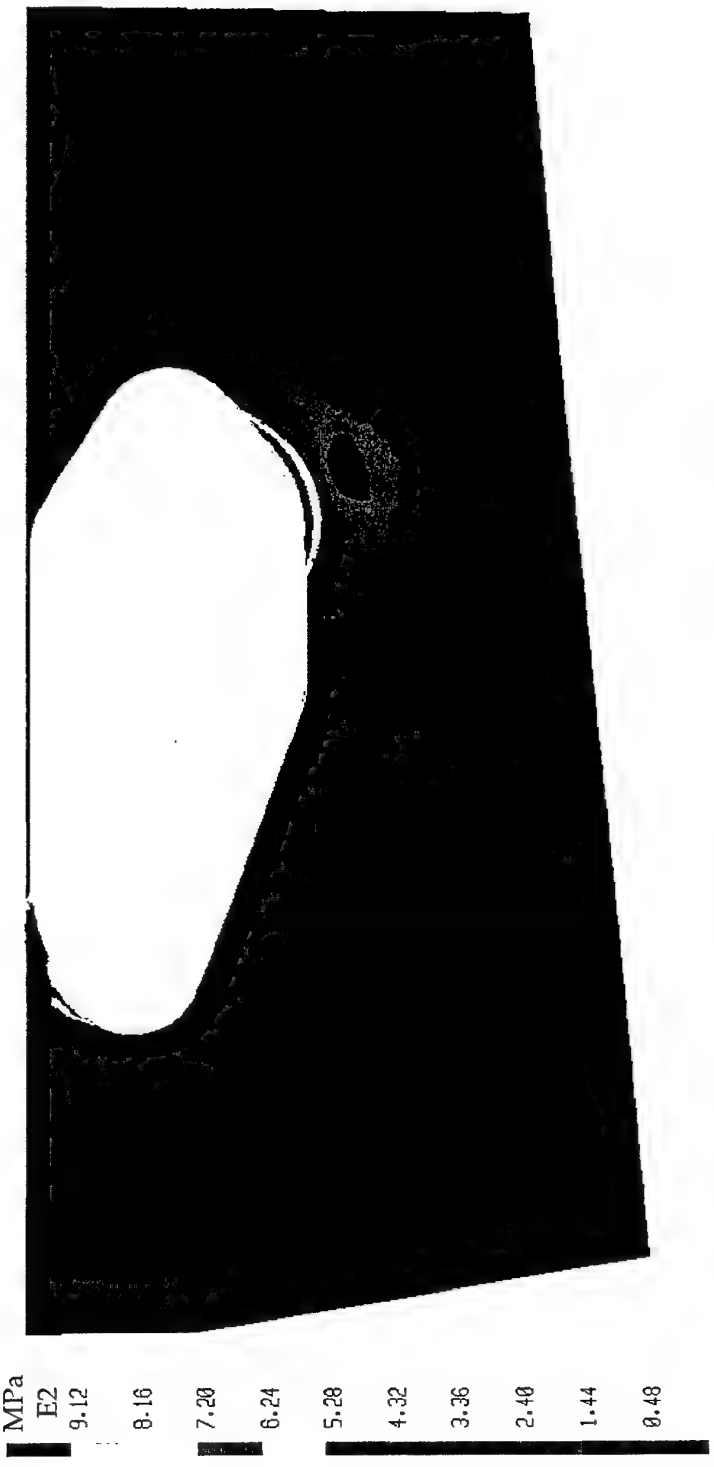

Figure 54: Von-Mises Stress Distribution: Intermediate, Plastic FE, 1st CPLT cycle, Residual.

Figure 55: Von-Mises Stress Distribution: Large, Plastic FE, 1st CPLT cycle, Residual.

APPENDIX 1

A1.1 OEM FE MODEL MODIFICATIONS

Close examination of the OEM model showed that parts of the model were not geometrically representative of current RAAF F-111 WPF's or the AMRL wing number A18-824 which was used in the testing program. Therefore during the calibration of the FEA model a number of modifications were made to create a more accurate representation of the F-111 wing structure and thus improve the overall results being produced. This Appendix describes these modifications:

A1.1.1 ELEMENT COUPLING

The 2D elements (shell) that are directly connected to the 3D elements (brick) cannot transfer the moments to the brick elements because the brick elements do not have the necessary rotational degrees of freedom. In this scenario the shell rotations have no way of being reacted into the bricks.

It was found that by coupling the rotational degrees of freedom of shell elements to brick elements with generalised constraint equations, which are based upon the local geometry, an improved local stress field is transferred to the brick element. PAFEC provides an automated facility to generate the generalised constraint equations and this facility was utilised.

A1.1.2 MATERIAL PROPERTIES

The Young's Modulus in the original OEM FE model was defined as 29000 ksi with a Poisson's ratio of 0.32. The material characterisation work conducted in [4] indicated that Young's Modulus for D6ac steel with the same heat treatment process should be 30023 ksi (205 GPa). Poisson's ratio was left untouched at 0.32.

A1.1.3 TITANIUM WEB

Geometry:
The titanium web is represented by 2D elements and is attached to Stiffener #3 between the upper and lower wing skin surfaces of the WPF. The web lies directly beneath FFVH#13 and is attached to stiffener #3 via a series of bolts. This web significantly affects the local stress field expected within this region. Inspection of the OEM FE model and AMRL wing A18-824 showed that the FE model did not sufficiently represent the dimensions of the titanium web contained within A18-824. The AMRL wing had an extra hole and the thickness distribution was different to that represented in the original OEM FE model. It was therefore necessary to modify the geometry and web properties to emulate those from the OEM drawing.

Offset:
The OEM FE model had the titanium web aligned in the plane of stiffener #3. In the wing the web is connected to the one side of the stiffener and is offset approximately 5.3mm centerline to centerline. In order to better represent the effect of the neutral axis offset of the web the complete web was moved out of the plane of the stiffener by this amount.

Bolt Connectivity:
The original NASTRAN OEM FE model used stiffness elements to represent the Connectivity to the upper and lower wing skin Stiffeners and the vertical inboard and outboard Stiffeners. These elements were converted into the PAFEC equivalents and an investigation into their representation of a bolt connection was undertaken.

A simple 2 element representative FE model was generated and sample loads applied. Three different types of connectivity were tested; 1) Stiffness elements, 2) Repeated Freedoms and 3) Rigid Links. It was found the 2) and 3) gave very similar results, however 1) provided unacceptable differences in all 6 degrees of freedom. Based upon this finding the stiffness elements were replaced with repeated freedoms to transfer the load from the web to the attachment Stiffeners.

Mesh Density:
The accuracy of the loads transferred into Stiffener #3 from the titanium web are partially dependent upon how accurately the web is modelled. In order to obtain a level of confidence that the web was numerically conditioned, two modifications were made. The first involved quadrupling the 2D mesh density and the second involved converting the 2D web representation into a 3D mesh. The effect of performing these 2 modifications was minimal.

A1.1.4 ELEMENT DISCONTINUITY'S

Several meshing areas with the OEM FE model showed element discontinuities. This may have been in the original NASTRAN data deck or a result of the conversion to PAFEC. These areas were improved.

A1.1.5 ELEMENT TYPES

As noted in [6], the original NASTRAN QUAD4 type elements could have been changed to the PAFEC equivalent "Semi-Loof" type elements. This modification was performed and the PAFEC 43210 series of elements replaces the plane stress/plane strain elements previously used.

A1.1.6 BEAM OFFSETS

The original NASTRAN data deck was not fully converted correctly as the beam offsets information was lost in translation. This has not been corrected as the original file has been lost.

A1.2 OEM/AMRL FE MODEL MODIFICATIONS

The modifications made to the OEM/AMRL series of models were not extensive and are listed below.

1. Removal of the original coarse meshed elements.
2. Re-numbering of the nodes and elements in the substructure model to avoid conflicts.
3. Restraining all relevant off shell directions[6] for the newly inserted stiffener and cross web plate elements.
4. The original OEM FE model contained only one 3D brick element though the thickness of the wing. The AMRL substructure model was refined to have two 3D brick elements through the thickness (discussed in Section A1.3.4). At the junction between the two models a set of generalised constraints were written to transfer the load through this discontinuous boundary.

A1.3 SUBSTRUCTURE FE MODEL MODIFICATIONS

A1.3.1 ORIENTATION

The original OEM FE model of the F-111 stub wing contained the substructure region at an orientation that made manipulating the mesh and processing the results difficult. To obtain the most accurate geometric representation of the intermediate and large geometries AMRL imported these geometries into the FE model via IGES format from AUTOCAD drawing. As a result there was a mismatch between the imported orientation and existing FFVH#13 orientation.

The simplest way to avoid any rotation mismatches that were occurring was to rotate the whole FE model so that Stiffener #3 lay directly in the X-Y plane. The fact that the stiffener was now in the X-Y plane, ie. the global axis system, resulted in a much quicker viewing of the stress and strain distributions as no rotation, were required from the global axis system to the in-plane axis system.

---

[6] Shell elements only allow 5 degrees of freedom so depending upon the local orientation of the elements 1 degree of freedom must be manually removed from the analysis.

However, the boundary conditions discussed in Section 2.3.3 were in the old axis system. The PAFEC FE package provides an option called LOCAL.DIRECTIONS which allows users to rotate nodal information into any axis system. The reverse rotation angle was calculated and applied to all boundary nodes and thus resulted in the displacement field been applied in the appropriate direction.

A1.3.2 MESH DENSITY

The mesh density around FFVH#13 was reworked serval times as a result of the very high variation in stresses and strains. The mesh densities required for the plastic analyses were significantly finer than those required for just an elastic analysis. Additional 3D plate elements were required to maintain mesh consistency in the region of the upper outboard corner of FFVH#13.

A1.3.3 STIFFENER THICKNESS TRANSITION

The nominal Stiffener #3 thickness is 5mm which originally flowed all the way up to the wing skin/stiffener interface. The resulting increased strains, due to this assumption, caused the upper corner to be unacceptable. The technique employed to improve this limitation was to apply separate thicknesses to layers of local elements at the interface. The problems associated with using this technique are discussed in Section 6.2.3.5.

A1.3.4 WING SKIN 3D ELEMENTS

As previously mentioned the original OEM FE model contained only one 3D brick element though the thickness of the wing. This was found to inadequately represent the effects of the underlying structure. The plate was meshed through the thickness in a ratio of .4 and .6 so that smaller elements were closest to the underlying structure. This also improved the reacting out of the coupling loads from the 2D shell elements.

A1.3.5 MISCELLANEOUS

The original AMRL FE model used plane strain elements to represent the stiffener. These elements were changed to the 'Semi-Loof' series of elements. In the current PAFEC level these elements are the only type of shell elements that allow a plastic analysis to be performed.

The coupling between the 2D and 3D elements, as described in Section A1.1.1, was also applied in all the FE model's. In addition, some 2D element discontinuities that flowed through from the original OEM FE model were corrected.

DISTRIBUTION LIST

Elastic/Plastic Finite Element Analysis of the F-111 Fuel Flow Vent Hole Number 13

J. Paul, P. Chapman and A. Searl

AUSTRALIA

DEFENCE ORGANISATION

Task Sponsor DTA-LC

S&T Program

Chief Defence Scientist
FAS Science Policy
AS Science Industry and External Relations
AS Science Corporate Management
} shared copy

Counsellor Defence Science, London (Doc Data Sheet)
Counsellor Defence Science, Washington (Doc Data Sheet)
Scientific Adviser to MRDC Thailand (Doc Data Sheet)
Director General Scientific Advisers and Trials/Scientific Adviser Policy and Command (shared copy)
Navy Scientific Adviser (3 copies Doc Data Sheet and 1 copy distribution list)
Scientific Adviser - Army (Doc Data Sheet and distribution list only)
Air Force Scientific Adviser
Director Trials

Aeronautical and Maritime Research Laboratory

Director
Chief, AED
F. Rose
K. Watters
P. Chapman
A. Searl
J. Paul (5 copies)
C. H. Wang
R. Allan

Electronics and Surveillance Research Laboratory

Director

DSTO Library

Library Fishermens Bend
Library Maribyrnong
Library DSTOS (2 copies)
Australian Archives
Library, MOD, Pyrmont (Doc Data sheet only)

Forces Executive

Director General Force Development (Sea) (Doc Data sheet only)
Director General Force Development (Land) (Doc Data sheet only)
Director General Force Development (Air)

Air Force
OIC ASI
ASI2A

S&I Program
Defence Intelligence Organisation
Library, Defence Signals Directorate (Doc Data Sheet only)

B&M Program (libraries)
OIC TRS, Defence Central Library
Officer in Charge, Document Exchange Centre (DEC), 1 copy
*US Defence Technical Information Centre, 2 copies
*UK Defence Research Information Center, 2 copies
*Canada Defence Scientific Information Service, 1 copy
*NZ Defence Information Centre, 1 copy
National Library of Australia, 1 copy

UNIVERSITIES AND COLLEGES

Australian Defence Force Academy
Library
Head of Aerospace and Mechanical Engineering
Deakin University, Serials Section (M list), Deakin University Library, Geelong, 3217
Senior Librarian, Hargrave Library, Monash University
Librarian, Flinders University

OTHER ORGANISATIONS

NASA (Canberra)
AGPS

OUTSIDE AUSTRALIA

4. ABSTRACTING AND INFORMATION ORGANISATIONS
INSPEC: Acquisitions Section Institution of Electrical Engineers
Library, Chemical Abstracts Reference Service
Engineering Societies Library, US
American Society for Metals
Documents Librarian, The Center for Research Libraries, US

5. INFORMATION EXCHANGE AGREEMENT PARTNERS
Acquisitions Unit, Science Reference and Information Service, UK
Library - Exchange Desk, National Institute of Standards and Technology, US
National Aerospace Laboratory, Japan
National Aerospace Laboratory, Netherlands

SPARES (10 copies)

Total number of copies: 63

DEFENCE SCIENCE AND TECHNOLOGY ORGANISATION
DOCUMENT CONTROL DATA

1. PRIVACY MARKING/CAVEAT (OF DOCUMENT)

2. TITLE

Elastic/Plastic Finite Element Analysis of the F-111 Fuel Flow Vent Hole Number 13

3. SECURITY CLASSIFICATION (FOR UNCLASSIFIED REPORTS THAT ARE LIMITED RELEASE USE (L) NEXT TO DOCUMENT CLASSIFICATION)

Document (U)
Title (U)
Abstract (U)

4. AUTHOR(S)

J. Paul, P. Chapman and A. Searl

5. CORPORATE AUTHOR

Aeronautical and Maritime Research Laboratory
PO Box 4331
Melbourne Vic 3001

6a. DSTO NUMBER	6b. AR NUMBER	6c. TYPE OF REPORT	7. DOCUMENT DATE
DSTO-TR-0454	AR-009-944	Technical Report	November 1996

8. FILE NUMBER	9. TASK NUMBER	10. TASK SPONSOR	11. NO. OF PAGES	12. NO. OF REFERENCES
M1/9/274	96/102	DTA-LC	80	15

13. DOWNGRADING/DELIMITING INSTRUCTIONS

None

14. RELEASE AUTHORITY

Chief, Airframes and Engines Division

15. SECONDARY RELEASE STATEMENT OF THIS DOCUMENT

Approved for public release

OVERSEAS ENQUIRIES OUTSIDE STATED LIMITATIONS SHOULD BE REFERRED THROUGH DOCUMENT EXCHANGE CENTRE, DIS NETWORK OFFICE, DEPT OF DEFENCE, CAMPBELL PARK OFFICES, CANBERRA ACT 2600

16. DELIBERATE ANNOUNCEMENT

No limitations

17. CASUAL ANNOUNCEMENT Yes

18. DEFTEST DESCRIPTORS

Finite element analysis, Plastic deformation, F-111 aircraft, Stress relaxation, Durability

19. ABSTRACT

A detailed plasticity finite element stress analysis is presented for a fatigue critical location, at Fuel Flow Vent Hole #13 (FFVH#13) in the Wing Pivot Fitting of the Royal Australian Air Force's F-111 aircraft. The D6ac material behaviour was represented by a unified constitutive model which is considered to be particularly accurate for modelling plastic deformation through several cycles of non-symmetric loading. The aim of the present work is to generate the residual stress distributions following one (or more) applications of Cold Proof Load Test, as an input to the Durability And Damage Tolerance Analyses (DADTA) for FFVH#13. The mesh refinements and the selection of boundary conditions for a substructure model representing the immediate vicinity of FFVH#13 are discussed in detail. The results from the numerical analysis were correlated with full-scale wing test strain data and showed good agreement. The residual stress distributions obtained here are considered to be significantly more accurate than what has previously been used for the DADTA of FFVH#13.